Title

Investigation of Spire and Cappuccino in Drosophila Oogenesis: Tool Development and Screening for Interactors

Author

Bailey, Hannah

Publication Date

2024

Peer reviewed|Thesis/dissertation

UNIVERSITY OF CALIFORNIA

Los Angeles

Investigation of Spire and Cappuccino in *Drosophila* Oogenesis: Tool Development and Screening for Interactors

A dissertation submitted in partial satisfaction of the

requirements for the degree Doctor of Philosophy

in Biochemistry, Molecular and Structural Biology

by

Hannah Marie Bailey

2024

ABSTRACT OF THE DISSERTATION

Investigation of Spire and Cappuccino in *Drosophila* Oogenesis:

Tool Development and Screening for Interactors

by

Hannah Marie Bailey

Doctor of Philosophy in Biochemistry, Molecular and Structural Biology

University of California, Los Angeles, 2024

Professor Margot Elizabeth Quinlan, Chair

The *Drosophila* oocyte has long served as a model for understanding oogenesis, the process of egg development. An essential structure in *Drosophila* oocytes is a cytoplasmic actin meshwork that persists during mid-oogenesis. This complex actin network is built by the collaboration of actin nucleators: Spire (Spir) and Cappuccino (Capu). Removal of the actin mesh, and the concurrent decrease in Spir and Capu expression, coincides with the onset of fast cytoplasmic streaming, mixing cytoplasmic contents and reinforcing the establishment of polarity. Analogous actin meshes, built by Spir and Capu, have been characterized in other systems. The function of these networks appears to differ based on the localization of Capu while the role of the *Drosophila* actin mesh, outside of restricting cytoplasmic streaming, remains uncertain. This is in part, due to the current limitations of imaging the egg chamber *ex vivo* during mesh removal and the requirement of mesh components during earlier stages of development.

To better characterize what the actin mesh does in oogenesis, we set out to generate improved tools for studying Spir and Capu. We established a gene-specific driver for Capu, *capu*-Gal4, that improved the rescue of *capu* null to 90% fertility. Using this driver, we uncovered evidence of additional roles for Capu in development outside of the actin mesh. Our attempts to improve transgene rescue of Spir were unsuccessful. In addition, we performed genome editing to endogenously tag Spir and Capu in *Drosophila*. With these tools, we confirmed the expression patterns of Spir and Capu and revealed previously undescribed localization in somatic cells. In addition, we employed knock-down screens to identify other genes that regulate the actin mesh or interact with Spir. Lastly, we have made progress in adapting long term live imaging methods to visualize the removal of the actin mesh.

In sum, this work contributes new insights into *Drosophila* oogenesis and establishes the groundwork for further developing tools for the *Drosophila* research community. More specifically, it demonstrates that subtle changes in the interaction of actin nucleators leads to the formation of actin-based structures that play distinct cellular roles and exemplifies the need for scrupulous genetic investigations.

The dissertation of Hannah Marie Bailey is approved.

Albert J. Courey

Alvaro Sagasti

Emil Reisler

Margot Elizabeth Quinlan, Committee Chair

University of California, Los Angeles

2024

To Spir and Capu,

“Alright then, keep your secrets.”

-Frodo Baggins

Lord of the Rings: The Fellowship of the Ring (Film)

TABLE OF CONTENTS

List of figures

List of tables

Acknowledgements

Thank you to my committee members for offering ideas, feedback, and advice as I embarked on this journey. I would specifically like to thank my committee chair and principal investigator, Dr. Margot Quinlan. Margot, your support and guidance has been invaluable to my growth as a scientist and person.

I would like to thank members of the Quinlan Lab over the years for their support and input. Thanks to Michelle Panzica and Kathryn Bremer for being my original girl gang. To Dylan Valenica for always agreeing to play Root. To Merin Rixen for being my travel buddy and confidant. To Menna, for being my first mentee in the lab and for her dedication to our research. I would also like to thank the Akin Lab for not only sharing their lab space and microscopes, but for supporting my baking hobby and always being up for friendly competition at game nights. Also, a huge thank you to the friends and mentors I met in undergrad at Otterbein. To Will King for being the most reliable third wheel and always willing to listen. And to my undergraduate PI, Dr. John Tansey, for pushing me to apply to a PhD program and taking me to conferences to share my work but also to learn more about what it meant to be part of the scientific community.

I would like to highlight that Chapter 3 is a manuscript in preparation, “Flexible geometry of *Drosophila* formin Cappuccino in actin mesh formation” and acknowledge the co-authors. Authors Peter Cullimore and Liam A Bailey contributed to assisting with fly data and generation of a custom correlation code, respectively. Chapter 4 is an abbreviated version of a manuscript in preparation, “Do Spir and MyosinV interact in *Drosophila* oogenesis?” While the included portion is work I assisted with, the fly genetics and project were led by Joseph Ong, biochemical study by Michelle Panzica, yeast screens and mesh imaging by Emma Carley, and additional fly work by Merin Rixen. Margot E. Quinlan was the principal investigator for all studies.

I would like to thank the NIH for supporting the UCLA CMB Training Grant, which funded one year of my research. Special thanks to the *Drosophila* community for their feedback at many fly meetings, to the *Drosophila* stock centers, and to the people at FlyBase for keeping an incredible tool available and curated. None of this work would have been possible without the generosity and dedication of the fly community.

I extend my gratitude to UCLA staff who keep our department running smoothly. Special thanks go to the following individuals: Marla Gonzales, for keeping the Biochemistry program organized and for always sharing a laugh. Ricky Ruiz, for going above and beyond to keep our research running, this does not go unnoticed or unappreciated. And to Martha Rivas, for working hard to keep our lab spotless and for her cheerful presence that always brightened my mornings.

Thanks to my family and friends for their support over the last six years. Thanks to my parents for supporting me in my pursuit of a PhD 2,000 miles away from home– even though they've been counting down the days until I move back. I would also like to extend my thanks to my two triplet brothers, Liam and Jacob, for fueling an academic competition that sometimes kept me going through my PhD. Liam, I never dreamed I would be publishing a manuscript with you. But your guidance and support over the years, from me crying over AP calculus to crying over code, has meant more to me than I can write in words.

Lastly, but most importantly, I would like to thank Brodie for being my constant source of support. There have been plenty of ups and downs, including ups and downs on the 5, but you always saw them through. Thank you for being my Reviewer 2, my sounding board, my voice of reason, my comic relief. While I dedicated this document to Spir and Capu for all of the headaches they gave me, I really couldn't have gotten through this without you.

Vita

Education

M.S., Biochemistry, Molecular and Structural Biology — April 2020
University of California, Los Angeles

B.S., Biochemistry and Molecular Biology — April 2018
Otterbein University

Research Experience

Graduate Student Researcher — January 2018 – June 2024
Laboratory of Dr. Margot E. Quinlan
Department of Chemistry and Biochemistry
University of California, Los Angeles

Undergraduate Researcher — September 2014 – April 2018
Laboratory of Dr. John T. Tansey
Department of Chemistry
Otterbein University

Publications

Bailey, HM, Cullimore P, Bailey, LA, Quinlan, ME. Flexible geometry of *Drosophila* formin Cappuccino in actin mesh formation. *Manuscript in preparation*

Ong, JO, Bailey, HM, Panzica, M, Carley, E, Rixen, M, Quinlan, ME. Do Spir and MyosinV interact in *Drosophila* oogenesis? *Manuscript in preparation*

Bradley, AO, Vizcarra, CL, Bailey, HM, Quinlan, ME. Spire stimulates nucleation by Cappuccino and binds both ends of actin filaments. MBoC. 2020 Feb 13; doi: 10.1091/mbc.E19-09-0550

Abstracts and Speaking Engagements

Bailey, HM, What the mesh do? An investigation of Spire and Cappuccino in *Drosophila* oogenesis. Technical talk, Dissertation Seminar. UCLA, Los Angeles, CA, 2024

Bailey, HM, Alternate roles for the actin formin Cappuccino during Drosophila oogenesis. Poster, The Allied Genetics Conference 2024, Metro Washington, DC, 2024

Bailey, HM, Behind the Science Stories. Workshop moderator, The Allied Genetics Conference 2024, Metro Washington, DC, 2024

Bailey, HM, Investigating the actin mesh in the Drosophila oocyte. Technical Talk, gBSA Summer Seminar Series, UCLA, Los Angeles CA, 2023

Bailey, HM, Multiple roles for the actin mesh in oocytes? Poster, 64th Annual Drosophila Research Conference, Chicago, Illinois, 2023

Bailey, HM, AID-ing our understanding of the Drosophila actin mesh. Poster, Cell Biology ASCB 2022 Annual Meeting, Washington, DC, 2022

Bailey, HM, Developing tools to study the actin mesh during Drosophila oogenesis. Poster, 63rd Annual Drosophila Research Conference, San Diego, CA, 2022

Bailey, HM, Developing tools to study the actin mesh during Drosophila oogenesis. Poster, Cell Biology ASCB 2021 Virtual Annual Meeting, Online, 2021

Awards
Summer Mentored Research Fellowship (2021)
Cellular and Molecular Biology Training Grant (2020-2021)
UCLA Chemistry and Biochemistry Excellence in Research Fellowship (2020)
Edwin W. Pauley Fellowship (2019)

Mentorship
Peter Cullimore — Summer 2023
Graduate student in Cell and Developmental Biology

Jiayuan Sun — November 2019 – June 2022
Undergraduate student in Chemistry and Biochemistry

Merin Rixen — Winter 2022
Graduate student in Biochemistry, Molecular and Structural Biology

Nikki Cheung — Fall 2021
Graduate student in Biochemistry, Biophysics, and Structural Biology

Michael Martinyak — September 2020 – November 2021
Undergraduate student in Molecular, Cell and Developmental Biology.

Sophia Yu — September 2020 – June 2021
Undergraduate student in Pre-Human Biology and Society

Bryan Christian — Winter 2020
Graduate student in Biochemistry, Molecular and Structural Biology

Teaching
TA – CHEM 153A (Biochemistry Lecture) — Fall 2023
TA – CHEM 156 (Physical Biochemistry) — Spring 2019
TA – CHEM 153L (Biochemistry Lab) — Winter 2018

Service
Scientific Pen Pal — 2022-2024
Letters to a Pre-Scientist

Organizing Chair — 2021-2022
gBSA Summer Seminar Series Committee at UCLA

Chapter 1: Introduction

Oogenesis, the development of the oocyte, is critical to egg production in all organisms. This process includes the synthesis and accumulation of RNAs and proteins. This accumulation is essential for oocyte maturation and further development to a viable embryo post fertilization (Yamaguchi and Yoshida, 2018). Networks of filamentous actin are involved in the spatiotemporal regulation of these mRNAs and proteins. Understanding how these actin structures are regulated lends to a greater understanding of oogenesis and guides studies of complex actin networks in other systems.

Drosophila melanogaster is a powerful model organism to study oogenesis

Drosophila melanogaster is a widely utilized model organism for studying development, neuroscience, and other biological processes. As one of the first organisms used for genetic analysis, their relatively short lifecycle and low cost of maintenance has made them powerful tools in the laboratory for over the past 100 years. A single mating pair may produce hundreds of offspring in under two weeks (McLaughlin and Bratu, 2015), thus facilitating the ability to collect large datasets in small periods of time. In addition, the genome and heredity of these organisms is highly characterized making it possible to methodically study genes of interest (Adams, 2000).

Robust tools for genetic manipulation exist for *Drosophila*. Classical, unbiased mutagenic approaches include chemical mutagens such as ethyl methanesulfonate (Ohnishi, 1977). This produces random DNA mutations throughout the genome, characterized as alleles, and have uncovered genes essential for proper oogenesis. Targeted modification includes taking advantage of transposable elements for gene exchange and site-specific integration through introduction of landing sites in the genome. Specific transposon recognition sites within the genome facilitate mutation, insertion, removal, and tagging of genes (Venken et al., 2011). Advances in CRISPR/Cas9 mediated genome editing has allowed for insertion, deletion, or modification of conceivably any site within the genome (Bier et al., 2018; Kanca et al., 2019; Li-

Kroeger et al., 2018). Utilizing these tools, transgenic organisms can be produced efficiently and implemented in studying genes involved in oogenesis to determine function.

Drosophila Oogenesis

Drosophila oogenesis can be broken into fourteen stages of egg development based on changes to cell morphology (King, 1970; Quinlan, 2016) (Figure 1-1). The egg chamber is a syncytium as a result of incomplete cytokinesis, consisting of 1 oocyte and 15 nurse cells, connected by ring canals. A layer of follicle cells surround the egg chamber and later a subset will become the eggshell (Wu et al., 2008). The oocyte is transcriptionally inactive, receiving a majority of the required RNAs and proteins for development from the nurse cells via ring canals. The localization of mRNAs, such as gurken (grk), bicoid (bcd), oskar (osk), and nanos (nos) is essential for the establishment of the anteroposterior (AP) and dorsoventral (DV) axes of the embryo and is initiated during mid-oogenesis (Becalska and Gavis, 2009; Little et al., 2015; Rongo et al., 1995).

Mid-oogenesis (stages 7-10A) is characterized by slow streaming and the persistence of an isotropic actin mesh throughout the oocyte. During this timeframe, establishment of the body axes begin, with the localization of *osk* at the posterior pole (Figure 1-1). Slow streaming is a seemingly random pattern of cytoplasmic flows (~25nm/s). This flow is driven by kinesin-1 bound cargo walking along microtubules throughout the oocyte (Ganguly et al., 2012; Palacios, 2002; Serbus, 2005) (Figure 1-2) and microtubule sliding (Lu et al., 2016). An isotropic actin mesh suppresses the kinesin movement and streaming speeds, maintaining the polarized arrangement of microtubules and allowing for directed transport of polarity factors (Dahlgaard et al., 2007). Similar meshworks have been identified in oocytes of other organisms including mouse (Azoury et al., 2008), starfish (Mori et al., 2011), and *C. elegans* (Panzica et al., 2017). Currently, how these critical actin meshworks are maintained and regulated is not understood.

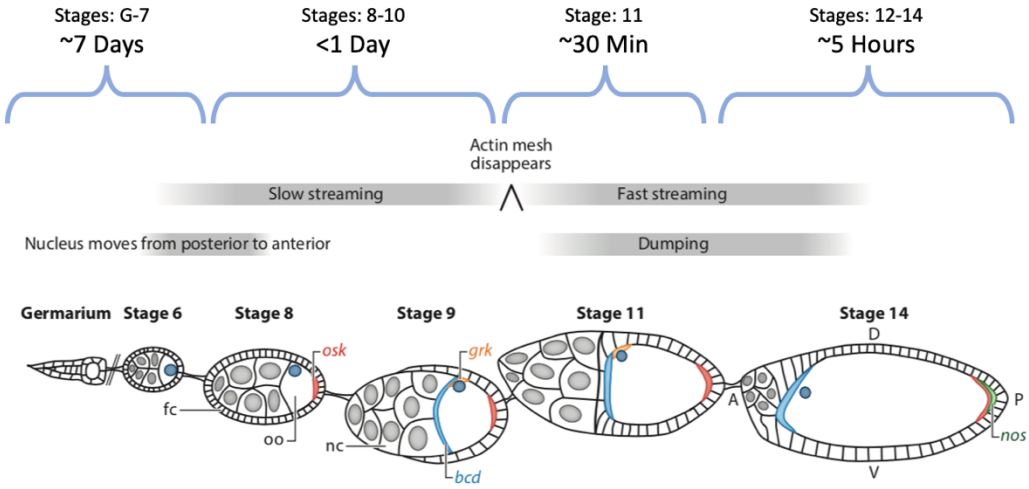

Figure 1-1: An Overview of Drosophila melanogaster oogenesis.

Each egg chamber is comprised of 1 oocyte (oo) and 15 nurse cells (nc), surrounded by ~1,000 follicle cells (fc). Proper localization via anchoring of mRNA polarity factors, osk, grk, bcd, and nos is linked to specific developmental stages. The approximate timeline of oogenesis (brackets) as described in Shimada, et al., 2011 (Shimada et al., 2011). Figure adapted from Quinlan, 2016 (Quinlan, 2016). Abbreviations: A, anterior; bcd, bicoid mRNA; D, dorsal; fc, follicle cells; grk, gurken mRNA; nc, nurse cells; nos, nanos mRNA; oo, oocyte; osk, oskar mRNA; P, posterior; V, ventral.

In late oogenesis (stages 10B-14) fast streaming begins with the disappearance of the actin mesh (Figure 1-2) and microtubule reorganization (Quinlan, 2016). Shortly thereafter, comes nurse cell dumping, during which the nurse cell contents are deposited in the oocyte. Following dumping, the nurse cells degenerate, resulting in a mature egg which can be fertilized.

Fast streaming is a highly coordinated process, and is conserved in a wide range of species including *C. elegans* (McNally et al., 2010) and *Arabidopsis* (Tominaga and Ito, 2015). During *Drosophila* oogenesis it is characterized by an approximate ten-fold increase in streaming rate (~300nm/s) (Quinlan, 2016). The timing of this increase is crucial for development as premature onset or inhibition of fast streaming leads to eggs that fail to develop (Quinlan, 2016; Theurkauf, 1994). This process has been linked to the continual asymmetric distribution of mRNAs and proteins in the oocyte as the nurse cells dump their contents (Becalska and Gavis, 2009). The molecular mechanism controlling the transition from slow to fast streaming remains unclear, due to the inability to directly observe the progression from mid

to late oogenesis. Critical components identified thus far include molecular motors (Ganguly et al., 2012; Lu et al., 2016; Palacios, 2002; Serbus, 2005) and the regulation of cytoskeletal elements including microtubules (Theurkauf, 1994; Theurkauf et al., 1992) and actin (Dahlgaard et al., 2007). Defects in any of these aspects of oogenesis can prevent oocytes from polarizing correctly and lead to female sterility (Manseau and Schupbach, 1989).

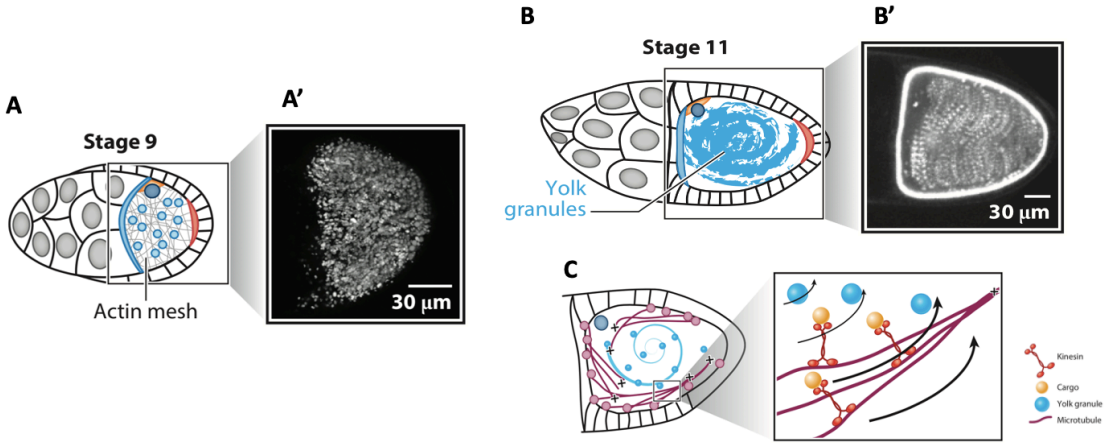

Figure 1-2 Streaming During Oogenesis (Quinlan, 2016).

A. An isotropic actin mesh fills the oocyte from stages 7-9, thus restricting yolk granule motion (A'). B. Stage 11 the actin mesh disappears, and streaming begins, yolk granules flow throughout the oocyte (B') C. Depiction of Streaming. Kinesin-1 bound cargoes migrate along microtubules surrounding the cortex of the stage 11 oocyte, this migration generates a fluid flow that propels yolk granules.

Role of Actin and Actin Binding Proteins in Oogenesis

Actin filaments play numerous roles within oogenesis as they make up the ring canals that connect the nurse cells (Hudson and Cooley, 2010; Tilney et al., 1996), line the cortex of the oocyte to anchor polarity factors (Chang et al., 2011; Tanaka et al., 2011), and form the isotropic actin mesh that fills the oocyte during mid-oogenesis (Dahlgaard et al., 2007). The mesh is a transient structure, existing during only stages 5 and 10A of oogenesis. The temporal regulation of the actin mesh is crucial for proper polarity establishment, as the mesh suppresses kinesin driven streaming, maintaining the polarized arrangement of microtubules required to get proper posterior delivery of mRNAs (Dahlgaard et al., 2007; Drechsler et al., 2019).

First characterized by Dahlgaard et al in 2007, the actin mesh requires the actin nucleators Spire (Spir) and Cappuccino (Capu) for its assembly (Dahlgaard et al., 2007). These nucleators, along with several other proteins have been linked to the formation of posterior filamentous actin as well (Tanaka et al., 2011). Capu, a member of the formin-family of actin nucleators (Quinlan et al., 2005), has been linked to control of the timing of cytoplasmic streaming (Bor et al., 2015; Dahlgaard et al., 2007; Quinlan, 2013). An increase in Capu expression has also been linked to an increase in mesh density, negatively affecting fertility by preventing the onset of fast streaming (Bor et al., 2015; Dahlgaard et al., 2007; Quinlan, 2013). Spir, a member of the WH2 class of actin nucleators (Quinlan et al., 2005), is also required to assemble the mesh but is not sufficient for mesh assembly in the absence of Capu (Dahlgaard et al., 2007). In the absence of Capu the actin mesh is not present and premature fast streaming occurs (Dahlgaard et al., 2007; Quinlan, 2016). Therefore, Spir and Capu are thought to work together to assemble the actin mesh within the developing oocyte (Dahlgaard et al., 2007). The mechanism by which the mesh is removed remains unclear, but the timing and expression levels of Spir and Capu have been found to alter the process (Dahlgaard et al., 2007; Quinlan, 2013). Mutations in these proteins results in dorsoventral defects, as posterior polarity factors do not properly localize (Bor et al., 2015; Quinlan, 2016).

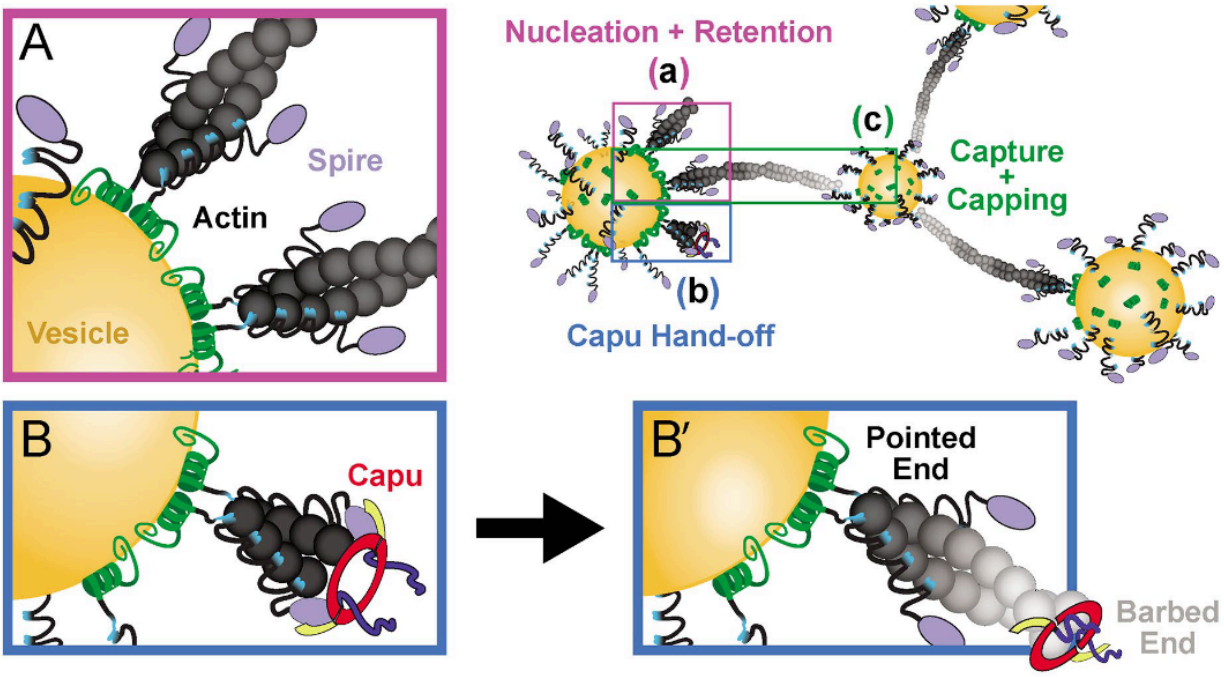

Figure 1-3: Proposed interactions of Capu and Spir utilized in forming actin networks in vivo (Bradley et al., 2019).

Spir is found to localize to vesicles where it can (a) nucleate actin filaments, (b) nucleate filaments and hand-off to Capu for elongation of the filament and (c) bind to the barbed end of filaments to capture and cap growth of the filament. These interactions provide a model as to how the actin mesh is produced.

Not only are Spir and Capu in the same pathway, but they also directly interact to synergistically assemble actin filaments (Bradley et al., 2019; Montaville et al., 2014; Quinlan, 2013). Proper regulation of this interaction is required, as separation of Capu from Spir is just as important as their association (Quinlan, 2013). Mechanisms describing this interaction include the hand-off model (Quinlan, 2013), and the ping-pong model (Montaville et al., 2014) - both leading to coordinated actin growth. The protein domain of Spir reveals an mFYVE domain, which leads to its localization to membranes (Tittel et al., 2015; Vizcarra et al., 2011). Within mouse oocytes, Spir localizes to vesicles (Pylypenko et al., 2016a; Schuh and Ellenberg, 2008), and unpublished super-resolution microscopy from the Quinlan lab supports this localization within *Drosophila* oocytes. Based on these data, models from bead-based assays of Spir and Capu localization effectively predict dynamics within the oocyte (Bradley et al., 2019). Spir is

found on vesicles, where clustering of Spir results in an enhanced affinity for the pointed end of actin filaments and bind to actin to form nuclei (Figure 1-3A). On the vesicle, Spir retains the pointed end of the filament and Capu separates from Spir to elongate the filament (Figure 1-3B). The vesicles within the oocyte may be connected due to filament capture of another Spir-containing vesicle (Figure 1-3C) (Bradley et al., 2019) thusly building an actin meshwork. Capu localization has been found to vary based on function of the overall actin network. In melanocytes, mammalian homolog, FMN1, is released from Spir positive vesicles to disperse melanosomes (Alzahofi et al., 2020). Conversely, in the mouse oocyte, FMN2 is retained on vesicles leading to the actin network exhibiting a pushing force to centrally position the mitotic spindle during metaphase (Almonacid and Verlhac, 2021; Schuh and Ellenberg, 2008). This established an intriguing line of investigation to determine Capu's localization in the developing *Drosophila* oocyte that could lead to a greater understanding of the function of the actin mesh.

Little else is known about the requirement of other actin binding proteins to build and recycle this mesh and if they directly interact with Spir and Capu. A few potential interaction partners and regulators include actin crosslinkers, actin/MT crosslinkers, molecular motors, and proteins involved in actin filament depolymerization and severing. Identification of these interaction partners is not exclusive for our understanding of the *Drosophila* actin mesh. Thus far, the proteins identified in the *Drosophila* oocyte mesh have also been found to be conserved in mouse oocytes. Therefore, knowing other interaction partners can lead to a greater understanding of complex actin networks in other systems.

Obstacles to Studying Oogenesis

A standard method used to study oogenesis is to excise the ovaries (Gutzeit and Koppa, 1982), tease apart egg chambers, and image them using confocal microscopy. While this method has yielded numerous discoveries and further understanding of development, it cannot be used to study the transition from stage 10 to 11, when the actin mesh dissipates, and fast

streaming begins. Despite efforts since the 1980s (Gutzeit and Koppa, 1982), the transition from slow to fast streaming has not been visualized. Dissected egg chambers will progress to stage 10A in development but will arrest at that stage. The failure to progress past stage 10A is likely due to maternal factors found within the fly. *Ex vivo* egg chambers are only viable for 1-5 hours, thus leading to challenges studying key transitionary stages during oogenesis. Therefore, the onset and regulation of streaming cannot be studied using extracted ovaries. With the development of new imaging methods of the *Drosophila* abdominal imaging, progress has been made to characterize these processes (Balachandra and Amodeo, 2024; Koyama et al., 2020; Martin et al., 2018). At this time the onset of late oogenesis and fast streaming remains undescribed.

Along with limitations to imaging, studying the specific role of actin binding proteins in mesh maintenance and regulation has remained troublesome. This is due to the pivotal role that these proteins play in prior stages of oogenesis. Deleterious alterations to these genes early on can halt oogenesis prior to mesh formation. Therefore, finer temporal regulation of candidate proteins, including Spir and Capu, is advantageous to study their role in specifically regulating the actin mesh during mid oogenesis.

Overview of the dissertation

To address the limitations in studying *Drosophila* oogenesis we set out to improve temporal regulation of Spir and Capu in the egg chamber and made advances to develop endogenously tagged *Drosophila* lines for Spir and Capu (**Chapter 2**). This work made it possible to study the influence localization of Capu has on oogenesis (**Chapter 3**) by rescuing *capu* null oocytes via expression of a membrane bound Capu isoform.

As a major question in the lab remains to understand the composition and regulation of the *Drosophila* actin mesh during oogenesis we made progress in screening for mesh components in a targeted manner. Firstly, Spir's interaction with MyosinV was evaluated

(**Chapter 4**), and from this work we were inspired to screen Rab candidates using readily available *Drosophila* stocks (**Chapter 5**). Other mesh components were screened from a list of proposed interaction partners and regulators including crosslinkers, molecular motors, and actin filament regulators. As attempts to use temporal regulation via induced degradation were unsuccessful (**Appendix III**), RNAi was utilized for initial screening (**Chapter 6**).

Lastly, development and optimization of both new and existing protocols for working with *Drosophila* have been established. Progress was made towards developing Long Term Live Imaging (**Chapter 7**) in hopes of characterizing the mid- to late-oogenesis transition. As a reference, current standing workflows for genome editing of Spir and Capu in *Drosophila* (**Appendix I**) and primary antibody staining conditions optimized (**Appendix II**) are reported here.

References

Adams, M. D. (2000). The Genome Sequence of Drosophila melanogaster. *Science* 287, 2185–2195.

Almonacid, M. and Verlhac, M.-H. (2021). A new mode of mechano-transduction shakes the oocyte nucleus, thereby fine tunes gene expression modulating the developmental potential. *C. R. Biol.* 343, 223–234.

Alzahofi, N., Welz, T., Robinson, C. L., Page, E. L., Briggs, D. A., Stainthorp, A. K., Reekes, J., Elbe, D. A., Straub, F., Kallemeijn, W. W., et al. (2020). Rab27a co-ordinates actin-dependent transport by controlling organelle-associated motors and track assembly proteins. *Nat. Commun.* 11, 3495.

Azoury, J., Lee, K. W., Georget, V., Rassinier, P., Leader, B. and Verlhac, M.-H. (2008). Spindle Positioning in Mouse Oocytes Relies on a Dynamic Meshwork of Actin Filaments. *Curr. Biol.* 18, 1514–1519.

Balachandra, S. and Amodeo, A. A. (2024). Bellymount-Pulsed Tracking: A Novel Approach for Real-Time In vivo Imaging of Drosophila Oogenesis. 2024.03.31.587498.

Becalska, A. N. and Gavis, E. R. (2009). Lighting up mRNA localization in Drosophila oogenesis. *Development* 136, 2493–2503.

Bier, E., Harrison, M. M., O'Connor-Giles, K. M. and Wildonger, J. (2018). Advances in Engineering the Fly Genome with the CRISPR-Cas System. *Genetics* 208, 1–18.

Bor, B., Bois, J. S. and Quinlan, M. E. (2015). Regulation of the formin cappuccino is critical for polarity of *D rosophila* oocytes: Capu is Autoinhibited In Vivo. *Cytoskeleton* 72, 1–15.

Bradley, A. O., Vizcarra, C. L., Bailey, H. M. and Quinlan, M. E. (2019). Spire stimulates nucleation by Cappuccino and binds both ends of actin filaments. *Mol. Biol. Cell* 31, mbc.E19-09-0550.

Chang, C.-W., Nashchekin, D., Wheatley, L., Irion, U., Dahlgaard, K., Montague, T. G., Hall, J. and St. Johnston, D. (2011). Anterior–Posterior Axis Specification in *Drosophila* Oocytes: Identification of Novel *bicoid* and *oskar* mRNA Localization Factors. *Genetics* 188, 883–896.

Dahlgaard, K., Raposo, A. A. S. F., Niccoli, T. and St Johnston, D. (2007). Capu and Spire Assemble a Cytoplasmic Actin Mesh that Maintains Microtubule Organization in the Drosophila Oocyte. *Dev. Cell* 13, 539–553.

Drechsler, M., Lang, L. F., Al-Khatib, L., Dirks, H., Burger, M., Schönlieb, C.-B. and Palacios, I. M. (2019). *Optical flow analysis reveals that Kinesin-mediated advection impacts on the orientation of microtubules in the* Drosophila *oocyte*. Cell Biology.

Ganguly, S., Williams, L. S., Palacios, I. M. and Goldstein, R. E. (2012). Cytoplasmic streaming in Drosophila oocytes varies with kinesin activity and correlates with the microtubule cytoskeleton architecture. *Proc. Natl. Acad. Sci.* 109, 15109–15114.

Gutzeit, H. and Koppa, R. (1982). Time-lapse film analysis of cytoplasmic streaming during late oogenesis of Drosophila. *J. Embryol. exp. Morph* 67, 101–111.

Hudson, A. M. and Cooley, L. (2010). *Drosophila* Kelch functions with Cullin-3 to organize the ring canal actin cytoskeleton. *J. Cell Biol.* 188, 29–37.

Kanca, O., Zirin, J., Garcia-Marques, J., Knight, S. M., Yang-Zhou, D., Amador, G., Chung, H., Zuo, Z., Ma, L., He, Y., et al. (2019). An efficient CRISPR-based strategy to insert small and large fragments of DNA using short homology arms. *eLife* 8, e51539.

King, R. C. (1970). *Ovarian development in Drosophila melanogaster*. Academic Press.

Koyama, L. A. J., Aranda-Diaz, A., Su, Y.-H., Balachandra, S., Martin, J., Ludington, W., Huang, K. C. and O'Brien, L. E. (2020). Bellymount enables longitudinal, intravital imaging of abdominal organs and the gut microbiota in adult Drosophila. *PLOS Biol.* 19.

Li-Kroeger, D., Kanca, O., Lee, P.-T., Cowan, S., Lee, M. T., Jaiswal, M., Salazar, J. L., He, Y., Zuo, Z. and Bellen, H. J. (2018). An expanded toolkit for gene tagging based on MiMIC and scarless CRISPR tagging in Drosophila. *eLife* 7, 27.

Little, S. C., Sinsimer, K. S., Lee, J. J., Wieschaus, E. F. and Gavis, E. R. (2015). Independent and coordinate trafficking of single Drosophila germ plasm mRNAs. *Nat. Cell Biol.* 17, 558–568.

Lu, W., Winding, M., Lakonishok, M., Wildonger, J. and Gelfand, V. I. (2016). Microtubule–microtubule sliding by kinesin-1 is essential for normal cytoplasmic streaming in *Drosophila* oocytes. *Proc. Natl. Acad. Sci.* 113, E4995–E5004.

Manseau, L. J. and Schupbach, T. (1989). cappuccino and spire: two unique maternal-effect loci required for both the anteroposterior and dorsoventral patterns of the Drosophila embryo. *Genes Dev.* 3, 1437–1452.

Martin, J. L., Sanders, E. N., Moreno-Roman, P., Jaramillo Koyama, L. A., Balachandra, S., Du, X. and O'Brien, L. E. (2018). Long-term live imaging of the Drosophila adult midgut reveals real-time dynamics of division, differentiation and loss. *eLife* 7,.

McLaughlin, J. M. and Bratu, D. P. (2015). Drosophila melanogaster Oogenesis: An Overview. In *Drosophila Oogenesis* (ed. Bratu, D. P.) and McNeil, G. P.), pp. 1–20. New York, NY: Springer New York.

McNally, K. L., Martin, J. L., Ellefson, M. and McNally, F. J. (2010). Kinesin-dependent transport results in polarized migration of the nucleus in oocytes and inward movement of yolk granules in meiotic embryos. *Dev. Biol.* 339, 126–140.

Montaville, P., Jégou, A., Pernier, J., Compper, C., Guichard, B., Mogessie, B., Schuh, M., Romet-Lemonne, G. and Carlier, M.-F. (2014). Spire and Formin 2 Synergize and Antagonize in Regulating Actin Assembly in Meiosis by a Ping-Pong Mechanism. *PLoS Biol.* 12, e1001795.

Mori, M., Monnier, N., Daigle, N., Bathe, M., Ellenberg, J. and Lénárt, P. (2011). Intracellular Transport by an Anchored Homogeneously Contracting F-Actin Meshwork. *Curr. Biol.* 21, 606–611.

Ohnishi, O. (1977). Spontaneous and Ethyl Methaneslfonate-induced mutations controlling viability in Drosophila Melanogaster. 1. Recessive Lethal Mutations. *Genetics* 87, 519–527.

Palacios, I. M. (2002). Kinesin light chain-independent function of the Kinesin heavy chain in cytoplasmic streaming and posterior localisation in the Drosophila oocyte. *Development* 129, 5473–5485.

Panzica, M. T., Marin, H. C., Reymann, A.-C. and McNally, F. J. (2017). F-actin prevents interaction between sperm DNA and the oocyte meiotic spindle in C. elegans. *J. Cell Biol.* 216, 2273–2282.

Pylypenko, O., Welz, T., Tittel, J., Kollmar, M., Chardon, F., Malherbe, G., Weiss, S., Michel, C. I. L., Samol-Wolf, A., Grasskamp, A. T., et al. (2016). Coordinated recruitment of Spir actin nucleators and myosin V motors to Rab11 vesicle membranes. *eLife* 5,.

Quinlan, M. E. (2013). Direct interaction between two actin nucleators is required in Drosophila oogenesis. *Development* 140, 4417–4425.

Quinlan, M. E. (2016). Cytoplasmic Streaming in the *Drosophila* Oocyte. *Annu. Rev. Cell Dev. Biol.* 32, 173–195.

Quinlan, M. E., Heuser, J. E., Kerkhoff, E. and Dyche Mullins, R. (2005). Drosophila Spire is an actin nucleation factor. *Nature* 433, 382–388.

Rongo, C., Gavis, E. R. and Lehmann, R. (1995). Localization of oskar RNA regulates oskar translation and requires Oskar protein. *Development* 121, 2737–2746.

Schuh, M. and Ellenberg, J. (2008). A New Model for Asymmetric Spindle Positioning in Mouse Oocytes. *Curr. Biol.* 18, 1986–1992.

Serbus, L. R. (2005). Dynein and the actin cytoskeleton control kinesin-driven cytoplasmic streaming in Drosophila oocytes. *Development* 132, 3743–3752.

Shimada, Y., Burn, K. M., Niwa, R. and Cooley, L. (2011). Reversible response of protein localization and microtubule organization to nutrient stress during Drosophila early oogenesis. *Dev. Biol.* 355, 250–262.

Tanaka, T., Kato, Y., Matsuda, K., Hanyu-Nakamura, K. and Nakamura, A. (2011). Drosophila Mon2 couples Oskar-induced endocytosis with actin remodeling for cortical anchorage of the germ plasm. *Development* 138, 2523–2532.

Theurkauf, W. (1994). Premature microtubule-dependent cytoplasmic streaming in cappuccino and spire mutant oocytes. *Science* 265, 2093–2096.

Theurkauf, W. E., Smiley, S., Wong, M. L. and Alberts, B. M. (1992). Reorganization of the cytoskeleton during Drosophila oogenesis: implications for axis specification and intercellular transport. *Development* 115, 923–936.

Tilney, L. G., Tilney, M. S. and Guild, G. M. (1996). Formation of actin filament bundles in the ring canals of developing Drosophila follicles. *J. Cell Biol.* 133, 61–74.

Tittel, J., Welz, T., Czogalla, A., Dietrich, S., Samol-Wolf, A., Schulte, M., Schwille, P., Weidemann, T. and Kerkhoff, E. (2015). Membrane Targeting of the Spir·Formin Actin Nucleator Complex Requires a Sequential Handshake of Polar Interactions. *J. Biol. Chem.* 290, 6428–6444.

Tominaga, M. and Ito, K. (2015). The molecular mechanism and physiological role of cytoplasmic streaming. *Curr. Opin. Plant Biol.* 27, 104–110.

Venken, K. J. T., Schulze, K. L., Haelterman, N. A., Pan, H., He, Y., Evans-Holm, M., Carlson, J. W., Levis, R. W., Spradling, A. C., Hoskins, R. A., et al. (2011). MiMIC: a highly versatile transposon insertion resource for engineering Drosophila melanogaster genes. *Nat. Methods* 8, 737–743.

Vizcarra, C. L., Kreutz, B., Rodal, A. A., Toms, A. V., Lu, J., Zheng, W., Quinlan, M. E. and Eck, M. J. (2011). Structure and function of the interacting domains of Spire and Fmn-family formins. *Proc. Natl. Acad. Sci. U. S. A.* 108, 11884–11889.

Wu, X., Tanwar, P. S. and Raftery, L. A. (2008). Drosophila follicle cells: Morphogenesis in an eggshell. *Semin. Cell Dev. Biol.* 19, 271–282.

Yamaguchi, M. and Yoshida, H. (2018). Drosophila as a Model Organism. In *Drosophila Models for Human Diseases* (ed. Yamaguchi, M.), pp. 1–10. Singapore: Springer Singapore.

Chapter 2: Building tools to improve study of Spir and Capu in the *Drosophila* egg chamber

Introduction

Drosophila melanogaster have a vast genetic toolkit for investigating protein function. A commonly used system is that of GAL4/UAS which expresses two transgenes (Brand and Perrimon, 1993, Figure 2-1A): the 'driver' Gal4 – a sequence specific transactivator that binds the second transgene. The first Gal4 driver lines were generated via random insertion in the *Drosophila* genome. Expression of the Gal4 is driven by the genomic enhancer in which the Gal4 was inserted. The 'transgene' expression vector comprises multiple upstreaming activating sequences (UAS) and cDNA from any gene of interest for expression. Gal4 binds the UAS, inducing expression of the gene of study (Brand and Perrimon, 1993). Modifications and improvements have been made to this system, allowing for expression in the female germline (Rørth, 1998) and targeted insertion of Gal4 within the *Drosophila* genome, allowing for generation of gene-specific drivers (Diao et al., 2015; Venken et al., 2011).

Capu and Spir are maternally expressed proteins and null expressing females are sterile (Manseau and Schupbach, 1989). *In-situ* hybridization reveals *spir* and *capu* expression to be highest from early oogenesis to mid-oogenesis (Emmons et al., 1995; Wellington et al., 1999). Functional and expression data indicate that Spir and Capu must go away during late oogenesis to permit fast streaming (Dahlgaard et al., 2007; Quinlan, 2013). Transgenes have been used to further characterize the functional role of Spir and Capu in oogenesis. As the expression of Spir and Capu are in the germline, the Gal4 drivers utilized have been predominately *maternal alpha tubulin*-Gal4 (*mat*α-Gal4) and *nanos*-Gal4 (*nos*-Gal4) (Dahlgaard et al., 2007; Quinlan, 2013), or a combination, known as the triple maternal driver (containing: *pCOG*-Gal4, *NGT40*-Gal4, and *nos*-Gal4) (Rosales-Nieves et al., 2006). Nanos, like Spir and Capu, is a member of the posterior class genes as its loss disrupts abdominal segmentation in the embryo (Manseau and Schupbach, 1989). *nanos* is highly expressed during early oogenesis, decreased during mid-oogenesis, and re-expressed during late oogenesis (Wang et al., 1994). *mat*α-Gal4 is linked to

αTub67c, an ovary and embryo specific tubulin gene that is highly expressed during oogenesis (Kalfayan and Wensink, 1982). Therefore, *nos*-Gal4 and *mat*α-Gal4 exhibit different expression patterns during oogenesis than *spir/capu* (Figure 2-1B). Bulk read out of oogenesis via fertility assay reveals an imperfect rescue with *nos*-Gal4 (Figure 2-1C) and *mat*α-Gal4 rescue (*data not shown*).

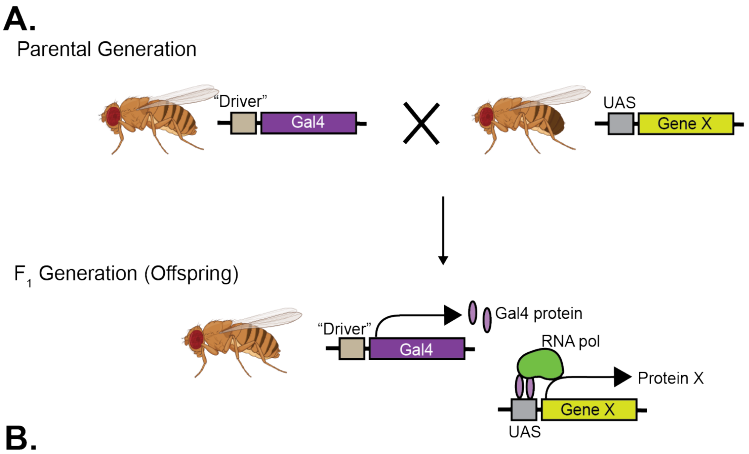

C.

Transgene* (capu[1])	% Hatched
nos > UASp::CapuA	56
nos > UASp::CapuA-GFP	36

Transgene* (spir[1]/Df(2L)Exel[6046])	% Hatched
nos > UASp::SpirB	48
nos > UASp::SpirB-GFP	59

*Quinlan, 2013

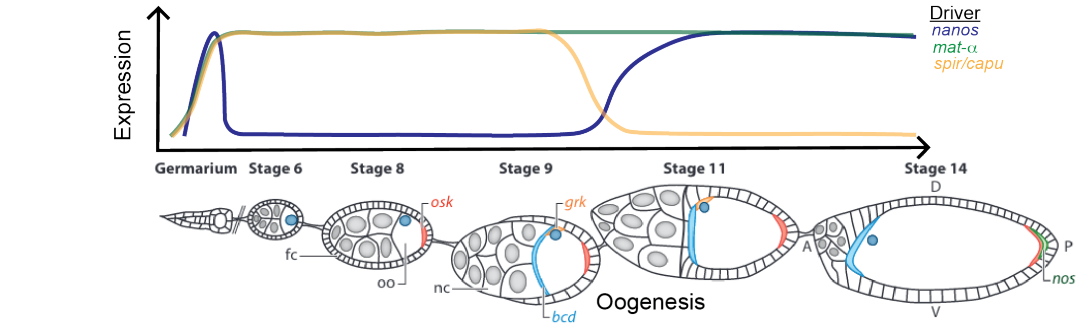

Figure 2-1: Transgene expression in Drosophila using the GAL4/UAS system.

(A.) Schematic of Gal4 expression and transactivation of UAS in Drosophila. Parental flies expressing Gal4 and UAS transgene are crossed to give rise to offspring that contain both components of the system. Expression of Gal4 activates the expression of the transgene of interest (Gene X) by binding the UAS to recruit RNA polymerase and initiate translation. (B.) Predicted expression pattern of commonly used drivers for germline cells in Drosophila oogenesis. Patterns are based on published data for nanos (Wang et al., 1994), maternalα-tubulin (αTub67c) (Kalfayan and Wensink, 1982), and spir/capu (Emmons et al., 1995; Quinlan, 2013; Wellington et al., 1999). Approximate expression levels are based off of reported modENCODE data for the ovary as reported on FlyBase (Brown et al., 2014). (C.) Bulk fertility data of transgene rescue of spir and capu null oocytes. Rescue data shown using nanos-Gal4-vp16 driver from (Quinlan, 2013).

Bulk fertility rates of rescue for *spir* and *capu* nulls, using the available Gal4 lines for germline expression, indicate room for improvement. This motivated the Quinlan lab to generate gene specific Gal4 lines for *spir* and *capu.* This work was largely carried out by Peter Bohall. The aim was with improved rescue characterization of weaker Spir and Capu mutants would be possible. Therefore, a modified Trojan-Gal4 design strategy was employed (Lee et al., 2018; Venken et al., 2011), inserting Gal4-K10 at the MI05737 (*capu*) or MI05646 (*spir*) landing sites (Figure 2-2A, B).

Rescue using *capu*-Gal4-K10 (*capu*-Gal4) was successful, improving fertility of Capu-GFP in bulk assay two-fold, from 36% (*nos*) to ~80% (*capu*) (Figure 2-2A'). The generated *spir*-Gal4-K10 did not rescue fertility (Figure 2-2B'). We hypothesize this is due to transcriptional regulation sites in close proximity to the selected MiMIC landing site (MI05646) resulting in excision of the Gal4. Therefore, we needed a new strategy to improve *spir* null rescue.

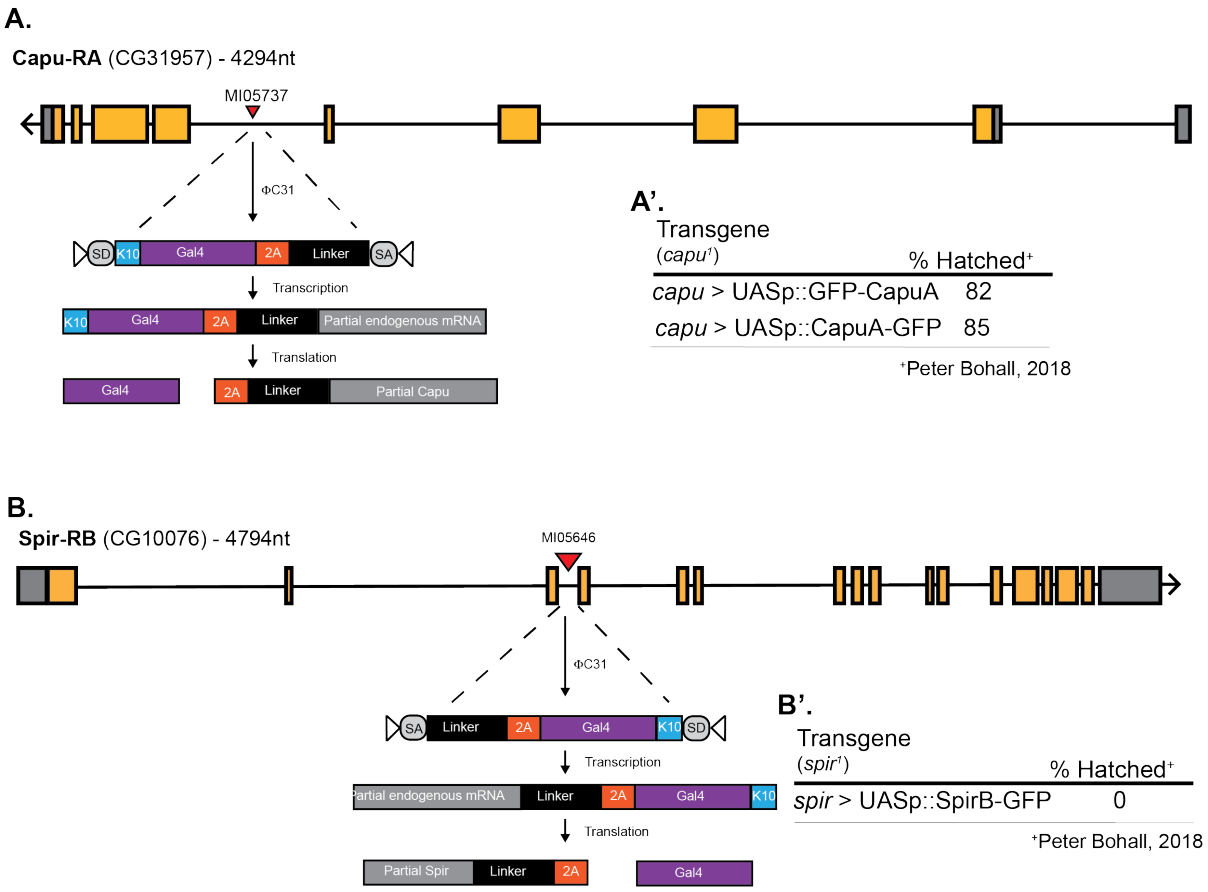

Figure 2-2: Generation of gene specific Gal4 drivers.

(A.) capu-Gal4-K10 generation. Overall insertion method shown in the diagram. The Gal4 expressing cassette was inserted in capu at MiMIC landing site MI05737. A': fertility data of rescue of capu null with Capu transgenes using this driver. Fertility is improved by two-fold in comparison with nos-Gal4, Peter Bohall, 2018 unpublished. (B.) spir-Gal4-K10 generation. Overall insertion method is identical to Capu. The Gal4 expressing cassette was inserted in spir at MiMIC landing site MI05646. The rescue of spir null oocytes using this driver is unsuccessful, Peter Bohall, 2018 unpublished.

Results

Rescuing spir null oocytes using the capu-Gal4 driver

As Spir and Capu have similar expression patterns in development and function to build the same actin mesh, we first asked if *spir* null oocytes can be rescued using the *capu*-Gal4 driver. As *spir* and *capu* are located on chromosome 2L, generation of a *spir* null background with *capu*-Gal4 required recombination. The recombination positions of *spir* (2-54) and *capu* (2-11) made success likely, and the following fly line was generated:

$$w^{+};\ \frac{spir^{KG00320},\ capu\text{-Gal4-K10}}{CyO}\ ;\ +$$

We first asked if fertility is rescued using the recombinant driver to express wildtype Spir transgenes (Figure 2-3A). We observed a hatch rate of 18%, indicating failed rescue of bulk fertility. The data are an improvement from *spir*-Gal4 (0%), but the rescue is still less than *nos*-Gal4 (48-59%) (Quinlan, 2013). Examination of the actin structures in SpirB rescue egg chambers revealed an abundance of actin production throughout oogenesis (Figure 2-3B, a'-a''') in comparison to wildtype (Figure 2-3B, b'-b'''). We observe a cytoplasmic actin mesh in the nurse cells and oocyte that persists throughout oogenesis. The presence of the actin in all germ cells and lack of loss of the actin mesh serves as an explanation of the failed rescue in bulk assay, as dumping and fast streaming does not occur properly in late oogenesis (Figure 2-3B, b'''). With these data in mind, we conclude that *capu*-Gal4 is too strong of a germline driver to properly rescue *spir* nulls - resulting in overexpression. We postulate that due to the autoinhibition domain in Capu, rescue and overexpression with Capu transgenes are less deleterious to oogenesis. Spir lacks such an autoinhibitory domain and therefore could be more sensitive to overactivity when overexpressed.

A.

Transgene ($spir^{KG00320}/spir^{1}$)	% Hatched
capu > UASp::SpirB-GFP	18
capu > UASp::GFP-CapuA	80

B.

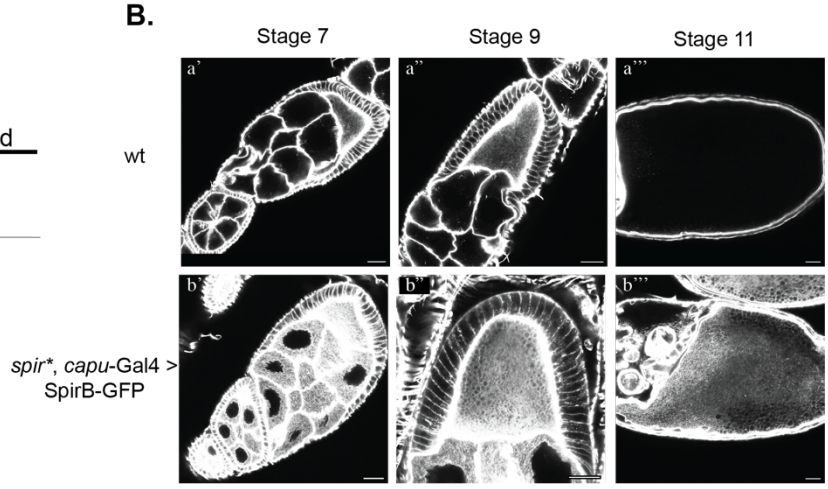

Figure 2-3: Transgene rescue of spir null oocytes with capu-Gal4.

(A.) Bulk fertility data of spir null rescue. CapuA rescues spir null to the same rate as capu nulls, around 80%. SpirB-GFP transgene rescue is slightly improved from the spir-Gal4 driver but overall fails to rescue fertility to the same rate as nos-Gal4 (Quinlan, 2013). (B.) Mesh staining of egg chambers of wildtype (a'-a''') and Spir transgene rescue (b'-b'''). Staining for actin in oocytes using AlexaFluor488 phalloidin (1uM, Invitrogen) allowed for observation of increased actin structures with SpirB-GFP rescue.

Therefore, to combat one potential cause of overexpression of transgenes (Gal4 stability), we sought out methods to decrease the half-life of the Gal4. To favor proteasomal degradation of Gal4 we selected to add an ornithine decarboxylase proline-glutamate-serine-threonine-rich (PEST) sequence, residues 422-461 of mouse ornithine decarboxylase, to the C-terminus of Gal4 (Nern et al., 2011). Addition of PEST to GFP has been shown to rapidly decrease protein half-life (Kitsera et al., 2007) and been used in *Drosophila* neuronal tissues to alter Gal4 activity (Nern et al., 2011), making addition of this motif a viable starting point. Following the same workflow as *capu*-Gal4, we generated flies expressing *capu*-Gal4-PEST-K10 (*capu*-Gal4-PEST, Figure 2-4A). This again rescued Capu transgenes (~80% fertility) but did not rescue Spir (Figure 2-4B). Consequently, we concluded that the current transgene tools available are insufficient to rescue *spir* null egg chambers and an entirely different approach was required.

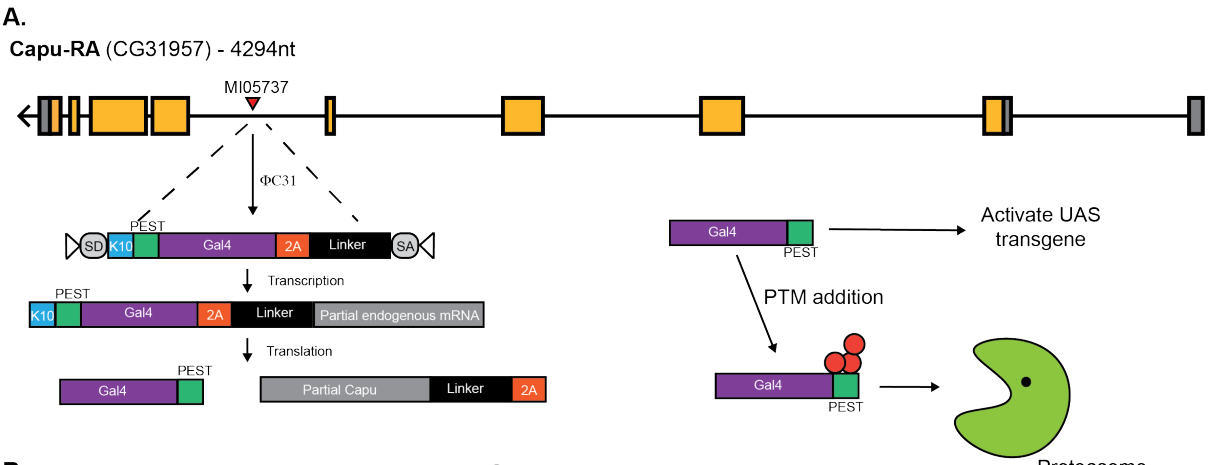

B.

Transgene (*capu*^{HK3})	% Hatched
capu-Gal4-PEST-K10	0

Transgene (*capu*^{1})	% Hatched
capu-PEST > GFP-CapuA	90
capu-PEST > CapuA-GFP	81

C.

Transgene (*spir*^{KG00320}/*spir*^{1})	% Hatched
capu-PEST > UASp::SpirB-GFP	19
capu-PEST > UASp::SpirB	10

Transgene (*spir*^{KG00320}/*capu*^{1})	% Hatched
capu-PEST > UASp::GFP-CapuA	87
capu-PEST > UASp::CapuA-GFP	84

Figure 2-4: Transgene rescue using capu-Gal4-PEST.

(A). Schematic of PEST insertion at MiMIC landing site MI05737. Gal4-PEST is expressed under the control of capu. The PEST sequence allows for posttranslational modifications to bind and target the Gal4 to the proteasome for degradation and therefore decreases the half-life of the Gal4. (B, C)Tables of fertility assays for rescue with capu-Gal4-PEST-K10. (B.) Capu rescues have a high rescue rate of fertility in bulk assays that is maintained with the recombinant with the spir mutant. (C.) Spir rescue with Capu-Gal4-PEST is a small improvement over Capu-Gal4 rescue, it is still worse than rescue with nos-Gal4.

Endogenous Tagging of Spir and Capu: CRISPR/Cas9 mediated HDR

As rescue of *spir* null backgrounds via transgenes remained unsuccessful, we turned to CRISPR/Cas9 mediated homology directed repair (HDR) to insert endogenous tags in the *spir* and *capu* loci. Advantages of genome editing include flexibility of insertion and labeling the gene of interest in all tissues and cell types (Sternberg et al., 2014).

Rapid advances have been made towards increasing efficiency of CRISPR/Cas9 mediated HDR in *Drosophila* (Bier et al., 2018; Kanca et al., 2019; Meltzer et al., 2019). Following established guidelines, we selected to edit the C-termini of Spir and Capu as transgene rescue was not hindered with C-terminal GFP addition (Bor et al., 2015; Quinlan,

2013). To amplify efficiency of immunolabeling we included spaghetti-monster fluorescent proteins (smFP) – fluorescent proteins containing modified loops to include multiple epitope tags (Nern et al., 2015), in our repair constructs. Concurrently, we generated lines containing the smFP and AID motif, in an attempt investigate the importance of temporal regulation of Spir and Capu in actin mesh maintenance.

The AID motif, a small 44 amino acid degradation system is part of the auxin-inducible degradation system, derived from plants. This system requires the degradation (AID) tag on the protein of interest, expression of TIR1 (a Skip-Cullin-Fbox Ubiquitin E3-ligase from *Oryza sativa*), and the plant hormone auxin. Upon treatment with auxin, cells will degrade >90% of the AID-tagged protein within 30 minutes (Nishimura et al., 2009). Auxin binds to TIR1, creating an active ubiquitin ligase complex which recognizes and ubiquitinates the AID tag. Following ubiquitination, the protein is targeted to the proteasome for degradation. Temporal and tissue-specific degradation occurs by regulating the expression of TIR1 and had been shown to work in the *Drosophila* ovary (Bence et al., 2017). Our attempts at using this system were unsuccessful and are explored further in **Appendix III**.

Overviews of editing (Figure 2-5A, B), guide RNAs (gRNA) selected (Figure 2-5C) and strategies for cloning (**Appendix I**) have been included for reference. Briefly, Spir editing utilized short flanking homology arms on the repair template (200nt) and a self-linearizable plasmid to increase efficiency of HDR (Kanca et al., 2019). Capu editing followed earlier CRISPR/Cas9-mediated HDR workflows, using large homology arms (850nt) and circular repair plasmids (Bence et al., 2017; Gratz et al., 2015). We employed a dual guide RNA strategy to induce double strand breaks proximal to the stop codon and terminal to the 3'UTR of our gene of interest, as we were looking to insert a large repair (~5kb) in the genome. This strategy has been demonstrated to improve efficiency of HDR of large inserts (>1kb) and work in the female germline (Bence et al., 2017).

We received multiple fly lines from BestGene that were positively identified to include the fluorescent eye reporter for each modification. To confirm desired genomic editing and expression, the following standard workflow was employed: genomic PCRs, fertility assays, western blotting, mesh staining, and immunofluorescence (IF) of the epitope tag. We report here characterization of the lines selected to use in further experimentation.

Genomic PCR (*data not shown*) verified insertion at the C-termini to generate Spir-smGFP-HA (Spir-HA) and Capu-smmRuby2-OLLAS (Capu-OLLAS). In bulk fertility assays we observed a great improvement of hatch rate for endogenously tagged Spir over wildtype transgene rescue. This finding is consistent for all C-terminal tags inserted using this workflow (Figure 2-5D). For Capu-OLLAS we determined the average fertility rate of homozygous females to be 4%, indicating failed rescue (Figure 2-5D). We identified expression of Spir-HA (Figure 2-5E') and Capu-OLLAS (Figure 2-5E") in western blots of whole ovary lysate from homozygous females (molecular weight range, 180-250kDa). In continuing our characterization, we determined sterility in homozygous Capu-OLLAS flies to be as a result of failure to form the actin mesh during (Figure 2-5F). Spir-HA are wildtype for mesh presence and removal (Figure 2-5F).

To complete our characterization, we wanted to determine if the localization pattern observed in our endogenously tagged egg chambers were similar to transgene rescue. Overall, we found that the expression level of both Spir and Capu is markedly lower than transgene rescue, as attempts to image fluorescence in live egg chambers was unsuccessful (*data not* shown). We report that the endogenous Spir-HA localization pattern matches transgenes, as we observe clear localization of Spir at the oocyte cortex and cytoplasm via IF (Figure 2-5G). We were surprised to also visualize Spir in somatic cells, specifically the migrating border cell cluster and anterior pole cells (Figure 2-5G'). Spir has not been previously reported to localize to these cell types and removal of Spir does not alter border cell migration. For Capu-OLLAS, we observed a similar localization pattern in IF to transgene rescue. As Capu-OLLAS homozygotes

are infertile, we elected to not work with these lines further and implemented an alternative tagging strategy.

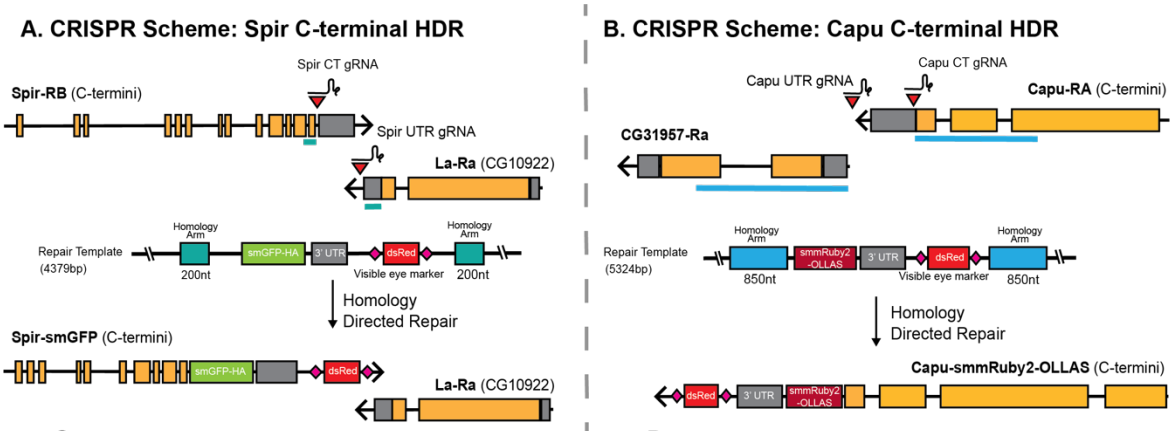

C.

Guide RNA	Target Strand	Protospacer Sequence (5' -> 3')
Spir-CT	+	CCCTGGATCTGACGCCCGTC
Spir-UTR	+	CAAACTAAAGAACAAGATTC
Capu-CT	-	GCGTCGCAACGTATCCACCA
Capu-UTR	-	GTGTTCGAATCGTTTCGCGA

D.

CRISPR Tagged	% Hatched
Spir-smGFP-HA	88
Spir-mScarlet-HA	94
Capu-smmRuby2-OLLAS	4

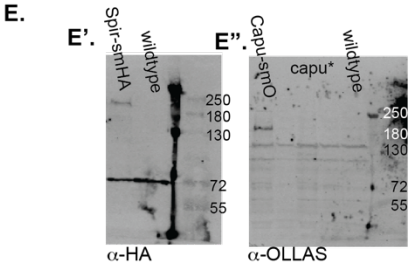

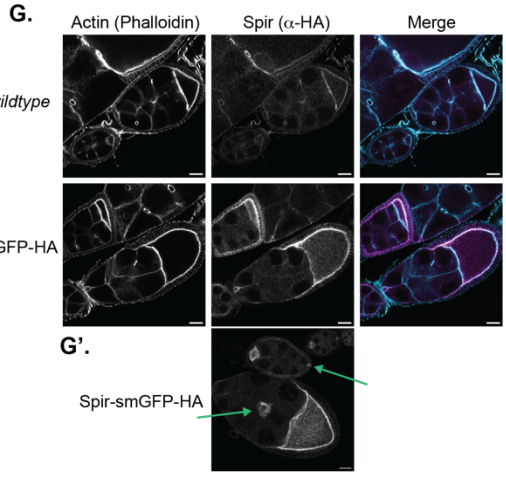

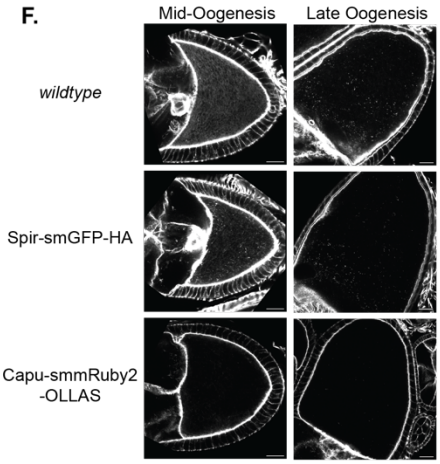

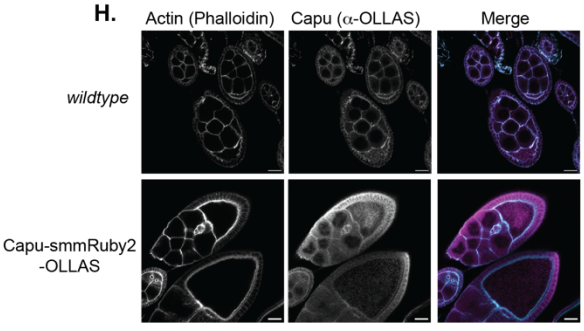

Figure 2-5: CRISPR/Cas9 mediated HDR for endogenous tagging of Spir and Capu.

(A.) CRISPR/Cas9 strategy used to C-terminally tag Spir isoforms. A two-guide method was employed to cleave out the 3'UTR of Spir and insert the tag, 3'UTR, and removable eye marker (3xP3 dsRed). Homology arms of 200nt each mediated HDR. (B.) CRISPR/Cas9 strategy used to C-terminally tag Capu isoforms. Again, the two-guide method was employed to insert a fluorescent tag at the C-terminal end of Capu. Homology of 850nt mediated HDR. (C.) Table of guide RNA protospacer sequences used to cleave Spir and Capu for C-terminal editing. The guides were selected for sequence specificity, proximal PAM (NGG), and proximity to desired editing site. CRISPR Optimal Target Finder http://targetfinder.flycrispr.neuro.brown.edu/index.php generated possible target sites. (D.) Fertility of CRISPR tagged lines. All C-terminal modifications of Spir were successful with high fertility rate of homozygotes (~90%). Capu-smmRuby2-OLLAS flies had a maximal fertility of 4%. (E.) Western blot of fly ovary lysate to identify expression of tagged constructs. (E'.) Spir-smGFP-HA homozygous ovary lysate (1:1000 rabbit anti-HA, CST). A positive band was identified between 180-250 kDa. (E".) Capu-smmRuby2-OLLAS western blot (1:1000 rat anti-OLLAS, Novus Biologicals). A positive band was again identified between 180-250kDa. (F.) Actin mesh staining of endogenously tagged lines using AlexaFluor488-Phalloidin. Images are representative. Spir-smGFP-HA oocytes contain a mesh during mid-oogenesis, Capu-smmRuby2-OLLAS oocytes do form an actin mesh during mid-oogenesis. (G.) Immunofluorescence of Spir-HA localization pattern. A strong cortical and cytoplasmic localization pattern is observed from early to late oogenesis (1:500 rabbit anti HA, CST). (G'.) Spir expression is also observed in the migrating border cell cluster (left arrow) and anterior polar cells (right arrow). (H.) Immunofluorescence of Capu-smmRuby2-OLLAS localization pattern is comparable to transgene data (1:1000 rat anti-OLLAS, Novus Biologicals).

Generation of endogenously tagged Capu: MiMIC insertion

Although CRISPR/Cas9 mediated HDR generated sterile flies, we still aimed to endogenously tagged Capu. As we found success generating *capu*-Gal4, we decided to establish Capu knock-in lines following a similar workflow. The MiMIC landing sites are integrated attP recombination sites in the *Drosophila* genome (Diao et al., 2015; Venken et al., 2011). Therefore, using the same recombination scheme, we should be able to insert any sequence into Capu at the same landing site. We modified the Gal4 insertion plasmid to contain the genomic sequence of CapuA from MI05737 through the 3'UTR (transcript nucleotides 26,540 – 30,215) for insertion (Figure 2-6A, cloning workflow **Appendix I**). As a proof of principle, we first inserted wildtype, untagged Capu at the landing site.

To validate the MiMIC lines received from injection, we followed an identical workflow, as established with the CRISPR/Cas9 edited flies. A majority of the lines screened by genomic PCR indicated the expression cassette was inserted in the reverse orientation for proper coding (*data not shown*). This quickly narrowed down the number of lines to validate further. Of those inserted correctly, we determined that the modified MiMIC insertion was successful, because

fertility assays of our wildtype Capu control matched that of *capu*-Gal4 driven transgene rescue (~80%, Figure 2-6B).

As this result was positive, we moved forward with generating C-terminally tagged Capu variants, meGFP, meGFP-AID, and mScarlet-OLLAS. We did not characterize the Capu-meGFP-AID flies as the AID project was abandoned prior to their receipt from BestGene. Consistently, Capu-meGFP and Capu-mScarlet-OLLAS rescue fertility to 80% (Figure 2-6B) and contain an actin mesh comparable to wildtype egg chambers (Figure 2-6C). Similarly to Spir, we determined expression of endogenously tagged Capu to be below the limit of detection in live samples (*data not shown*). IF of egg chambers expressing Capu-meGFP and -mScarlet-OLLAS exhibited consistent localization patterns with transgene rescue (Figure 2-6D). Endogenous tagging of Capu also uncovered localization to somatic cells: the migrating border cell cluster and posterior pole cells (Figure 1-6D', arrows). This is similar to what we observed for Spir-HA egg chambers and the role of Spir and Capu in these cells remains undetermined. Due to the high rates of fertility in homozygous females, we are satisfied with the endogenously tagged Capu lines generated and the modified MiMIC insertion pipeline established.

With both of the editing strategies described, we have generated endogenous expression patterns for Spir and Capu in oogenesis. Generally, the expression patterns match that reported using transgenes but at lower levels (Dahlgaard et al., 2007; Quinlan, 2013) and revealed localization in previously undescribed cell types.

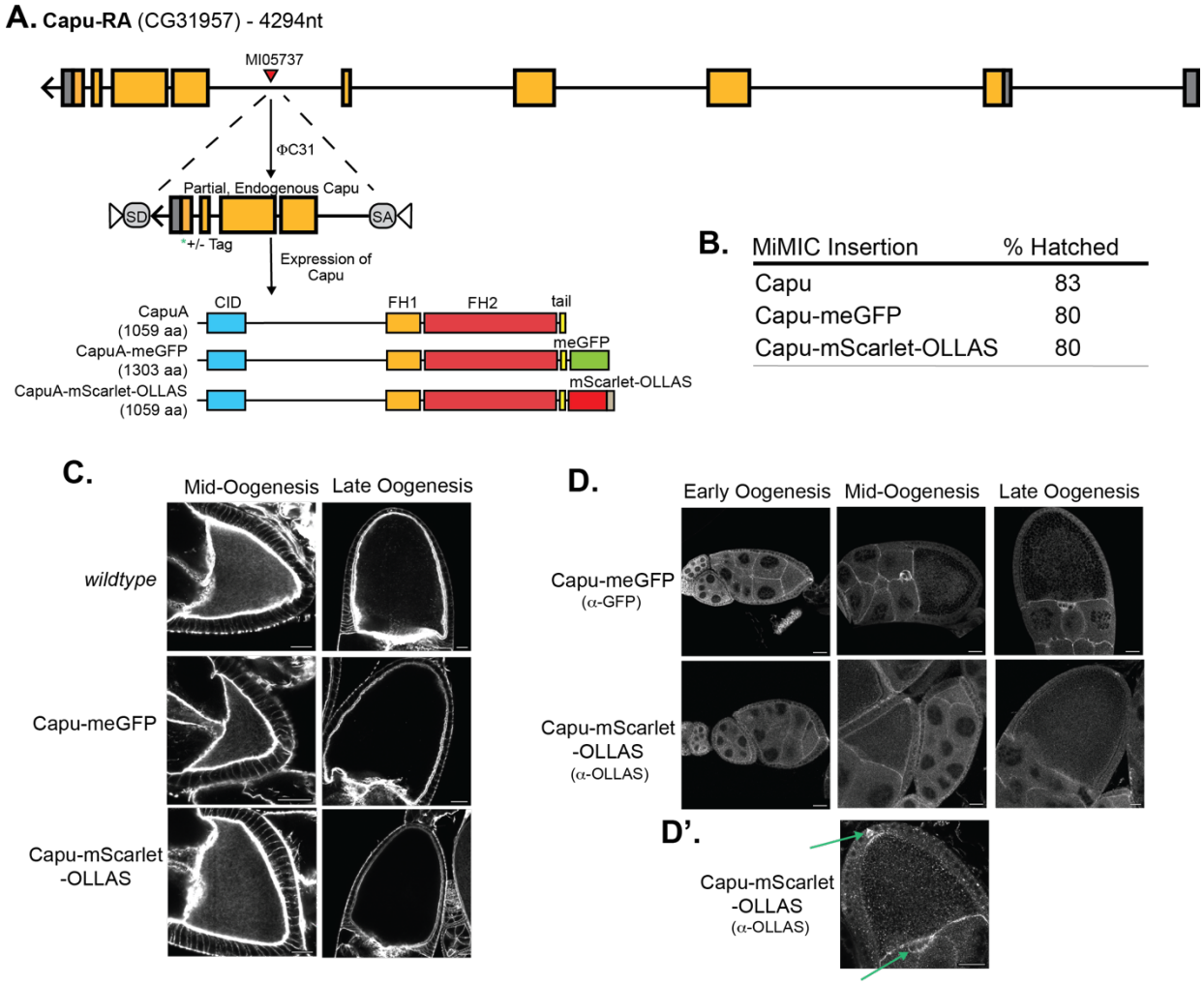

Figure 2-6: MiMIC insertion scheme to endogenously tag Capu.

(A.) Scheme for C-terminal insertion of tags in Capu. Three fly lines were generated using the MI05737 landing site: wildtype Capu (CapuA), Capu-meGFP, and Capu-mScarlet-OLLAS. (B.) Fertility rates of homozygous edited females. All rescue bulk fertility to ~80%, which is comparable to transgene rescue by capu-Gal4. (C.) Mesh staining of C-terminal edited Capu lines using AlexaFluor488-Phalloidin. Wildtype timing is observed. (D.) Immunofluorescent staining of Capu. anti-GFP staining of Capu-meGFP (1:2,500 chicken anti-GFP, Abcam). anti-OLLAS staining of Capu-mScarlet-OLLAS (1:2,000 rat anti-OLLAS, Novus Biologics). Staining patterns match that of transgene expression. (D') Endogenous tagging of Capu reveals localization at the migrating border cell cluster and posterior pole cells (arrows).

Co-imaging of Spir and Capu

We have generated and established *Drosophila* lines individually expressing endogenously tagged Spir and Capu. To characterize the temporal and positional interactions of Spir and Capu throughout oogenesis we set out to combine these tools. As previously stated,

live imaging was not possible due to low fluorescence signal. Consequently, all colocalization attempts were performed using immunofluorescent labeling and confocal imaging.

We set out to probe the Spir/Capu interaction by staining for Spir-smGFP-HA and Capu-mScarlet-OLLAS in a heterozygous background. The signal we observed for Capu-OLLAS was low and inconsistent, resulting in a lack of Spir/Capu colocalization in the oocyte (Figure 2-7A). We theorized that one explanation for the lack of overlap was due to low staining efficiency as a result of expressing a single copy of tagged Capu. Another hypothesis we established is preferential interaction exists between untagged, endogenous Spir and Capu. Therefore, to remove the possibility of interacting with untagged proteins and improve labeling efficiency, we recombined Spir-HA and Capu-OLLAS, obtaining egg chambers homozygous for the edited genes.

We were successful in recombing Spir-smGFP-HA and Capu-mScarlet-OLLAS, as small-scale fertility of homozygous females produced offspring (*data not shown*). Co-staining Spir-HA and Capu-OLLAS was inefficient, as we observed no clear colocalization. Again, we determined the Capu-OLLAS signal to be low and inconsistent and do not trust the biological significance in the lack of overlap (Figure 2-7B). We considered the lack of colocalization in the recombinant egg chambers to be due to the difference in epitope availability. Spir-HA contains 11xHA tags as they are incorporated in the smFP and while Capu has only 3xOLLAS. Another possibility is that the only commercially available OLLAS antibody is not as efficient as HA antibodies available (interpreted from Figure 2-6). As a result, we have been motivated to generate yet another endogenously tagged Capu line, Capu-smGFP-Myc. Myc epitopes have high availability of antibodies for optimization and hold promise to improve staining efficiency of endogenous Capu. The Capu-smGFP-Myc line has been received and is still in the validation workflow at this time.

In a final attempt, we recombined Spir-mScarlet-HA with *capu*-Gal4 driver and rescued *capu* null egg chambers with CapuA-meGFP. Transgene expression of Capu-GFP is too high to

permit antibody staining (*data not shown*). Therefore, co-imaging using this genetic background included staining of Spir-HA and capturing direct fluorescence of Capu-GFP in fixed samples. We were able to observe both Spir and Capu signal in the oocyte and further analyzed the images acquired to determine the degree of overlap (Figure 2-7C, D). Using JaCoP plugin in FIJI (Bolte and Cordelières, 2006), we determined Pearson's correlation coefficients of Capu's overlap with Spir in the oocyte cytoplasm, dorsal cortex, and posterior cortex (Figure 2-7D, E). The coefficients indicate a positive correlation and higher degree of overlap at the cortex over the oocyte cytoplasm. We postulate this finding is due to a higher degree of Spir-HA localization at the cortex. It is important to note that these data are not entirely reliable, due to limitations and differences in staining that exist between Spir and Capu. Improving staining and analysis workflows is important for further understanding the Spir/Capu interaction during oogenesis.

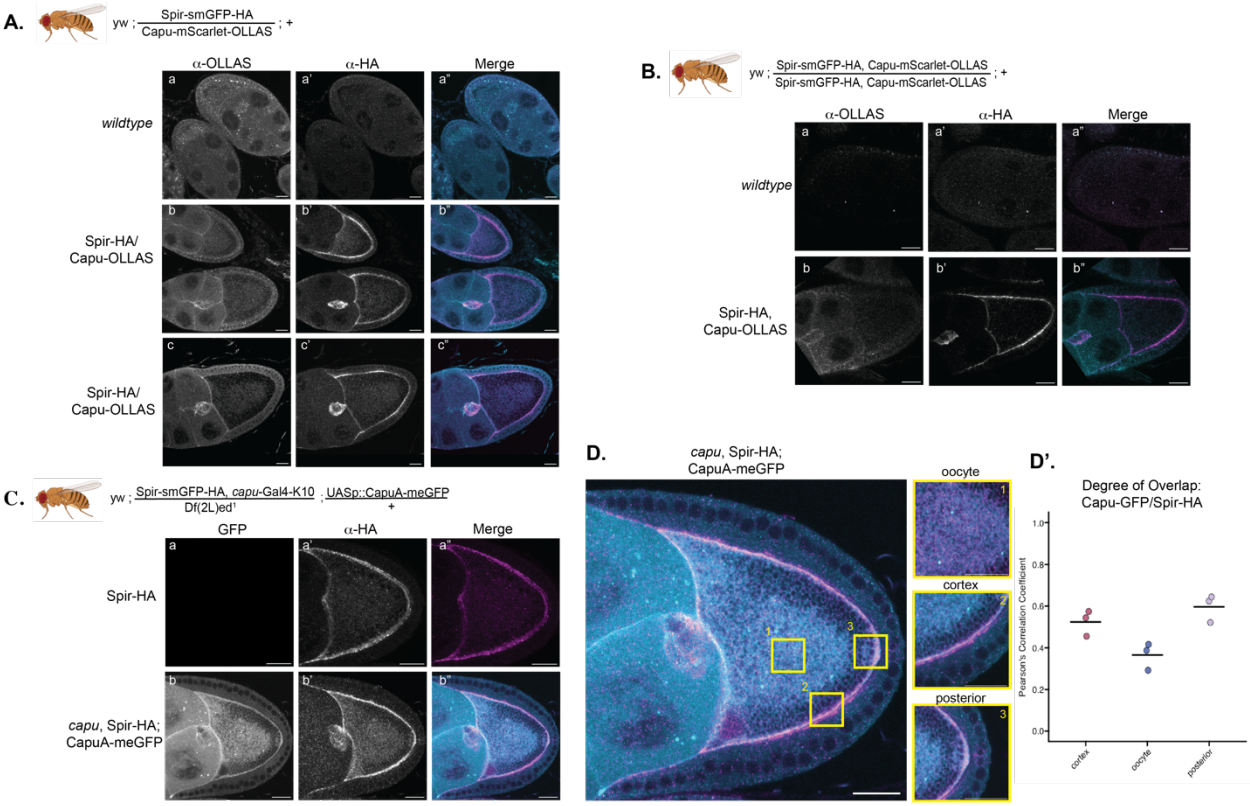

Figure 2-7: Co-imaging of Spir and Capu in the Drosophila oocyte.

(A.) Co-labeling attempts of heterozygous Spir (HA; 1:1000 rabbit anti-HA, CST) and Capu (OLLAS; 1:2,500 rat anti-OLLAS, Novus Biologicals) egg chambers. Capu-OLLAS signal is weak (b, c) and slightly improved when swapping secondary colors (c-c"). (B.) Imaging of homozygous Spir (HA; 1:1000 rabbit anti-HA, CST) and Capu OLLAS; 1:2,500 rat anti-OLLAS, Novus Biologicals) egg chambers. Labeling efficiency of Capu-OLLAS was low, further optimization of staining conditions is required. (C.) Co-visualization of heterozygous Spir-HA (1:1000 rabbit anti-HA, CST) in a transgene rescue background of Capu (GFP, direct fluorescence). This yielded the best signal observed with the co-imaging attempts. (D.) Analysis of degree of overlap in Spir and Capu signal from co-imaging. Regions of interest were the (1) oocyte cytoplasm, (2) dorsal oocyte cortex, (3) posterior oocyte cortex. (D'.) Measurement of the degree of co-incidence was evaluated using Pearson's correlation coefficient (FIJI: JaCoP, n=3). There is a slightly higher degree of overlap at the cortexes than the oocyte cytoplasm.

Discussion

Through this work we were able to establish that transgene rescue of *capu* nulls is successful using the Capu specific driver, *capu*-Gal4 (Figure 2-2). As attempts to improve transgene rescue of *spir* null rescue remains unsuccessful (Figures 2-3 – 2-4), a new *spir*-Gal4 driver is required. Such a driver was recently generated for the Quinlan Lab by the Gene Disruption Project using CRISPR/Cas9 mediated MiMIC insertion (CRIMIC) in the first intron of

Spir (Li-Kroeger et al., 2018). More information can be found at their website: https://flypush.research.bcm.edu/pscreen/crimic/info.php?CRname=CR71188. We hope that this version of *spir*-Gal4 proves successful for driving expression of Spir transgenes. To further improve transgene rescue of *spir* and *capu* null egg chambers, trading germline-specific elements (UASp/K10+) for those that express strongly in somatic and germline cells (UASz/p10) could be of interest (Masukawa et al., 2021). This theory is motivated from endogenous Spir/Capu localization we observed in somatic cells of the egg chamber.

To elucidate the role of Spir and Capu in actin mesh maintenance, we set out to determine where and when they interacted during oogenesis. CRISPR/Cas9 mediated HDR successfully generated endogenously tagged Spir at the C-termini (Figure 2-5). ΦC31 recombinase mediated insertion at MiMIC landing site MI05737 in Capu led to the generation of endogenously tagged Capu at the C-termini (Figure 2-6). While the general localization patterns observed match published transgene rescue data, we also find surprising localization of Spir (Figure 2-5, G') and Capu (Figure 2-6, D') to the migrating border cell cluster and posterior pole cells. This localization opens a new line of investigation to determine the role for Spir and Capu in these cells. We speculate that the function of Spir and Capu in the border cell cluster and pole cells has remained undescribed due to 1) the dramatic negative effect of premature fast steaming and 2) compensatory mechanisms regulating the cytoskeleton.

We attempted to co-image Spir and Capu localization and were met with mixed results (Figure 2-7). We attribute this to differences in labeling efficiency and an inability to detect the fluorescent tags in live samples. Some degree of overlap was measured (Figure 2-7D), but further improvements and optimization of Capu staining is required. As we aim to determine the dynamics of Spir and Capu in the oocyte, improving fluorescence intensity of live samples is integral. We consider adding other tags such as SNAP- or Halo (Erdmann et al., 2019).

In sum, we have generated multiple *Drosophila* lines expressing endogenous tags for our genes of interest. Using these, we confirmed previous transgene expression patterns and

have made progress in furthering our understanding of Spir and Capu in oogenesis. The fly lines and workflows established will aid in future study of these actin nucleators in *Drosophila*. For example, Spir-smGFP-HA lines are already being used to study Spir in *Drosophila* neurons by collaborators at McGill University, Montreal, Quebec, Canada.

Methods

Fly Line Generation

capu-Gal4-PEST-K10 Generation

capu-Gal4-k10 driver was generated by fist adding the K10 3' UTR terminator site to replace the Hsp70 3'UTR within the Trojan-Gal4 plasmid, pBS-KS-atB2-SA(0)-T2A-Gal4 (Addgene, Plasmid #62899). To this a short PEST motif was added c-terminally to the Gal4. This plasmid was then sent for injection to be integrated in the MiMIC landing site of Capu, MI057537 by BestGene (Chino Hills, CA).

CRISPR: Capu-smmRuby2-OLLAS

Capu was tagged with smmRuby2-OLLAS (Addgene #59761, quick change to mutate to fluoresce) at its endogenous locus using CRISPR/Cas9 mediated homologous recombination. To generate tagged flies, we followed a combined approach using dual gRNA sequences (Bence et al., 2017)and 850nt homology arms (Gratz et al., 2015). gRNA sequences for the C-termini of Capu (5' GCGTCCGCAACGTATCCACCA 3') and following the 3'UTR (5' GTGTTCGAATCGTTTCGCGA 3') were selected using the CRISPR Optimal Target finder (http://targetfinder.flycrispr.neuro.brown.edu/index.php). Oligonucleotides were cloned into pCFD3-dU6:3gRNA (Addgene #49410) and cloned using the previously designed strategy (Port et al., 2014). 850nt homology sequences with the PAM removed were cloned into Puc19. The repair template includes a C-terminal smmRuby2-OLLAS, the endogenous 3'UTR of Capu, and

the fluorescent eye reporter 3xP3_dsRed flanked by two PiggyBac recombinase sites. Plasmids expressing the guide RNAs and donor template were mixed and co-injected in embryos *nos-Cas9* embryos (BDSC 78782,(Ren et al., 2013)) at concentrations of 100ng/μL and 250ng/μL respectively. Offspring were screened via fluorescence of the 3xP3_dsRed for integration of the repair within the genome. Clones were balanced on chromosome II and Cas9 expressing chromosome removed. All injections and initial screening were completed by BestGene (Chino Hills, CA). Proper insertion of C-terminal tag was confirmed via genomic PCR (forward primer: 5' CCCGACCAGTTCTTCGAGTA 3', reverse primer: 5' ACACTCGTCCGAGTAAACGC 3') and western blot prior to further experimentation.

CRISPR: Spir-FP-HA

Spir was tagged with smGFP-HA (Addgene #63166, mutagenized to fluoresce) and mScarlet-HA (mScar-HA) at its endogenous locus using CRISPR/Cas9 mediated homologous recombination. To generate tagged flies, we followed a combined approach using dual gRNA sequences (Bence et al., 2017)and short homology arms (Kanca et al., 2019). gRNA sequences for the C-termini of Spir (5' GCCCTGGATCTGACGCCCGTC 3') and following the 3'UTR (5' GCAAACTAAAGAACAAGATTC 3') were selected using the CRISPR Optimal Target finder (http://targetfinder.flycrispr.neuro.brown.edu/index.php). Oligonucleotides were cloned into pCFD3-dU6:3gRNA (Addgene #49410) and cloned using the previously designed strategy (Port et al., 2014). 200nt homology sequences with the PAM removed were cloned into homologous recombination vector, a self-linearizable Puc57 (Kanca et al., 2019). The repair template includes a C-terminal fluorescent protein with HA, the endogenous 3'UTR of Spir, and the fluorescent eye reporter 3xP3_dsRed flanked by two PiggyBac recombinase sites. Spir-mScarlet-HA repair contains loxP removable fluorescent eye reporter. Plasmids expressing the guide RNAs and donor template were mixed and co-injected in embryos *nos-Cas9* embryos (BDSC 78782,(Ren et al., 2013)) at concentrations of 100ng/μL and 250ng/μL respectively.

Offspring were screened via fluorescence of the 3xP3_dsRed for integration of the repair within the genome. Clones were balanced on chromosome II and Cas9 expressing chromosome removed. All injections and initial screening were completed by BestGene (Chino Hills, CA). Proper insertion of C-terminal tag was confirmed via genomic PCR (forward primer: 5'GGGGATTCAACCTGTTCTCCT 3', reverse primer: 5'TGTGCAAGTGCGTTCTGAAG 3') and western blot prior to further experimentation.

Capu MiMIC Tagged Line Generation

The full genomic sequence of Capu, coding and non-coding, from MiMIC landing site MI05737 to end of the gene was inserted in pBS-KS-atB2-SA(0)-T2A-Gal4 (Addgene, Plasmid #62899). For C-terminal tagging, fluorescent protein sequences were inserted to the sequence. This plasmid was then sent for injection to be integrated in the MiMIC landing site of Capu, MI057537 (yw; Mi{MIC}capu^{MI05737} Bloomington, BDSC 42745) by BestGene (Chino Hills, CA).

Drosophila Stocks and Lab Generated Stocks

UASp::CapuA-meGFP-K10 (Quinlan, 2013), w[1118] (Bloomington, BDSC 3605), Df(2L)ed1/CyO (Bloomington, BDSC 5330), *capu*-Gal4-K10; + (Peter Bohall, unpublished), yw; spir^{KG00320} / SM6a (Bloomington, BDSC 13087), spir^{1}/CyO (Bloomington, BDSC 5113), capu^{1}/ CyO (Bloomington, BDSC 5094), capu^{HK3}/CyO (Manseau and Schupbach, 1989).

Fertility Assays

Approximately 100 test females were crossed to 50 wildtype (wt) males and raised on apple plates for 2 nights at 25°C. On day 3, to synchronize egg laying, flies were pre-cleared on a fresh apple plate containing yeast paste for 1.5 hours. The plate was changed, also containing yeast paste, and eggs laid over the following 3-hour time period were collected. Approximately 200 eggs were laid during that window. Eggs were moved to a fresh apple plate using a paint brush and incubated at 25°C for 24 hours. The number of eggs that hatched during that window

were recorded. Each trial was repeated with independent crosses three times. The data reported in the table is an average across the three trials to get the fertility rate.

Microscopy and staining

All microscopy images were collected on a Zeiss LSM 700 (Banerjee Lab, UCLA) or Zeiss LSM 780 confocal microscope (Akin Lab, UCLA). Flies were raised at 25°C and fed yeast paste for 16-24 hours prior to imaging.

The actin mesh was stained as described (adapted from (Dahlgaard et al., 2007; Quinlan, 2013)) using 1μM AlexaFluor488-phalloidin (Thermo Fisher Scientific, A12379) or 1μM AlexaFluor647-phalloidin (Thermo Fisher Scientific, A22287) for 45minutes.

Immunofluorescent staining of the HA (Spir-FP-HA), GFP (capu-GFP) and OLLAS (capu-FP-OLLAS) was performed by dissecting ovaries in cold 1XPBS, and fixing in 5% PFA (Electron Microscopy Solutions, 15714), diluted in 0.16X PBS with Heptane, protocol is modified from (Robinson and Cooley, 1997). Primary antibody conditions can be found in the figure legends. Optimal primary antibody conditions can be found in **Appendix II.** All samples were incubated in primary solution overnight at 4°C. 1:200 secondary complementary to primary species was used with conjugated fluorescent probe for 2 hours at room temperature. Sometimes with AlexaFluor647-phalloidin counterstain in the last hour of secondary incubation (Thermo Fisher Scientific, A22287).

Further analysis of microscopy images was performed in FIJI. JaCoP in FIJI was used to analyze the degree of overlap in microscopy data (Bolte and Cordelières, 2006). Data presentation of colocalization analysis was done in R using ggplot2.

Immunoblots

Levels of endogenous tagged construct in whole ovaries were detected as follows: whole ovaries of 10, 3-day old, flies were dissected in cold 1X-PBS. Samples were transferred to 1.5mL tubes, PBS removed and replaced with 10µL of PBS, 0.1% NP-40 and a protease inhibitor cocktail (Fisher, PIA32965). Ovaries were crushed and centrifuged at maximum speed at 4°C for 15 minutes. The supernatant was transferred to a fresh tube. SDS sample buffer was added to each sample and boiled for 10 minutes at 100°C. Samples were loaded in a 10% SDS-PAGE gel. PVDF membrane (Immobilon-FL, Fisher, IPFL 00010) was used and transferred at 100V for 90 minutes, cold, in Tris/glycine buffer with 10% methanol and 0.01% SDS. For detection of Spir-FP-HA rabbit anti-HA (C29F4) (Cell Signaling Technology (CST), 3724S) was used at 1:1000 overnight. For Capu-FP-OLLAS, rat anti-OLLAS (L2) (Novus Biologicals, NBP1-06713) was used at 1:1000 overnight. Detection was done using a LI-COR imager (LI-COR Biosciences, Odyssey Imaging System 9120, UCLA BIF).

References

Bence, M., Jankovics, F., Lukácsovich, T. and Erdélyi, M. (2017). Combining the auxin-inducible degradation system with CRISPR /Cas9-based genome editing for the conditional depletion of endogenous *Drosophila melanogaster* proteins. *FEBS J* 284, 1056–1069.

Bier, E., Harrison, M. M., O'Connor-Giles, K. M. and Wildonger, J. (2018). Advances in Engineering the Fly Genome with the CRISPR-Cas System. *Genetics* 208, 1–18.

Bolte, S. and Cordelières, F. P. (2006). A guided tour into subcellular colocalization analysis in light microscopy. *Journal of Microscopy* 224, 213–232.

Bor, B., Bois, J. S. and Quinlan, M. E. (2015). Regulation of the formin cappuccino is critical for polarity of *D rosophila* oocytes: Capu is Autoinhibited In Vivo. *Cytoskeleton* 72, 1–15.

Brand, A. H. and Perrimon, N. (1993). Targeted gene expression as a means of altering cell fates and generating dominant phenotypes. *Development* 118, 401–415.

Brown, J. B., Boley, N., Eisman, R., May, G. E., Stoiber, M. H., Duff, M. O., Booth, B. W., Wen, J., Park, S., Suzuki, A. M., et al. (2014). Diversity and dynamics of the Drosophila transcriptome. *Nature* 512, 393–399.

Dahlgaard, K., Raposo, A. A. S. F., Niccoli, T. and St Johnston, D. (2007). Capu and Spire Assemble a Cytoplasmic Actin Mesh that Maintains Microtubule Organization in the Drosophila Oocyte. *Developmental Cell* 13, 539–553.

Diao, F., Ironfield, H., Luan, H., Diao, F., Shropshire, W. C., Ewer, J., Marr, E., Potter, C. J., Landgraf, M. and White, B. H. (2015). Plug-and-Play Genetic Access to Drosophila Cell Types using Exchangeable Exon Cassettes. *Cell Reports* 10, 1410–1421.

Emmons, S., Phan, H., Calley, J., Wenliang, C., James, B. and Manseau, L. (1995). cappuccino, a Drosophila maternal effect gene required for polarity of the egg and embryo, is related to the vertebrate limb deformity locus. *Genes & Development* 9, 2482–2494.

Erdmann, R. S., Baguley, S. W., Richens, J. H., Wissner, R. F., Xi, Z., Allgeyer, E. S., Zhong, S., Thompson, A. D., Lowe, N., Butler, R., et al. (2019). Labeling Strategies Matter for Super-Resolution Microscopy: A Comparison between HaloTags and SNAP-tags. *Cell Chemical Biology* 26, 584-592.e6.

Gratz, S. J., Rubinstein, C. D., Harrison, M. M., Wildonger, J. and O'Connor-Giles, K. M. (2015). CRISPR-Cas9 Genome Editing in Drosophila. *Current Protocols in Molecular Biology* 111, 31.2.1-31.2.20.

Kalfayan, L. and Wensink, P. (1982). Developmental Regulation of Drosophila a-Tubulin Genes. *Cell* 29, 91–98.

Kanca, O., Zirin, J., Garcia-Marques, J., Knight, S. M., Yang-Zhou, D., Amador, G., Chung, H., Zuo, Z., Ma, L., He, Y., et al. (2019). An efficient CRISPR-based strategy to insert small and large fragments of DNA using short homology arms. *eLife* 8, e51539.

Kitsera, N., Khobta, A. and Epe, B. (2007). Destabilized green fluorescent protein detects rapid removal of transcription blocks after genotoxic exposure. *BioTechniques* 43, 222–227.

Lee, P.-T., Zirin, J., Kanca, O., Lin, W.-W., Schulze, K. L., Li-Kroeger, D., Tao, R., Devereaux, C., Hu, Y., Chung, V., et al. (2018). A gene-specific T2A-GAL4 library for Drosophila. *eLife* 7, e35574.

Li-Kroeger, D., Kanca, O., Lee, P.-T., Cowan, S., Lee, M. T., Jaiswal, M., Salazar, J. L., He, Y., Zuo, Z. and Bellen, H. J. (2018). An expanded toolkit for gene tagging based on MiMIC and scarless CRISPR tagging in Drosophila. *eLife* 7, 27.

Manseau, L. J. and Schupbach, T. (1989). cappuccino and spire: two unique maternal-effect loci required for both the anteroposterior and dorsoventral patterns of the Drosophila embryo. *Genes & Development* 3, 1437–1452.

Masukawa, M., Ishizaki, Y., Miura, H., Hayashi, M., Ota, R. and Kobayashi, S. (2021). Male-biased protein expression in primordial germ cells, identified through a comparative study of UAS vectors in Drosophila. *Sci Rep* 11, 21482.

Meltzer, H., Marom, E., Alyagor, I., Mayseless, O., Berkun, V., Segal-Gilboa, N., Unger, T., Luginbuhl, D. and Schuldiner, O. (2019). Tissue-specific (ts)CRISPR as an efficient strategy for in vivo screening in Drosophila. *Nat Commun* 10, 2113.

Nern, A., Pfeiffer, B. D., Svoboda, K. and Rubin, G. M. (2011). Multiple new site-specific recombinases for use in manipulating animal genomes. *Proceedings of the National Academy of Sciences* 108, 14198–14203.

Nern, A., Pfeiffer, B. D. and Rubin, G. M. (2015). Optimized tools for multicolor stochastic labeling reveal diverse stereotyped cell arrangements in the fly visual system. *Proc Natl Acad Sci USA* 112, E2967–E2976.

Nishimura, K., Fukagawa, T., Takisawa, H., Kakimoto, T. and Kanemaki, M. (2009). An auxin-based degron system for the rapid depletion of proteins in nonplant cells. *Nat Methods* 6, 917–922.

Port, F., Chen, H.-M., Lee, T. and Bullock, S. L. (2014). Optimized CRISPR/Cas tools for efficient germline and somatic genome engineering in Drosophila. *Proc Natl Acad Sci U S A* 111, E2967–E2976.

Quinlan, M. E. (2013). Direct interaction between two actin nucleators is required in Drosophila oogenesis. *Development* 140, 4417–4425.

Ren, X., Housden, B. E., Hu, Y., Roesel, C., Lin, S., Liu, L.-P., Yang, Z., Mao, D., Sun, L., Wu, Q., et al. (2013). Optimized gene editing technology for Drosophila melanogaster using germ line-specific Cas9.

Robinson, D. N. and Cooley, L. (1997). *Drosophila* Kelch Is an Oligomeric Ring Canal Actin Organizer. *The Journal of Cell Biology* 138, 799–810.

Rørth, P. (1998). Gal4 in the Drosophila female germline. *Mechanisms of Development* 78, 113–118.

Rosales-Nieves, A. E., Johndrow, J. E., Keller, L. C., Magie, C. R., Pinto-Santini, D. M. and Parkhurst, S. M. (2006). Coordination of microtubule and microfilament dynamics by Drosophila Rho1, Spire and Cappuccino. *Nature Cell Biology* 8, 367–376.

Sternberg, S. H., Redding, S., Jinek, M., Greene, E. C. and Doudna, J. A. (2014). DNA interrogation by the CRISPR RNA-guided endonuclease Cas9. *Nature* 507, 62–67.

Venken, K. J. T., Schulze, K. L., Haelterman, N. A., Pan, H., He, Y., Evans-Holm, M., Carlson, J. W., Levis, R. W., Spradling, A. C., Hoskins, R. A., et al. (2011). MiMIC: a highly versatile transposon insertion resource for engineering Drosophila melanogaster genes. *Nature Methods* 8, 737–743.

Wang, C., Dickinson, L. K. and Lehmann, R. (1994). Genetics of *nanos* localization in *Drosophila*. *Developmental Dynamics* 199, 103–115.

Wellington, A., Emmons, S., James, B., Calley, J., Grover, M., Tolias, P. and Manseau, L. (1999). Spire contains actin binding domains and is related to ascidian posterior end mark-5. *Development* 126, 8.

Chapter 3: Flexible geometry of *Drosophila* formin Cappuccino in actin mesh formation

Introduction

Drosophila oogenesis has long served as a model for studying polarization of developing cells. Careful regulation of the actin cytoskeleton and a range of actin-based structures are essential to cell polarity establishment and maintenance. Among these structures, the actin mesh, is poorly understood. It is a network of filamentous actin, that fills the developing oocyte specifically during developmental stages 5-10A (Dahlgaard et al., 2007). If the network is not built or persists beyond stage 10B, fertility is severely decreased (Bor et al., 2015; Dahlgaard et al., 2007; Quinlan, 2013). In both cases, polarized localization of mRNAs is disrupted. It is thought that the actin mesh indirectly impacts mRNA localization by restricting microtubule-dependent cytoplasmic streaming (Dahlgaard et al., 2007; Gutzeit and Koppa, 1982). Two proteins, specifically actin nucleators, Spire (Spir) (Quinlan et al., 2005) and Cappuccino (Capu) (Emmons et al., 1995) are required for proper formation of this meshwork (Dahlgaard et al., 2007). Their direct interaction results in synergistic actin assembly, which is required to build the mesh (Bradley et al., 2019; Quinlan, 2013). It follows that mutation of either gene leads to absence/loss of mesh. Downstream of mesh loss, premature onset of fast cytoplasmic streaming, loss of cell polarity, and infertility are observed. It is difficult to determine if the sole consequence of mesh absence is loss of cell polarity or if other processes are disrupted. Premature streaming is so severe that it may be masking other processes that require the mesh, Spir, and/or Capu. In fact, there exists evidence of other roles for Spir and Capu have been presented (Alzahofi et al., 2020; Chang et al., 2011; Scheffler et al., 2021; Schuh and Ellenberg, 2008; Stürner et al., 2022). Here we present evidence that Capu plays at least one alternate role in the Drosophila oocyte, which may be independent of Spir.

In the developing mouse oocyte, an analogous actin meshwork is built by mammalian homologs of Spir (Spire-1 and Spire-2) and Capu (Fmn-2) (Pfender et al., 2011; Schuh and Ellenberg, 2008). FMN2 and Spire-1/2 colocalize on Rab11-positive vesicles and the cortex, where they nucleate actin filaments. Myosin V (MyoV) movement along this network of actin

generates a pushing force – contraction – to centrally position the mitotic spindle and transport Rab11-positive vesicles in meiosis (Almonacid and Verlhac, 2021; Holubcová et al., 2013; Schuh and Ellenberg, 2008). Interestingly, the mammalian paralog, FMN1, is cytosolic in mouse melanocytes, which have Spire-1/2 abutting Rab27-positive melanosomes. In this case, MyoV drives dispersion of melanocytes, as opposed to contraction (Alzahofi et al., 2020).

The implication of the mouse oocyte and melanocyte models is that localization of the formin defines the structure built by Spir and Capu, thereby determining the consequences of their activity. Spir is enriched at the cortex in the *Drosophila* oocyte (Quinlan 2007, 2013). All Spir proteins contain a mFYVE domain, which binds negatively charged membranes, consistent with its presence on vesicles and in the cortex (Kerkhoff et al., 2001; Tittel et al., 2015). Based on transgene expression, Capu appears to be diffuse in the developing *Drosophila* oocyte, though it is enriched at the cortex of nurse cells (Bor et al., 2015; Dahlgaard et al., 2007; Quinlan, 2013). This localization initially surprised us based on the mouse oocyte data and the fact that Capu directly interacts with membrane-associated Spir to function (Quinlan, 2013). Therefore, we sought to determine the localization of endogenous protein and study the effect of altering Capu localization in the *Drosophila* oocyte.

A notable difference between FMN1 and FMN2 is the presence of an N-terminal glycine only in FMN2 that is predicted to be N-myristoylated by n-myristoyltransferase (NMT). Myristoylation may drive FMN2 to membranes, as observed in the mouse oocyte. Nine unique isoforms of Cappuccino are predicted in the fly (FlyAtlas2, FlyBase)(Leader et al., 2018; Öztürk-Çolak et al., 2024). A closer look at these isoforms reveals a myristoylation site in the N-terminal exon of isoforms D/E/F/J. CapuA is the canonical isoform expressed in the ovary. It does not have a predicted myristoylation site. The diffuse localization of CapuA, suggests that Spir, Capu, and the mesh may function more like the melanocyte – important for dispersion - than the mouse oocyte – driving contractile forces.

We created endogenously tagged genes to establish high resolution localization data for Spir and Capu. We then tested the impact of altering Capu localization, by utilizing transgene rescue with a new gene-specific driver. These experiments enabled us to identify an alternate role for Capu in oogenesis, linking a structure critical for organization of posterior determinants to the oocyte cortex, which appears to be independent of Spir.

Results

Capu localization

Because function is necessarily linked to localization, we decided to revisit the question of where Capu is found in the Drosophila oocyte. Previous work relied on transgene expression because multiple attempts by multiple groups to generate a specific antibody for immunofluorescence were unsuccessful. The *capu* gene has five potential start sites and 9 transcripts, but all of the splice variants share their C-termini. So, we took advantage of a MiMIC line (MI05735) to insert a C-terminal tag in the endogenous gene (Figure 3-S1A). As proof of principle, we first inserted a duplicate of the remaining gene, such that a full-length untagged version of Capu would be expressed under the same control as wild type. The *capu* insertion worked well, resulting in 83% fertility (Figure 3-S1B). We then inserted tags using the same method. We started with GFP because transgene rescue with Capu-GFP has been successful (Quinlan 2013). Homozygous females expressing Capu-GFP were fertile at levels comparable to those with the untagged gene, 80%. Our efforts to image Capu-GFP in live samples or by immunofluorescence suggested that Capu is expressed at low levels (Figure 3-S1B,C, a-a”). Immunofluorescence revealed that Capu is largely diffuse in the oocyte, as observed with transgenes. We, therefore, inserted mScarlet-3XOLLAS (Figure 3-S1B, C, b-b”). The localization patterns detected with GFP and OLLAS are consistent with one another and similar to previously reported transgene expression (Dahlgaard et al., 2007; Quinlan, 2013; Rosales-Nieves et al., 2006). Broadly, Capu is diffuse throughout the egg chamber and enriched in the

nurse cell cortex. Interestingly, we observed Capu enriched at the oocyte cortex during mid oogenesis (stages 6-9) (Figure 3-S1C). However, we only observed cortical enrichment in the oocyte only in fixed samples. Perhaps cortical localization is masked by high levels of diffuse protein. In addition, we observed Capu in specialized follicle cells: the migrating border cell cluster (Figure 3-S1C, a' arrow) and posterior polar cells (Figure 3-S1C, b" arrow). Experiments using germline-specific drivers could not have revealed these previously undescribed localizations of Capu.

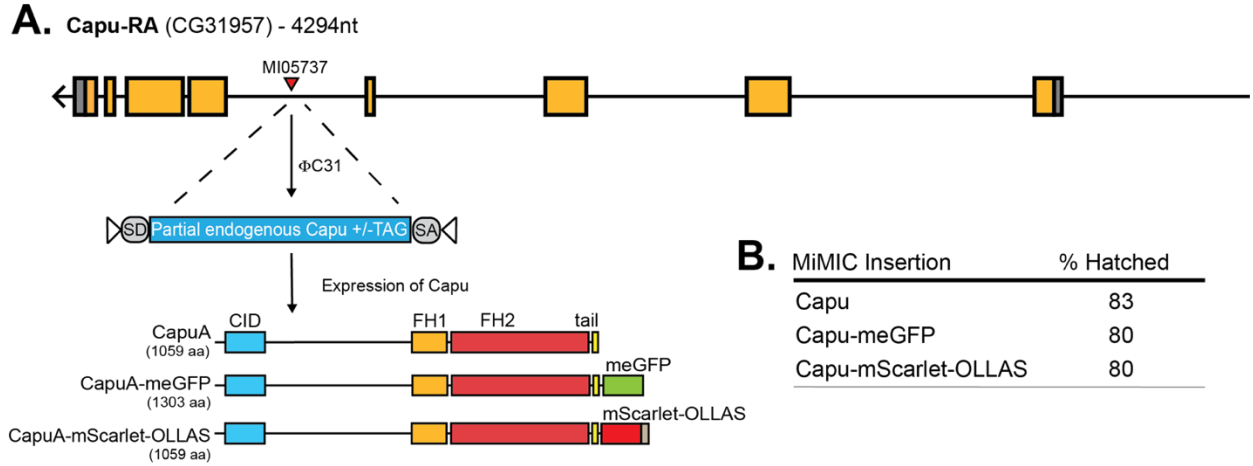

B.

MiMIC Insertion	% Hatched
Capu	83
Capu-meGFP	80
Capu-mScarlet-OLLAS	80

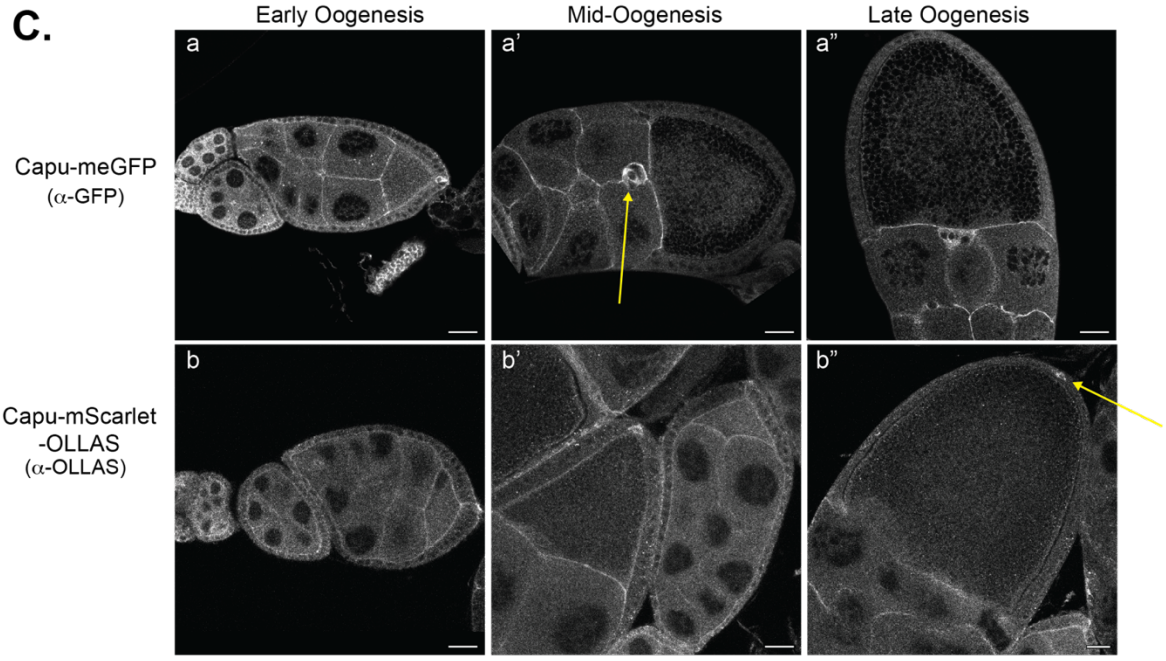

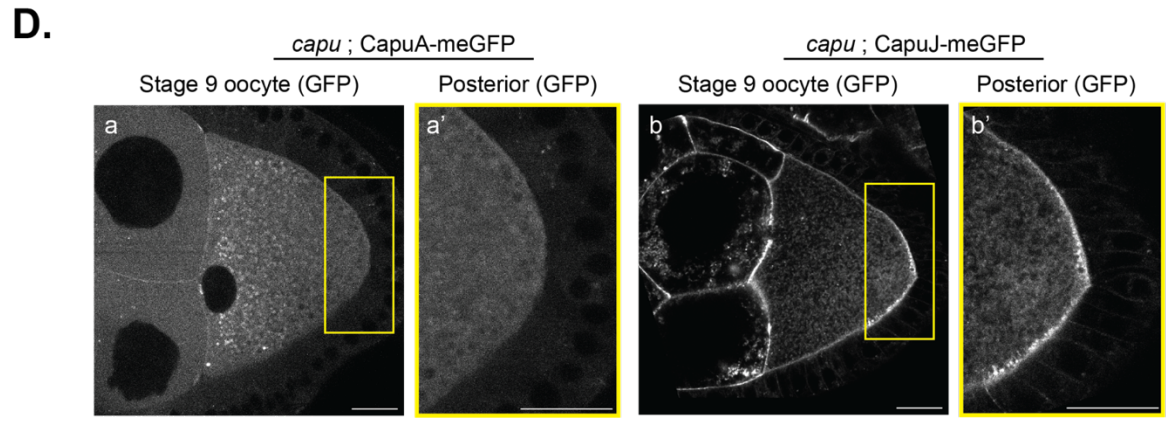

Figure 3-S1: Determining the localization of Capu.

(A.) Schematic of insert strategy used to generate endogenously tagged Capu lines. C-termini of Capu-RA is shown as an example, all isoforms of Capu contain MI05737. (B.) Fertility of endogenous tagged Capu lines generated. The % hatched is reported as the average of three independent trials, with the number counted being the sum total eggs collected from all trials. Fertility is reported as the percentage of eggs that hatched following 24 hours of being laid. All test female flies were crossed to wild-type males to evaluate the maternal contribution to the rescue rate. (C.) Immunofluorescent staining of endogenously tagged Capu in egg chambers over oogenesis. Capu-meGFP (a-a") and Capu-mScarlet-OLLAS (b-b") staining is consistent with transgene rescue data. Scale bars: 20μm. (D.) CapuA-meGFP (a-a') and CapuJ-meGFP (b-b') stage 9 egg chambers. Posterior localization pattern varies between isoforms, CapuJ (b') has a higher enrichment at the cortex. Scale bars: 20μm.

A capu-GAL4 driver

In the past, Capu transgene expression was usually driven by *nanos*-Gal4-vp16 (*nos*-Gal4) and always by germline specific drivers (Dahlgaard et al., 2007; Quinlan, 2013; Rosales-Nieves et al., 2006). While rescue of fertility in the null is observed, it is incomplete. For example, when driving CapuA or GFP-CapuA, fertility was 56 and 36%, respectively. Low fertility could reflect a requirement for alternate splice variants of Capu or a mismatch in Capu's spatial and/or temporal expression pattern with *nos*-Gal4. For example, *nos*-Gal4 does not drive expression in the border and polar cells. To test these possibilities, we built a gene-specific driver, *capu*-Gal4-K10 (*capu*-Gal4). We inserted Gal4-K10 at the MI05737 landing site within *capu,* using a modified Trojan-Gal4 design strategy (Lee et al., 2018; Venken et al., 2011). Expression driven by *capu*-Gal4 begins as early as stage 2A in the germarium, increases in intensity upon stage one and is continually expressed until the onset of late oogenesis (Figure 3-1C), a pattern that markedly differs from *nos*-Gal4 (Hudson and Cooley, 2014). Using *capu*-Gal4 driven CapuA-GFP to rescue a *capu* null background resulted in 90% fertility: a great improvement over *nos*-Gal4 driven rescue experiments (Table 1). Localization of CapuA matches that seen when the gene is driven by *nos*-Gal4: largely diffuse with enrichment at the nurse cell cortex (Figure 3-S1). We do not see follicle cell expression, presumably due to the 3'-UTRs used in the Gal4 driver and the pUASp insertion. Thus, we conclude that primarily germline expression of CapuA is sufficient to rescue fertility, consistent with expression data indicating that it is the major isoform expressed in the ovary (Leader et al., 2018). Further, the

process is sensitive to the timing of Capu expression. We, therefore, use only *capu*-Gal4 as a driver in the following studies.

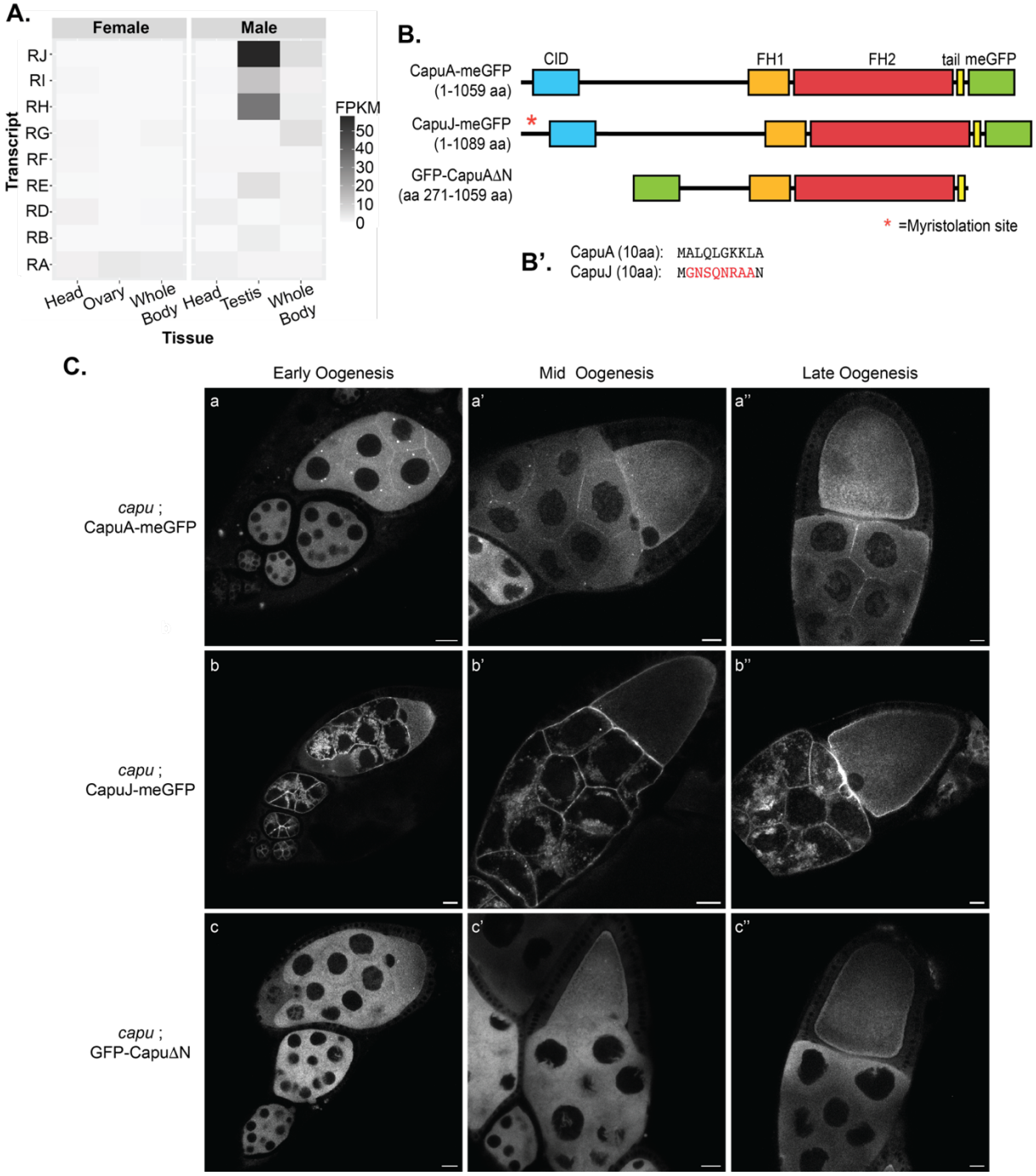

Figure 3-1: Myristoylation of Capu shows fertility loss.

(A) Heatmap of transcript expression data from FlyAtlas2, modified from Leader et al, 2018. (B) Domain maps of transgenes used in this study. CapuA-GFP, CapuJ-GFP, and GFP-CapuAΔN. Numbers in the parentheses are total amino acids of the constructs, not including the meGFP (GFP). Major domains indicated are; CID, Capu inhibitory domain (blue); FH1, formin homology 1 (orange); FH2, formin homology 2 (red); tail (yellow). A green box is included for each domain map to indicate their location within the construct. The red asterisk indicates the region of CapuJ where the myristoylation site can be found. (B") The first ten amino acids of CapuA and CapuJ, the predicted myristoylation motif is indicated in red. (C.)Capu localization in live egg chambers throughout oogenesis. (a-a")CapuA localization in live egg chambers is enriched at the nurse cell cortex, interface between the nurse cell and oocyte, and is largely diffuse in nurse cell and oocyte cytoplasm. (b-b") CapuJ exhibits an increased enrichment at the nurse cell cortexes, and nurse cell/oocyte interface. Cytoplasmic diffuse localization is lost in the nurse cells and there is a stronger cortical localization pattern in the oocyte during mid and late oogenesis. (c-c") CapuΔN localization is completely diffuse through the nurse cells and oocytes for all developmental stages. Scale bars: 20 μm.

Myristoylation of Capu alters localization and decreases fertility

Capu isoforms D/E/F/J are highly expressed in the male testis but not detected in the female ovary (Figure 3-1A)(Leader et al., 2018). As noted above, these isoforms share their first coding exon containing a predicted N-terminal myristoylation site, which could target Capu to membranes. We reasoned that by expressing one of these isoforms we could alter Capu localization in the oocyte. We selected CapuJ because the coding regions of CapuA and CapuJ only differ by their most N-terminal exons (Benson et al., 2012) (Figure 3-1B-B').

CapuJ-GFP is largely membrane bound (Figure 3-1C). Higher magnification imaging reveals strong cortical localization in the oocyte as well as punctate-like signal in the cytoplasm (Figure 3-S1D). In addition, there is an aggregate-like localization pattern in the nurse cell cytoplasm and an increase in signal at the nurse cell-oocyte interface (Figure 3-1C, b-b"). Based on the altered localization, we conclude that CapuJ is myristoylated when expressed in the *Drosophila* egg chamber.

We also considered GFP-CapuΔN, a truncated version of CapuA, which lacks the N-terminus through its autoinhibitory domain (CID; Figure 3-1B). GFP-CapuΔN was previously shown to rescue mesh formation and *oskar* localization when driven by *nos*-Gal4 (Dahlgaard et al., 2007). Live imaging of GFP-CapuΔN driven by *capu*-Gal4 reveals localization patterns similar to those previously reported with *nos*-Gal4 (Dahlgaard et al., 2007; Quinlan, 2013). GFP-

CapuΔN is completely diffuse; no cortical enrichment is detected in the nurse cells or at the nurse cell-oocyte interface (1C, c-c”).

As the spatiotemporal regulation is critical for formin regulation in other systems (Alzahofi et al., 2020; Azoury et al., 2008; Holubcová et al., 2013), we asked whether altering the localization in the *Drosophila* egg chamber influences Capu function and, therefore, fertility. Interestingly, CapuJ-meGFP-expressing flies were only 48% fertile. In addition, GFP-CapuΔN expressing flies were 43% fertile (Table 1). These marked decreases in fertilty demonstrate that Capu’s function is impaired when the N-terminus is altered, perhaps due to changes in localization.

Transgene (Df(2L)ed^{1}/*capu*-Gal4-K10)	% Hatched	Number counted
UASp::CapuA-meGFP	89.5	637
UASp::CapuJ-meGFP	47.8	694
UASp::eGFP-CapuΔN	43.1	800
Null/No Rescue	0.66	598

Table 3-1: Table of fertility data from the genetic rescue.

The genetic background is in parentheses, all transgenes are under UASp regulation. The % hatched is reported as the average of three independent trials, with the number counted being the sum total eggs collected from all trials. Fertility is reported as the percentage of eggs that hatched following 24 hours of being laid. All test female flies were crossed to wild-type males to evaluate the maternal contribution to the rescue rate.

CapuJ builds an actin mesh

A straightforward explanation for the decreased fertility with CapuJ rescue would be that the actin mesh is misregulated. To be assembled, the actin mesh requires direct interaction between Spir and Capu (Bradley et al., 2019; Dahlgaard et al., 2007; Quinlan, 2013). By restricting Capu’s localization within the oocyte, Capu’s actin assembly activity and synergy with Spir could be disrupted. We stained for the actin mesh in rescue egg chambers and found no difference in mesh presence (mid-oogenesis) or the timing of removal (late oogenesis) (Figure 3-2A). As previously reported (Dahlgaard et al., 2007) GFP-CapuΔN rescue exhibited formation of a denser actin mesh in the nurse cells. We attribute the apparently increased activity to loss

of autoinhibition. Similarly, *nos*-Gal4 driven expression of GFP-CapuΔN, but not GFP-CapuA, markedly decreased fertility when expressed in wild type background (Bor et al., 2015). Thus, both excess actin in nurse cells and hyperactive Capu in the oocyte may be contributors to the decreased fertility in GFP-CapuΔN rescue flies (Table 1). Therefore, we include CapuΔN in some of our studies but interpret it with care when comparing it to CapuA and CapuJ. Altogether these data demonstrate that membrane-bound Capu (CapuJ) retains actin assembly activity and is capable of forming an actin meshwork with wildtype timing, indistinguishable from cytosolic Capu (CapuA).

To functionally assess the actin mesh, we analyzed the cytoplasmic fluid flows, so-called cytoplasmic streaming, during mid and late oogenesis (Figure 3-2A, streaming-h, m-p). We analyzed timelapse images of streaming to determine velocity (PIVlab, MATLAB) and pattern (2DCorrelation, LiamABailey GitHub). To describe the pattern of motions, we measured the degree of correlation of motion and report the maximal radius at which the streaming topology remains half correlated (C(r)=0.5). No significant difference was observed during mid oogenesis for velocity or correlation between wildtype and rescues, leading us to conclude that the mesh is functional and streaming is properly regulated at this stage (Figure 3-S2). (Unless otherwise stated, we used one-way ANOVA and post-hoc Tukey-Kramer Multiple Comparisons Tests (TKMC) to determine significance, p=0.05)

We found differences in streaming during late oogenesis. While there was no significant difference in velocity (Figure 3-2B), we did find an intriguing difference in the pattern/correlation of fast streaming during late oogenesis (Figure 3-2C). In wildtype oocytes, at the (C(r)=0.5) of fast streaming, the radius is ~20 μm on average. CapuJ rescue oocytes were found to have a significantly lower radius of ~15 μm. The change is the opposite direction from the correlation pattern of *capu* null oocytes, which have significantly higher correlated radii (C(r)=0.5 radius of ~32 μm) compared to wildtype (p=1.09E-08). While interesting, the change in pattern correlation

is small and we do not predict that it is substantial enough to explain the fertility defect observed with CapuJ rescue (Table 1).

During oogenesis, the known role of Capu is its involvement in actin mesh formation, which regulates cytoplasmic streaming. By rescuing with membrane bound Capu, CapuJ, we have determined that actin mesh assembly and streaming are largely unaltered, leaving the reduction in fertility unexplained. This poses intriguing questions, such as: are there additional roles for Capu during *Drosophila* oogenesis? Further, could a role for the mesh, other than streaming regulation, be disrupted because the mesh organization is altered when CapuJ builds it?

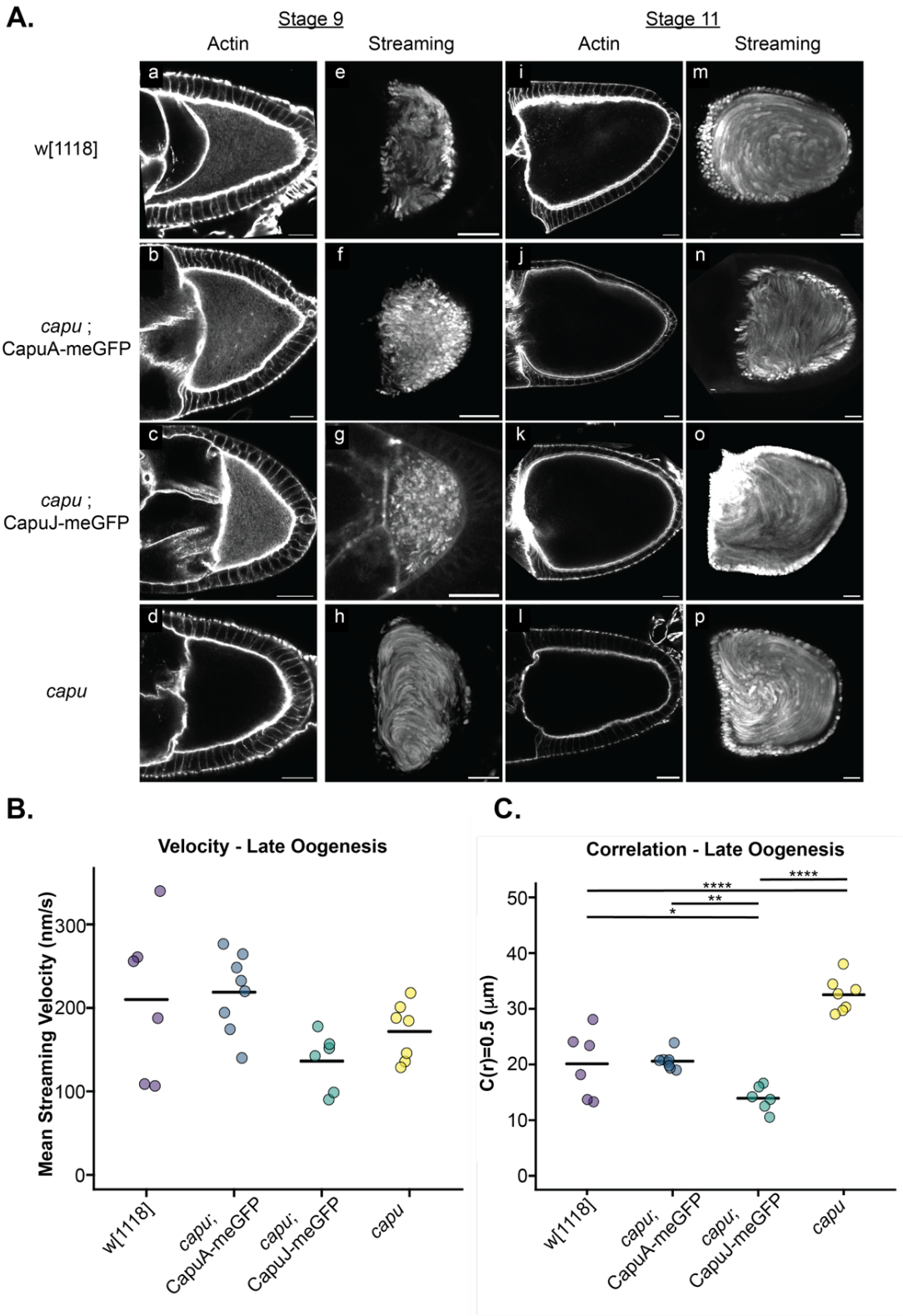
A.
Stage 9
Stage 11
Actin
Streaming
Actin
Streaming
w[1118]
capu ; CapuA-meGFP
capu ; CapuJ-meGFP
capu
a
b
c
d
e
f
g
h
i
j
k
l
m
n
o
p
B.
Velocity - Late Oogenesis
Mean Streaming Velocity (nm/s)
0
100
200
300
w[1118]
capu; CapuA-meGFP
capu; CapuJ-meGFP
capu
C.
Correlation - Late Oogenesis
C(r)=0.5 (μm)
0
10
20
30
40
50
****
**
*
****
w[1118]
capu; CapuA-meGFP
capu; CapuJ-meGFP
capu

Figure 3-2: Membrane-bound Capu is sufficient to rescue the actin mesh formation and timing.

*(A.) Stage 9 and 11 egg chambers stained with AlexaFluor488-phalloidin to examine the actin mesh in transgenic flies. This shows that for the CapuA (Df(2L)ed^{1}/capu-Gal4-K10; UASp::CapuA-meGFP/+) and CapuJ (Df(2L)ed^{1}/capu-Gal4-K10; UASp::CapuJ-meGFP/+) rescue, the actin mesh is properly formed (stage 9, a-d) and removed (stage 11, i-l) during oogenesis with a wildtype (w[1118]) control for comparison. capu null (Df(2L)ed^{1}/capu-Gal4-K10; +/+) included to show failed rescue. Maximum intensity projections of autofluorescent yolk granule motion over a period of 5 minutes for transgenic egg chambers mid-oogenesis (typical stage 9, e-h) and late oogenesis (stage 11, m-p) are shown for each background. Scale bars: 20μm. (B-C) Analysis of streaming velocities and pattern. Dot plots of streaming velocities and pattern (correlation radius =0.5), the bar in each dataset indicates the average value. N ≧ 6 for each stage 11 analyzed. (B) Late streaming velocity is not significantly different for any of the genotypes measured (~200nm/s), see methods for analysis. (d) Analysis of the late oogenesis streaming pattern, correlation (described in the methods), using a personalized code (2DCorrelation, LiamABailey, GitHub). The correlation pattern of streaming during late oogenesis in capu null oocytes is significantly increased (~32 μm, p****, 9.87E-06) in comparison to wildtype, 20μm. The CapuJ rescue has a significantly lower correlation pattern (15 μm) in comparison to wildtype (20 μm, p=*, 0.02648815), CapuA rescue (21 μm, p**, 0.00918752), and capu null (32 μm, p=****, 1.09E-08). All p values were determined via one-way ANOVA, post-hoc Tukey-Kramer Multiple Comparisons Test, see methods for more details.*

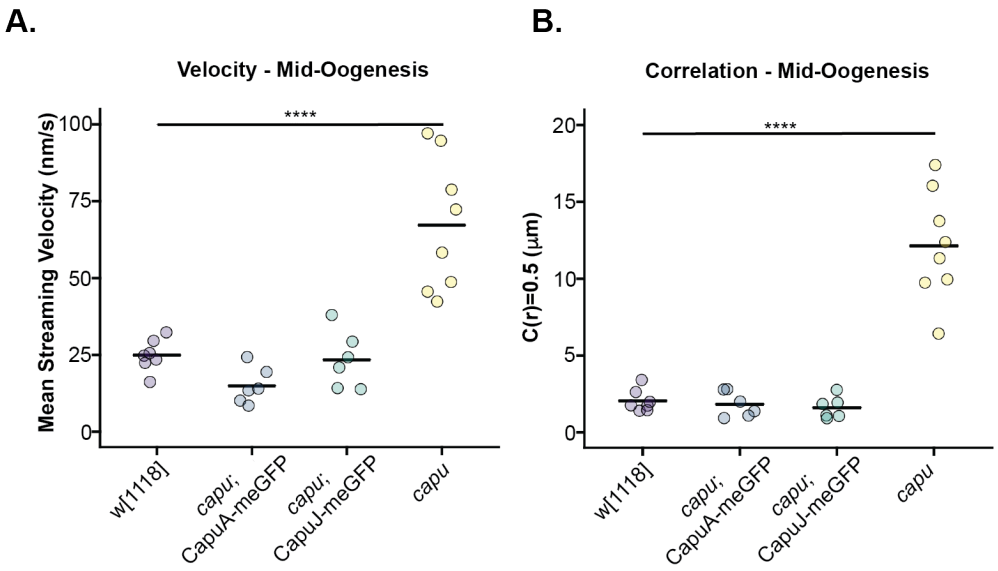

Figure 3-S2: Analysis of streaming velocities and pattern during mid-oogenesis.

*(A-B) Dot plots of streaming velocities and pattern (correlation radius =0.5), the bar in each dataset indicates the average value. N ≧ 6 for each stage 9 and stage 11 analyzed. (A) Quantification of streaming shows no significant differences between the wildtype and Capu rescue backgrounds during mid oogenesis (~25nm/s). capu null oocytes show premature fast streaming with a three-fold increase in streaming velocity (~65nm/s) and is significantly different from the other genotypes as indicated (p****, 0.00001652). (B) Analysis of the mid-oogenesis streaming pattern, correlation (described in the methods), using a personalized code (2DCorrelation, LiamABailey, GitHub). No significant difference exists between wildtype and CapuA rescue flies (~2μm). capu null oocytes exhibit a significant increase in correlation radius, ~13μm (p****,1.4E-08).*

Restricting Capu to membranes leads to disrupted posterior pole during mid-oogenesis

The actin mesh, microtubule organization and *oskar* localization are tightly correlated (Babu et al., 2003; Dahlgaard et al., 2007; Glotzer et al., 1997; Krauss et al., 2009; Serbus, 2005). In both *spir* and *capu* nulls, localization of polarity factors, including *oskar, nanos*, Vasa, and Staufen, is impaired (Dahlgaard et al., 2007; Ephrussi et al., 1991; Kim-Ha et al., 1991; Manseau and Schupbach, 1989; St. Johnston et al., 1991). A straightforward explanation is that delivery and maintenance fail due to disorganized microtubules and premature fast streaming. If this is the whole story, our analysis of the actin mesh and streaming in CapuJ-GFP-expressing flies would lead to the prediction that localization of polarity factors would not be altered. Nevertheless, we decided to inspect polarity determinant localization.

The altered localization pattern of CapuJ-GFP, including enrichment at the posterior oocyte cortex (Figure 3-S1D), and oocyte-nurse cell interface during mid-oogenesis, motivated us to examine both anterior and posterior factors. We used smiFISH (Calvo et al., 2021; Lu et al., 2023; Tsanov et al., 2016) to label polarity determinants, *gurken (grk)* and *bicoid (bcd)* at the anterior oocyte and *oskar (osk)* at the posterior, specifically in mid- to late-stage 9 egg chambers. We observed no difference in mRNA localization at the anterior when compared to wildtype (Figure 3-S3). This is consistent with previous studies that implicate microtubules in localization and anchoring of *grk* and *bcd* (Jaramillo et al., 2008; Trovisco et al., 2016; Weil et al., 2006).

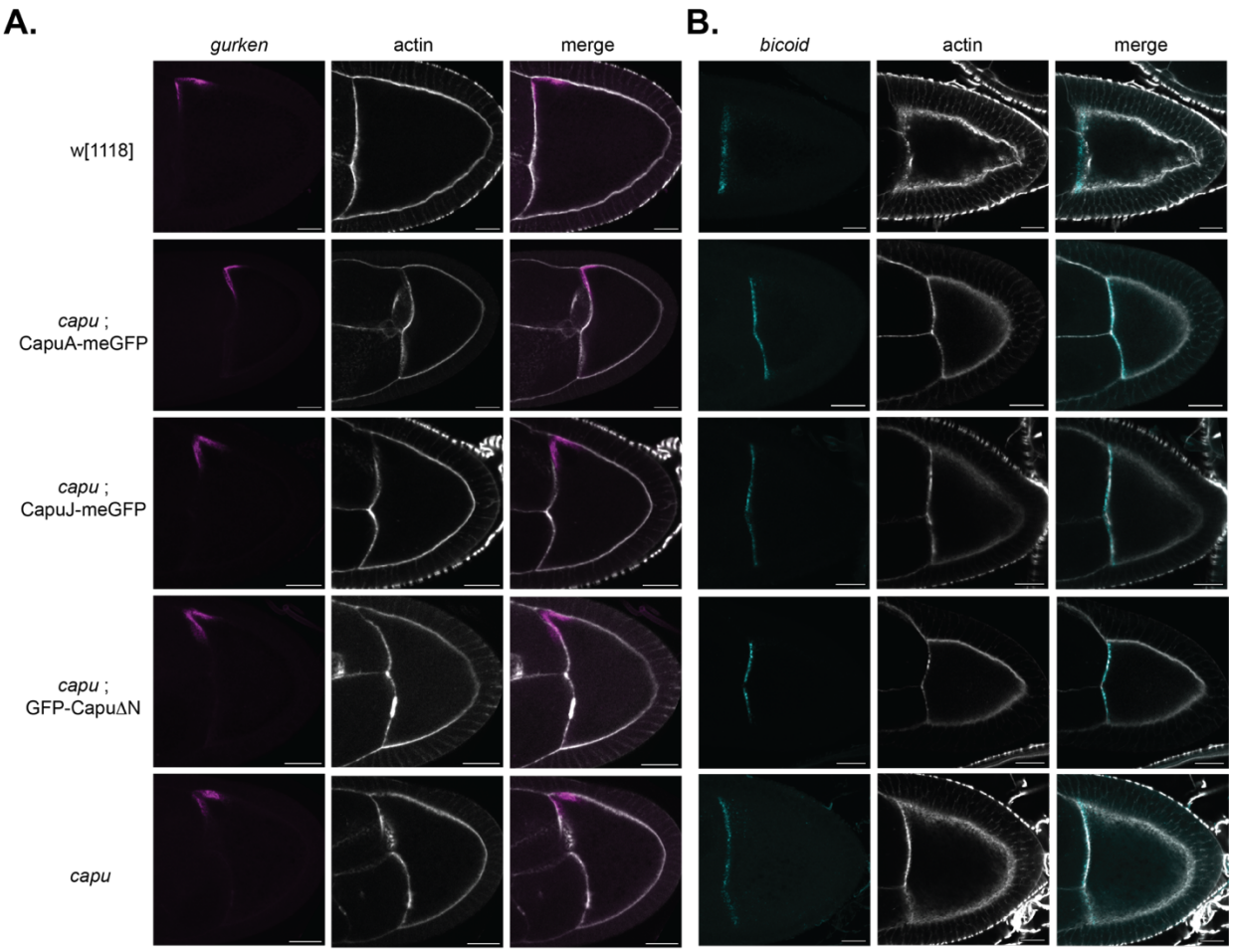

Figure 3-S3: Anterior mRNA localization is unaffected by altering Capu within the Drosophila egg chamber.

(A.) gurken mRNA localization was evaluated in stage 9 oocytes using smiFISH (Lu et. al, 2023). Cy3-labeled FLAP-X smiFISH probes recognized the entire mRNA sequence of grk. Scale bars: 20μm. (B.) bicoid mRNA localization was evaluated in stage 9 oocytes using smiFISH (Lu et. al, 2023). Cy3-labeled FLAP-X smiFISH probes recognized the 3'UTR of bcd. Scale bars: 20μm.

In contrast, *osk* mRNA at the posterior oocyte is altered in the CapuJ-GFP rescue background (Figure 3-3A). In stage 9 wildtype egg chambers *osk* is tightly localized to the posterior cap. Posterior localization of *osk* is completely lost if fast streaming is premature – as observed in *capu* null oocytes (Figure 3-3A). When CapuJ-GFP was expressed, we observed a localization pattern that differed from wildtype but was not nearly as dramatic as seen in the *capu* null. To describe and compare the localization patterns we measured the intensity profile of the smiFISH signal around the oocyte cortex (Figure 3-S4) and along the anterior/posterior axis in the center of the oocyte (Figure 3-3B). For all rescue backgrounds the localization of *osk*

around the cortex exhibited a greater spread at the posterior (Figure 3-S4). The most striking difference was observed in the anterior to posterior (AP) localization of *osk*. To characterize these differences, we measured the distance of the intensity peak from the posterior oocyte (distance), the full width of the intensity signal at half max (FWHM) and the amplitude of the intensity signal for each genotype (average amplitude). Wildtype *osk* was closely localized to the posterior oocyte (distance = 0.035, FWHM = 0.054) at high intensity (average amplitude 0.811) (Figure 3-3B-B'). CapuA-GFP and GFP-CapuΔN rescue had similar localization patterns to each other, with an increased spread (FWHM was twice that of wildtype, 0.12, Figure 3-3B-B'). The peak intensity was also shifted twice as far from the posterior (distance = ~0.8) with an overall 20% reduction in peak amplitude (average amplitude = ~0.65) (Figure 3-3B-B'). CapuJ-GFP rescue oocytes had the most dramatic changes in the AP localization pattern of *osk* (Figure 3-3B-B'). *osk* on average was reduced by 40% in intensity (average amplitude = 0.46) with a fourfold increase in distance from the posterior (distance = 0.15) and threefold increase in spread (FWHM = 0.17) in comparison to wildtype oocytes (Figure 3-3B-B'). To determine what was causing the spread in the average peak intensity, we analyzed individual oocyte trace data (Figure 3-3C-C'). From this we discerned that the average reduction was due to a significant difference in peak distance from the posterior (Figure 3-3C', p=2.02E-08) as opposed to increased spread of *osk* in individual oocytes (Figure 3-3C). This suggests that osk mRNA is organized but not tightly anchored at the posterior. It is also consistent with the distance from the posterior contributing more to fertility defects versus cortical spread.

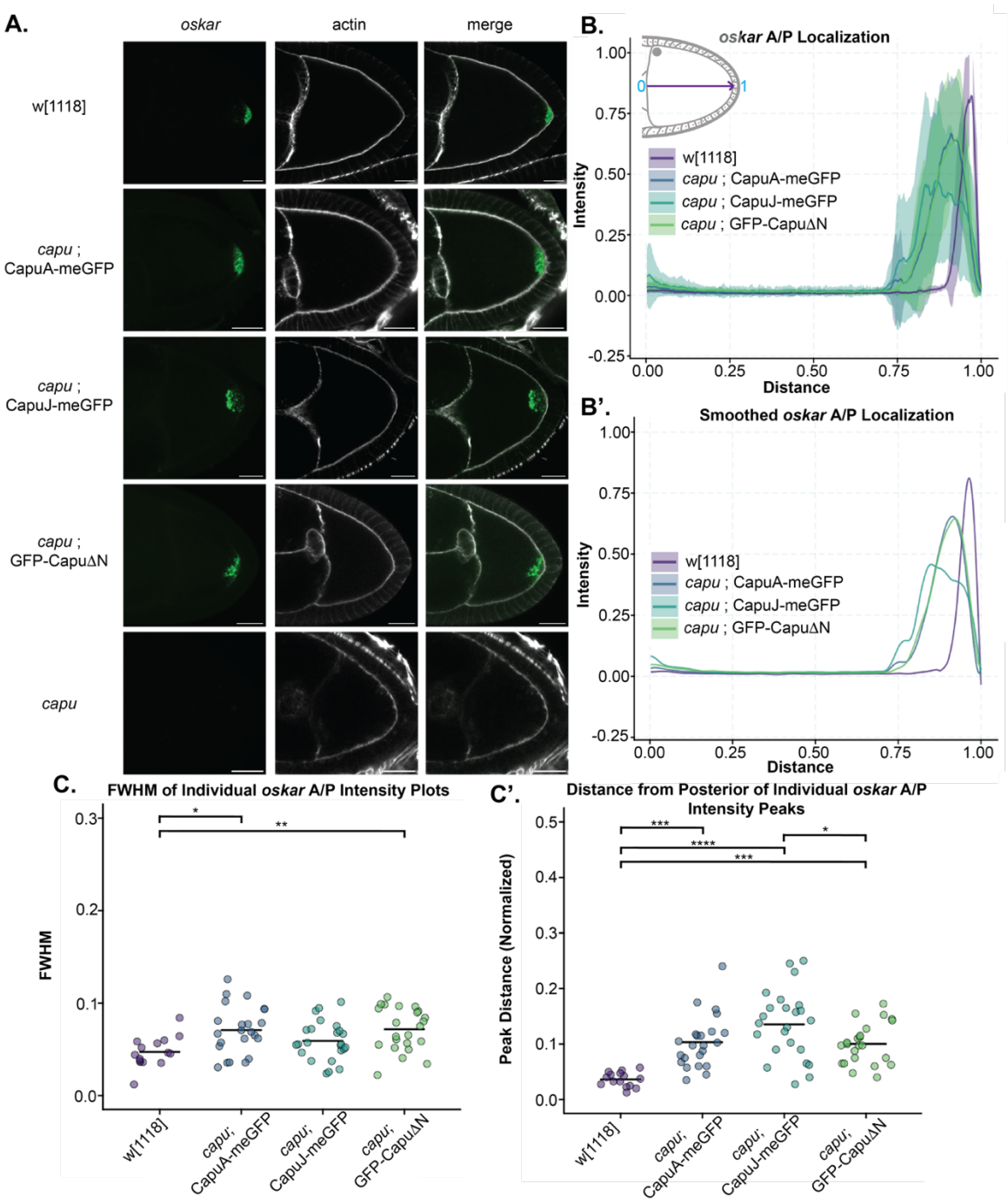

Figure 3-3: Expression of membrane bound Capu results in defected posterior mRNA localization.

*(A.) oskar mRNA localization was evaluated in stage 9 oocytes using smiFISH (Lu et. al, 2023). Cy3-labeled FLAP-X smiFISH probes recognized the 3'UTR of osk mRNA. To determine the localization within the oocyte, AlexaFluor647 Phalloidin was used as a counterstain. Scale bars: 20μm. (B.) Quantification of intensity line scans from the anterior to posterior oocyte for all genotypes overlaid. The anterior/posterior distance was from the nurse cell-oocyte interface to the posterior oocyte cortex-anterior follicle cell border. (B') Smoothed averages of individual genotype scans, a Savitzky-Golay filter was applied. (C) The full width of the peak intensity at half max of oskar in CapuJ rescue oocytes is not significantly different from wildtype. (C') Analysis of individual peaks, the distance from the posterior oocyte shifted significantly with CapuJ rescue in comparison to wildtype (p****, 2.025E-08). Wildtype (w[1118]) n= 15, CapuA rescue n = 23, CapuJ rescue n = 25, CapuΔN rescue n = 23. capu null oocytes were not analyzed for localization pattern due to the lack of signal within the oocytes at stage 9.*

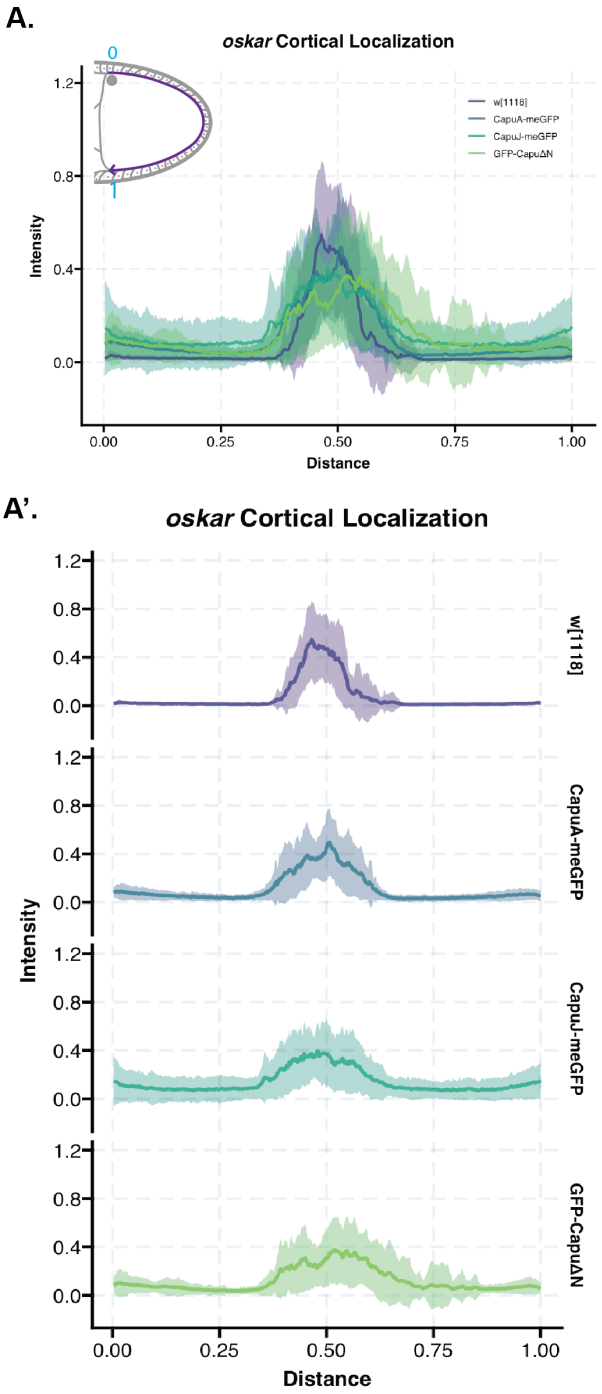

Figure 3-S4: oskar mRNA localization around the cortex is not significantly different between Capu rescue backgrounds.

(A.) Quantification of normalized intensity line scans around the oocyte cortex for all genotypes overlaid. Rescue oocytes exhibit a decreased posterior intensity with greater spread, compared to wildtype oocytes. (A') Individual genotype scans, average (solid line) with the standard deviation. Wildtype (w[1118]) n= 15, CapuA rescue n = 23, CapuJ rescue n = 25, CapuΔN rescue n = 23. capu null oocytes were not analyzed for localization pattern due to the lack of signal within the oocytes at stage 9.

When osk localization is disrupted, translation may not occur (Rongo et al., 1995). As the osk peak intensity was so variable with the CapuJ rescue we asked if osk was translated. If protein were absent in ~50% of egg chambers, we would have an explanation for infertility in the CapuJ-GFP background. However, immunofluorescence showed no failure to produce Oskar within the CapuJ-GFP rescue (Figure 3-S5). Oskar localization patterns are similar to mRNA localization patterns during stage 9 (Figure 3-3). When fast streaming begins Oskar that is not anchored can be swept away but there was no apparent difference in retention of Oskar protein at the posterior.

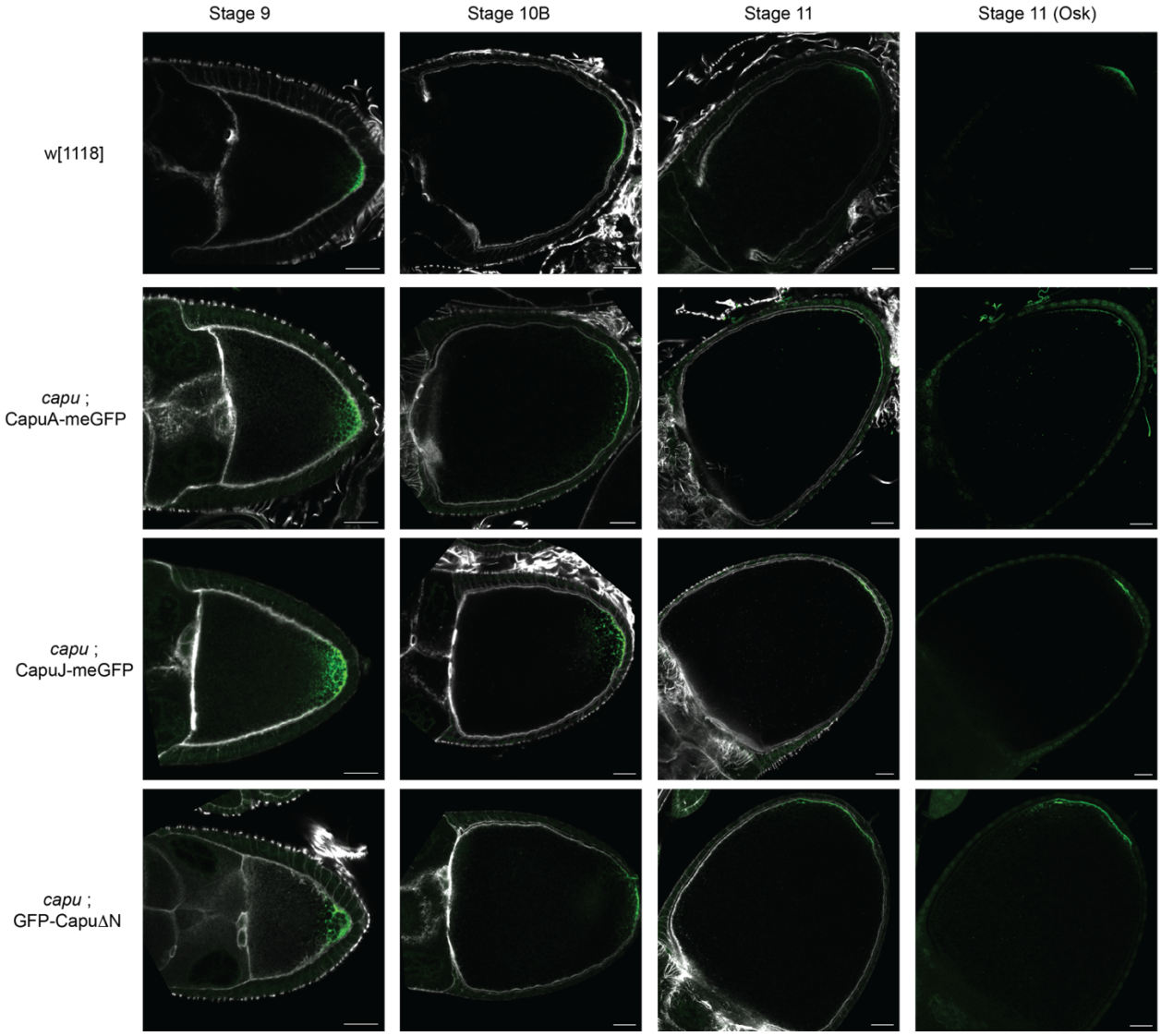

Figure 3-S5: Oskar translation occurs when Capu localization is altered.

(A.) Staining for Oskar (1:3000, gift from Ephrussi Lab) at mid (stage 9) and late oogenesis at the onset (stage 10B) and as streaming velocity increases (stage 11). At all stages and in all rescues, Oskar is present. Scale bars: 20μm.

MyoV is the major actin motor involved in mRNA localization at the posterior. Its direct competition with Kinesin-1 within the oocyte is important for transport, eventually taking over in the directed transport of mRNAs into the posterior and anchoring the transcripts, particularly *osk,* during mid-oogenesis (Krauss et al., 2009; Lu et al., 2020). Motor activity of MyoV is directional, migrating towards the growing barbed end of actin filaments and as a consequence

is influenced by the orientation of actin filaments within the oocyte. We asked if MyoV localization was altered when Capu remains bound to membranes in the oocyte. We observed a slight disruption of MyoV localization at the posterior in CapuJ-GFP rescues (Figure 3-4A). The localization around the cortex is consistent between all genetic backgrounds (Figure 3-S6B). The AP localization in CapuJ-GFP oocytes is spread slightly further towards the anterior (Figure 3-4B). Measurement of the spread of MyoV signal revealed CapuJ has approximately a 40% greater anterior spread (FWHM = 0.1) compared to wildtype MyoV localization (FWHM = 0.06). CapuA-GFP rescue also exhibited a less dramatic spread of signal towards the anterior on average (FWHM = 0.075) (Figure 3-4C'). In contrast, *capu* null oocytes fail to establish a posterior anchor (Figure 3-S6). Together, these data are consistent with altered *osk* mRNA and protein localization within the stage 9 oocyte and an altered posterior anchor organization due to membrane-bound Capu.

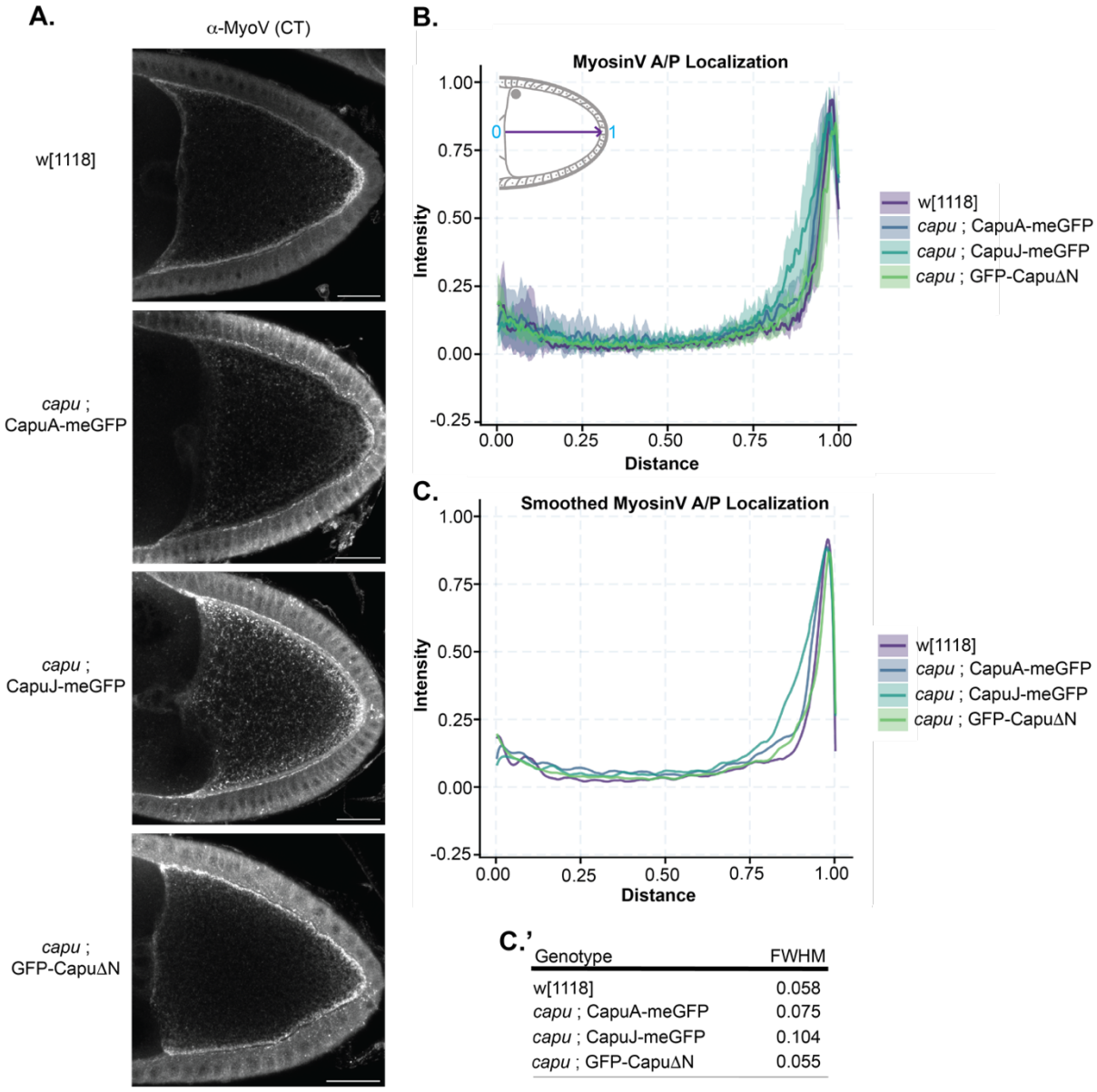

C.'

Genotype	FWHM
w[1118]	0.058
capu ; CapuA-meGFP	0.075
capu ; CapuJ-meGFP	0.104
capu ; GFP-CapuΔN	0.055

Figure 3-4: MyosinV at the posterior is slightly altered when expressing membrane bound Capu.

(A.) MyosinV localization was evaluated in stage 9 oocytes using immunofluorescence, using MyosinV-CT rabbit antiserum (Gift from the Ephrussi Lab). Scale bars: 20μm. (B.) Quantification of intensity line scans from the anterior to posterior oocyte for all genotypes overlaid. The anterior/posterior distance was from the nurse cell-oocyte interface to the posterior oocyte cortex-anterior follicle cell border. (C) Smoothed averages of individual genotype scans, a Savitzky-Golay filter was applied. (C') From this the full width of the curves at half max (FWHM) were determined. Wildtype (w[1118]) n= 6, CapuA rescue n = 10, CapuJ rescue n = 10, CapuΔN rescue n = 8.

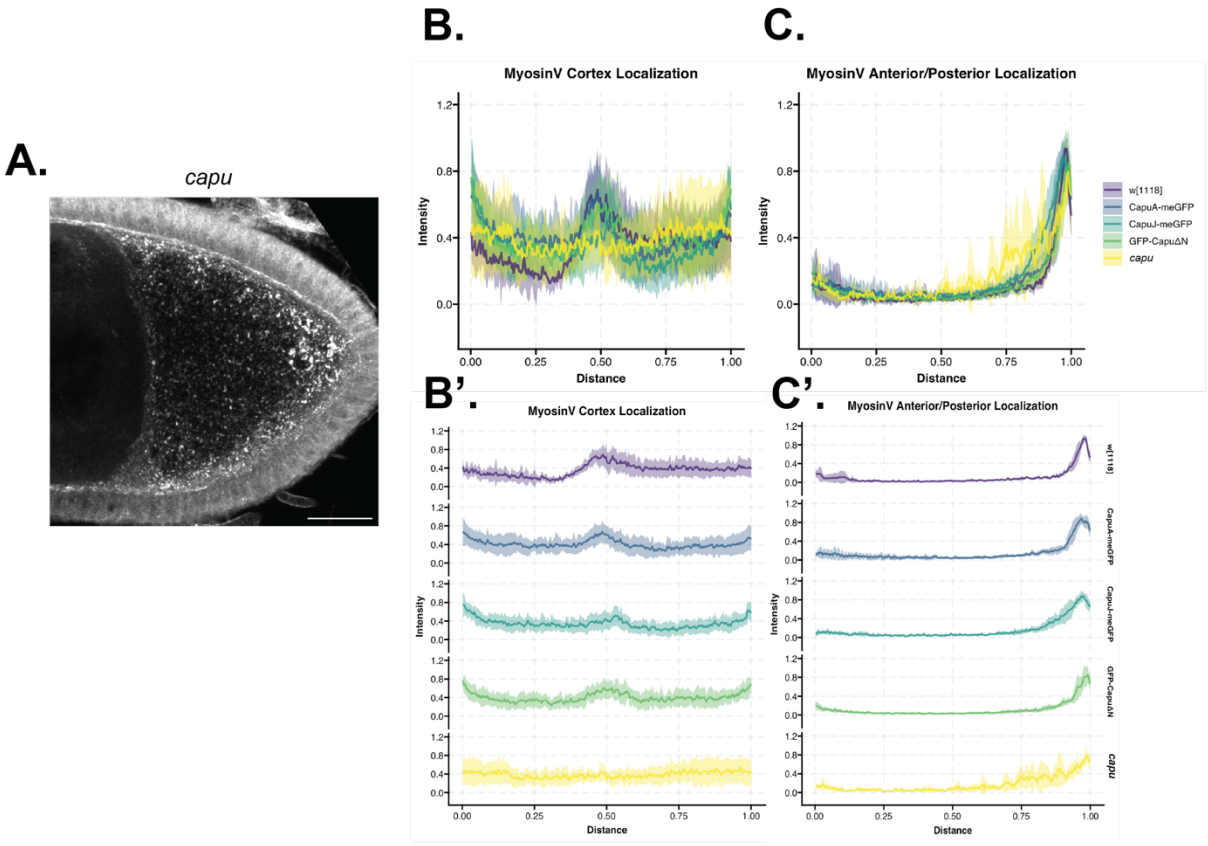

Figure 3-S6: MyosinV distribution is significantly disrupted in capu null oocytes.

(A) MyosinV localization in capu null stage 9 oocytes using immunofluorescence, using MyosinV-CT rabbit antiserum (gift from the Ephrussi Lab). Scale bar: 20µm. (B.) Quantification of intensity line scans around the oocyte cortex for all genotypes overlaid, with data from Figure 3-6. The localization is similar for wildtype and Capu rescue backgrounds. The posterior cap increase is lost in capu null oocytes (yellow line). (B') Individual genotype scans of cortical localization, average (solid line) with the standard deviation. Wildtype (w[1118]) n= 6, CapuA rescue n = 10, CapuJ rescue n = 10, CapuΔN rescue n = 8, capu null = 7. (C.) Quantification of intensity line scans from the anterior to posterior oocyte for all genotypes overlaid. capu null data are the yellow line. The anterior/posterior distance was from the nurse cell-oocyte interface to the posterior oocyte cortex-anterior follicle cell border. (C') Individual genotype scans of anterior/posterior scan, average (solid line) with the standard deviation Wildtype (w[1118]) n= 6, CapuA rescue n = 10, CapuJ rescue n = 10, CapuΔN rescue n = 8, capu null = 7.

Failed rescue with myristoylated Capu is not a classic posterior-group phenotype

Given the disruption to *osk* anchoring but apparent recovery of Oskar localization, we asked if posterior patterning was functionally rescued by looking at cuticles of offspring from the rescue lines. While CapuA-GFP cuticles were indistinguishable from those of wildtype, the preparations for CapuJ-GFP and GFP-CapuΔN embryos failed, repeatedly. They seemed to lack larvae inside their eggshells that were sufficient to withstand cuticle preparation.

Preliminary examination suggests that many offspring do not complete embryogenesis with these rescues.

As an alternate approach, we examined germ cell formation. Germ cell precursors are formed at the oocyte posterior and the process is highly sensitive to disruption of posterior axis determinants; proper localization of Oskar as well as mRNA binding proteins, Vasa, Tudor, and Aubergine are required (Santos and Lehmann, 2004). Penetrance of this phenotype is often evident even if fertility of the parental line and/or the body axes of the offspring are not strongly impacted. That is, female flies with mutations in classical posterior-group genes are grandchildless. We, therefore, asked whether the disruption in posterior organization we observed was hindering pole cell formation. The F1 offspring were crossed to wildtype males and their ovaries were examined as a bulk readout of pole cell formation. Wildtype ovary pairs were less frequently observed in the offspring of both CapuA-GFP and CapuJ-GFP rescues (averages of 68% and 84%, respectively) (Figure 3-5). However, given that the CapuJ-GFP offspring had wild type ovaries more often than the CapuA-GFP offspring, we conclude that fertility loss does not reflect a classical posterior-group phenotype. That is, while rescuing oogenesis with membrane bound CapuJ-GFP led to observed differences in the posterior pole, the flies that matured to adulthood were not “escapers” that exhibit signs of posterior defects; body patterning was correct and pole cells still formed.

The phenotype of GFP-CapuΔN rescue was more consistent with that of a traditional grandchildrenless phenotype. For the GFP-CapuΔN rescue, only 33% of offspring had wildtype ovaries (Figure 3-5). Even more had only one ovary. Thus, we conclude that GFP-CapuΔN failed to rescue fertility by a different mechanism than GFP-CapuJ. Apparently, hyperactivity, due to loss of autoinhibition, is more detrimental than mislocalization of Capu.

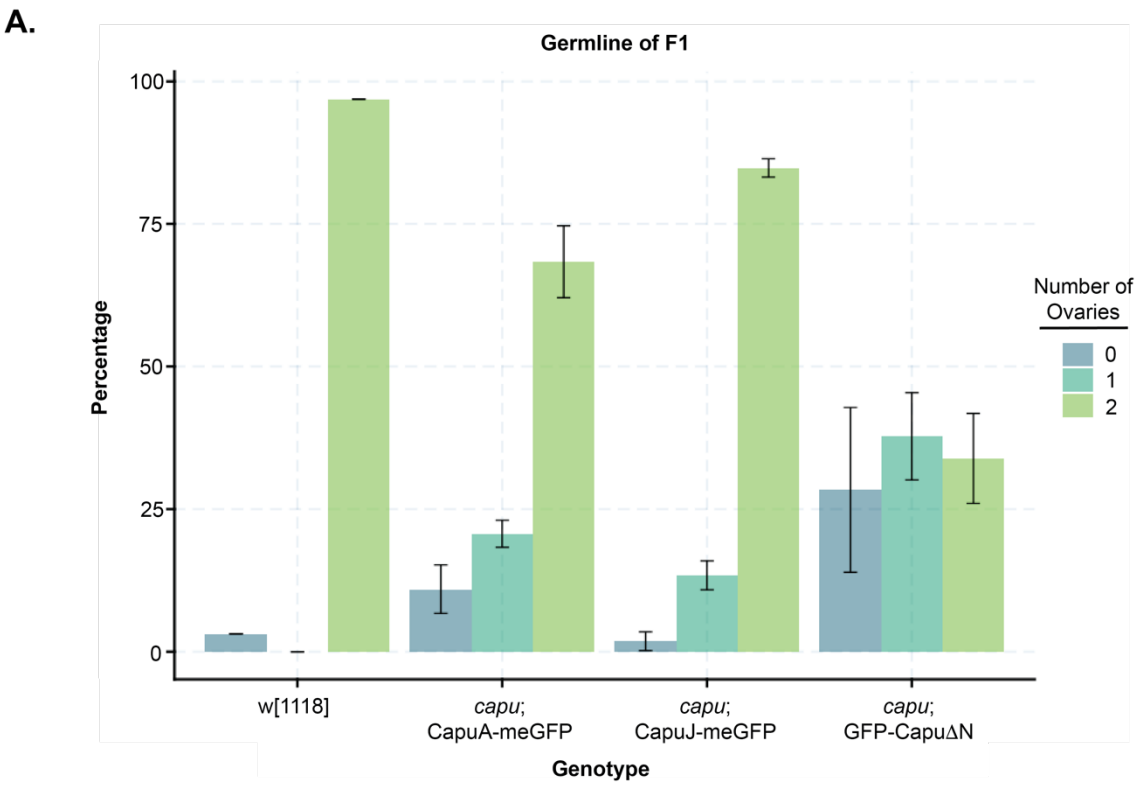

Figure 3-5: Membrane bound Capu rescue does not exhibit characteristics of the posterior group phenotype.

(A.) Progeny derived from CapuA or CapuJ rescue females do not show a significant decrease in germline development. Progeny females (F1) from the CapuA (Df(2L)ed^{1}/capu-Gal4-K10; UASp::CapuA-meGFP/+) and CapuJ (Df(2L)ed^{1}/capu-Gal4-K10; UASp::CapuJ-meGFP/+) rescue were crossed to wildtype (w[1118]) males and the offspring were allowed to develop. Dissected ovaries were classified as wildtype (two healthy ovary pairs, 2/light green), one ovary (where one ovary appeared wildtype in size and the other shrunken, 1/teal), or none (where when dissected there is somatic tissue but no germ cells are housed in the tissue, 0/blue). Wildtype (w[1118]) n= 32, CapuA rescue n = 130, CapuJ rescue n = 107, CapuΔN rescue n = 116.

Is the function of Capu at the posterior independent of Spir?

Spir and Capu function together to build the actin mesh during mid-oogenesis (Dahlgaard et al., 2007; Quinlan, 2013). Given that CapuJ-GFP localization is so different from CapuA-GFP but still builds a functional mesh, we asked if it impacts Spir localization. To better determine where Spir is localized, we used Crispr/Cas9 to add either smGFP-HA (Nern et al., 2015) or mScarlet-HA at the C-terminus. Fertility rates of females expressing homozygous Spir edits were 88% and 94%, respectively. As observed with immunofluorescence and similar to transgene localization, Spir is enriched at the oocyte cortex (Figure 3-S7A). Furthermore, we were able to confidently identify Spir-positive punctae which we presume to be vesicles. These

punctae are found throughout the oocyte but at higher concentrations near the cortex (Figure 3-S7B). Like Capu, we observed Spir expression in the border cells. We also observed Spir in the follicle cells surrounding the oocyte (Figure 3-S7A,B). Interestingly, the concentration of Spir at the posterior of the oocyte is lower than other places. We first noticed the decrease in Spir signal when comparing Spir and Capu localization. (Figure 3-6B, Figure 3-S7C). The decrease in posterior Spir was consistent in both endogenously tagged lines. Comparison of rescue with CapuA-GFP and CapuJ-GFP shows no apparent difference in Spir localization pattern (Figure 3-6), suggesting that Capu is not determining Spir localization. Decreased Spir at the posterior cortex and the fact that Spir localization is not impacted by the Capu isoform could indicate that Capu works independently of Spir at this location. Of note, now that we know that Spir is expressed in the follicle cells, in addition to the oocyte, further work is required to determine if this decrease is in one or both of these cell types.

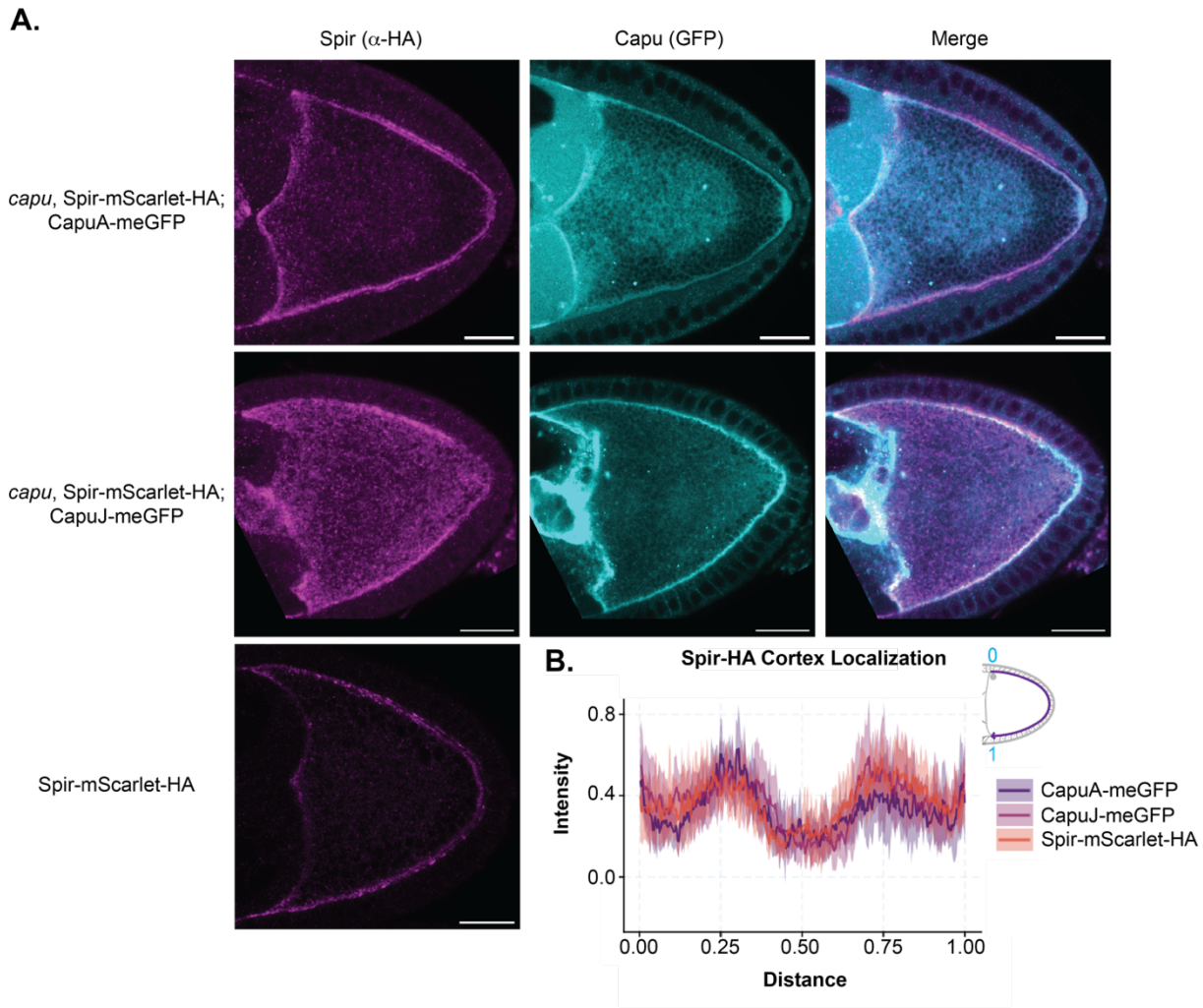

Figure 3-6: The posterior function of Cappuccino is potentially independent of Spire.

(A.) Co-imaging of stage 9 egg chambers expressing Capu-GFP (direct fluorescence of the transgene) or wildtype Capu and Spir-mScarlet-HA (endogenous tag, α-HA). There is a striking lack of Spir at the posterior end of the oocyte. Scale bars: 20μm. (B.) Quantification of Spir signal around the cortex of the oocyte. This shows a dip in intensity at the posterior in all backgrounds. Wildtype Capu background (Spir-mScarlet-HA) n= 9, CapuA rescue n = 7, CapuJ rescue n = 8.

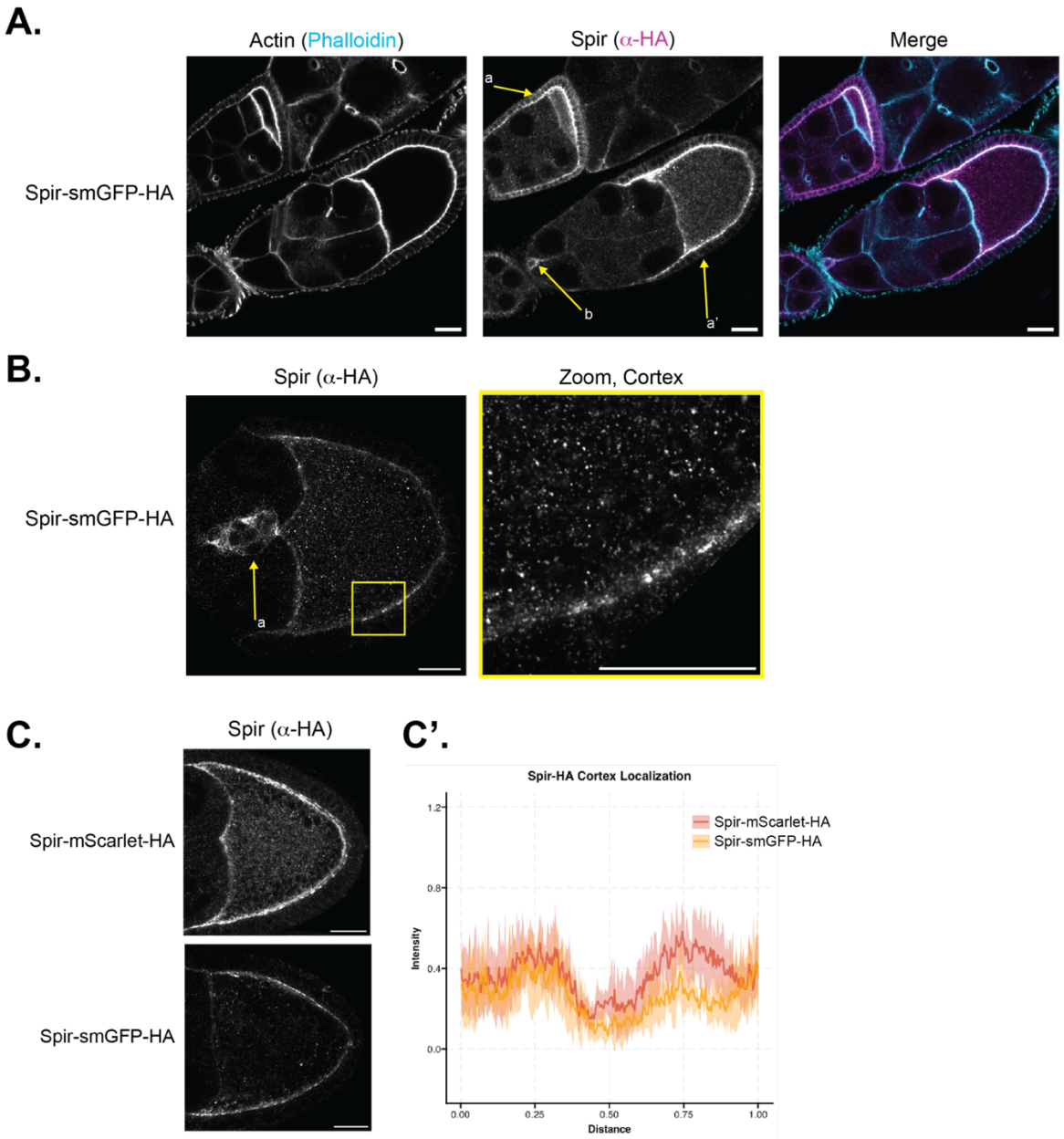

Figure 3-S7: Interrogation of Spir's localization in the developing egg chamber.

(A.) Immunofluorescence of endogenously tagged Spir. Signal is observed in the oocyte, follicle cells (arrows a, a') and migrating border cell cluster (arrow b). Counterstained with phalloidin to label actin. Scale bars: 20μm. (B.) Immunofluorescent imaging of endogenously tagged Spir in a stage 9 egg chamber using super resolution microscopy. Clear localization is observed in the migrating border cell cluster. Zooming in at the cortex (yellow box) reveals punctate signal along the membrane and in the cytoplasm. Scale bars: 20μm.(C.) Representative images, (Spir-HA, anti-HA 1:1000, CST) and (C') quantification of spir signal around the cortex of the oocyte. This shows a dip in intensity at the posterior with all endogenously tagged Spir generated. Wildtype Capu backgrounds; Spir-mScarlet-HA n= 9, Spir-smGFP-HA n = 7.

Discussion

In the developing mouse and fly oocytes, Spir and Capu (FMN2) fill the cytoplasm with an actin mesh (Azoury et al., 2008; Dahlgaard et al., 2007; Schuh and Ellenberg, 2008). FMN2 colocalizes with Spir on vesicles in the mouse oocyte (Pfender et al., 2011). We now confirm that Capu is not enriched with Spir on vesicles in the *Drosophila* oocyte. As suggested by transgene expression, endogenously edited genes reveal diffuse localization of Capu throughout the *Drosophila* oocyte (Figure 3-S1). We also detected relatively strong expression of Capu in specialized somatic cells, including the border cells and polar cells (Figure 3-S1). We did not pursue this observation, however, because our rescue experiments demonstrated that germline expression is sufficient for oogenesis (Table 3-1, CapuA rescue).

Localization of Spir and Capu is independent of one another within the *Drosophila* oocyte, as demonstrated by the lack of colocalization and the unaltered localization of Spir when CapuJ is expressed and enriched at membranes (Figure 3-6). We would not have predicted this independence based on their colocalization in the mouse oocyte and our finding that Spir is sufficient to drive Capu localization in S2 cells (Pfender et al., 2011; Vizcarra et al., 2011). Further, genetics demonstrate that the pair of actin nucleators must physically interact to function in *Drosophila* oogenesis (Quinlan, 2013). Together, these observations raise the questions of when, where, and for how long Spir and Capu interact? The data suggest that the interactions are transient and that Capu elongates barbed ends of filaments away from Spir-enriched surfaces (Bradley et al., 2019), which would likely impact the function of the structures built. Given that Spir and Capu bind with nanomolar affinity in vitro (Vizcarra et al., 2011), the data also suggest that the interactions are somehow down regulated in the oocyte. It follows that this regulatory mechanism is absent in S2 cells. Finally, the distinct localizations suggest that Spir and Capu may not always function as a team. If so, do one or both of these nucleators build structures other than the mesh? It has been difficult to address this question, as premature

fast steaming due to absence of the actin mesh has such drastic consequences on development.

We were particularly intrigued to detect a marked decrease in Spir intensity at the posterior of the oocyte, despite no change in Capu along the cortex (Figure 3-6). Even more intriguing, if CapuJ was the isoform of Capu expressed, we observed displacement of *osk* mRNA during mid oogenesis (Figure 3-3). In fact, in all three rescue backgrounds, CapuA, CapuJ, and CapuΔN, the spread of *osk* around the cortex was broader than observed in wildtype oocytes (Figure 3-S4). We propose that the increased region or *osk* retention reflects a role for Capu in posterior anchoring. That is, the anchoring site is expanded due to high levels of expression of any of the Capu the transgenes. However, altered A/P localization of *osk* was distinct to CapuJ expression (Figure 3-3A). Mislocalization of *osk* at the posterior has been investigated in a number of genetic backgrounds. Proper organization of the cytoskeleton and motor activity is required to transport and anchor *osk* in a posterior cap. Mutants of par-1, khc, didum among others often result in *osk* at a central dot, reflecting failure to transport *osk* along properly organized microtubules and capture it with MyoV at the posterior (Cha et al., 2002; Doerflinger et al., 2006; Doerflinger et al., 2022; Krauss et al., 2009; Lu et al., 2020; Parton et al., 2011; Zimyanin et al., 2008). In the absence of Long Osk, *osk* spreads continuously from the posterior, reflecting failure to anchor (Vanzo and Ephrussi, 2002). The CapuJ phenotype is distinct from both of these. While the average location of osk was spread broadly during stage 9, within any individual oocyte, the *osk* was tightly gathered (Figure 3-3C). We interpret this as evidence that altering Capu geometry (by myristoylation) reveals a role for Capu in stabilizing but not building the actual “posterior landing platform”. We observe *osk* translation both at the posterior and at what we are referring to as the displaced posterior landing platform (Figure 3-S5). The fact that *osk* is translated indicates that functional organization of posterior determinants is accomplished. Development of germ cells and deviation from typical posterior

group phenotypes further strengthens this interpretation. In the future, it will be important to identify the minimal elements of the landing platform.

Finally, if posterior determination is slightly perturbed but ultimately functional, why is fertility decreased when CapuJ is expressed? There could be additional structures built by Capu that are defective. There are previous reports of long posterior actin filaments that are induced by Long Oskar and Capu during mid-oogenesis that further anchor Short Oskar for continual delivery of posterior pole plasm components (Chang et al., 2011; Tanaka et al., 2011). We would assume that by greatly increasing the localization of Capu to the posterior oocyte (Figure 3-S1) that we would see a dramatic increase in filament formation. We were unable to observe such a phenomenon. Perhaps, this is due to technical challenges in distinguishing these filaments from the mesh. We also note that a recent publication suggests the previously described posterior actin filaments are projections, filopodia from the surrounding follicle cells (Mallart et al., 2024). Alternatively, decreased fertility could imply that the mesh has another role that cannot be effectively performed when built with CapuJ-GFP. This role would be in addition to limiting microtubule movement and regulating the transition from slow to fast streaming.

Materials and Methods

Drosophila Line Generation

CRISPR: Spir-mScarlet-HA

Spir was tagged with mScarlet-HA (mScarlet-HA) at its endogenous locus using CRISPR/Cas9 mediated homologous recombination. To generate tagged flies, we followed a combined approach using dual gRNA sequences (Bence et al., 2017)and short homology arms (Kanca et al., 2019). gRNA sequences for the C-termini of Spir (5’ GTCGGCCCTGGATCTGACGCCCGTC 3’) and following the 3’UTR (5’ GTCGGCAAACTAAAGAACAAGATTC 3’) were selected using the CRISPR Optimal Target finder (http://targetfinder.flycrispr.neuro.brown.edu/index.php). Oligonucleotides were cloned

into pCFD3-dU6:3gRNA (Addgene #49410) and cloned using the previously designed strategy (Port et al., 2014). 200nt homology sequences with the PAM removed were cloned into homologous recombination vector, a self-linearizable Puc57 (Kanca et al., 2019). The repair template includes a C-terminal mScarlet-HA, the endogenous 3'UTR of Spir, and they fluorescent eye reporter 3xP3_dsRed flanked by two PiggyBac recombinase sites. Plasmids expressing the guide RNAs and donor template were mixed and co-injected in embryos *nos-Cas9* embryos (BDSC 78782,(Ren et al., 2013)) at concentrations of 100ng/μL and 250ng/μL respectively. Offspring were screened via fluorescence of the 3xP3_dsRed for integration of the repair within the genome. Clones were balanced on chromosome II and Cas9 expressing chromosome removed. All injections and initial screening were completed by BestGene (Chino Hills, CA). Proper insertion of mScarlet-HA was confirmed via genomic PCR (forward primer: 5'GGGGATTCAACCTGTTCTCCT 3', reverse primer: 5'TGTGCAAGTGCGTTCTGAAG 3') and western blot prior to further experimentation.

UASp::CapuJ-meGFP-K10 Generation

CapuJ-meGFP transgene was generated by modifying our CapuA-meGFP expression vector. The coding sequence of CapuA-meGFP was amplified from pTIGER (Quinlan, 2013) lacking the first 238bp (N-terminal exon) to generate a generic Capu-meGFP plasmid in pDONR221. A gene fragment containing the first 326bp of CapuJ (CG93399-RJ) were cloned into the N-termini at a XhoI site. The insert was cloned into pPw (DGRC 1130) modified to include attB,pPw-attB1 via LR reaction. The final plasmid was then integrated at the attP2 landing site by BestGene.

capu-Gal4-K10 Generation

capu-Gal4-k10 driver was generated by fist adding the K10 3' UTR terminator site to replace the Hsp70 3'UTR within the Trojan-Gal4 plasmid, pBS-KS-atB2-SA(0)-T2A-Gal4 (Addgene, Plasmid

#62899). This plasmid was then sent for injection to be integrated in the MiMIC landing site of Capu, MI057537.

Other Drosophila Stocks

UASp::CapuA-meGFP-K10 (Quinlan, 2013), UASp::GFP-Capu-ΔN (Gift from St. Johnson lab (Dahlgaard et al., 2007)), w[1118] (Bloomington, BDSC 3605), Df(2L)ed1/CyO (Bloomington, BDSC 5330)

Fertility Assays

Approximately 100 test females were crossed to 50 wild-type (wt) males and raised on apple plates for 2 nights at 25°C. On day 3, to synchronize egg laying, flies were pre-cleared on a fresh apple plate containing yeast paste for 1.5 hours. The plate was changed, also containing yeast paste, and eggs laid over the following 3-hour time period were collected. Approximately 200 eggs were laid during that window. Eggs were moved to a fresh apple plate using a paint brush and incubated at 25°C for 24 hours. The number of eggs that hatched during that window were recorded. Each trial was repeated with independent crosses three times. The data reported in the table is an average across the three trials to get the fertility rate.

F2 Ovary Dissection/Germline Perdurance

Approximately 15 F2 females, progeny of the test flies, were crossed to 7 wild-type males. Female progeny from these crosses were then collected, aged to 3 days post-eclosion, and fattened overnight at 25°C. Their ovaries were then dissected in 1XPBS and classified in three categories: wildtype (two average size ovaries), 1 ovary, (one ovary with one shrunken ovary), or 0 ovaries (somatic tissue/both shrunken). Each trial was repeated with independent crosses three times. The data reported in the graph is an average across the trials, error bars are +/- one standard deviation.

Microscopy and staining

All microscopy images, live and fixed, were collected on a Zeiss LSM 780 confocal microscope. Flies were raised at 25°C and fed yeast paste for 16-24 hours prior to imaging.

The actin mesh was stained as described (adapted from (Dahlgaard et al., 2007; Quinlan, 2013)) using 1μM AlexaFluor488-phalloidin (Thermo Fisher Scientific, A12379) or 1μM AlexaFluor647-phalloidin (Thermo Fisher Scientific, A22287) for 45minutes.

Immunofluorescent staining of the HA (Spir-mScarlet-HA) and MyosinV was performed by dissecting ovaries in cold 1XPBS, and fixing in 5% PFA (Electron Microscopy Solutions, 15714), diluted in 0.16X PBS with Heptane, protocol is modified from (Robinson and Cooley, 1997). Samples were stained with 1:1,000 rabbit anti-HA (C29F4) (Cell Signaling Technology (CST), 3724S), 1:3,000 rabbit anti-Osk NT (gift from A. Ephrussi), or 1:500 rabbit anti-MyoV CT (gift from A. Ephrussi, preabsorbed with fixed and unblocked wildtype ovaries) respectively overnight at 4°C. 1:200 secondary was used, AlexaFluor568-Donkey α Rabbit (Invitrogen, A10042). Sometimes with AlexaFluor647-phalloidin counterstain (Thermo Fisher Scientific, A22287).

Live egg chambers were dissected under halocarbon 700 oil (Sigma-Aldrich, H8898). For GFP-fusion localization imaging, egg chambers were excited with 488 nm laser using 40X oil immersion objective. Images were captured at 1024x1024 resolution with 4 averaging. Z-stacks were collected with a range of 5-10 μm with 1 μm steps. Autofluorescent yolk granules were excited using UV 405nm laser. To track fluid flows, streaming, images were captured ever 5 seconds for a 5-minute duration. Maximum ‘z’-projections were created in Fiji for representation of motion throughout the movie for the oocyte.

Analysis of Streaming: Particle Image Velocimetry and Correlation Functions

Cytoplasmic streaming velocities were determined from confocal images using particle image velocimetry lab (PIV lab) MATLAB package generated by William Thielicke (Thielicke and Sonntag, 2021; Thielicke and Stamhuis, 2014).

ROIs were drawn around the oocyte and the background masked so only the area containing yolk (the oocyte cytoplasm) was interrogated. PIV algorithm used was FFT window deformation, a direct Fourier transformation correlation with multiple passes and deforming windows. The passes were interrogation areas of 30px with a 15px step (50%), decreasing to 20px and 10px. This allowed for interrogation areas that were specific to yolk and changing with pattern to be analyzed for each frame. Limits were selected to refine data, and PIV lab was permitted to interpolate missing data based on surrounding values. From this analysis the vector information was extracted for the motion stream and the mean streaming velocity was determined for each oocyte analyzed. Mid and late-stage oocytes were analyzed using this method.

Output raw files of vector information then further processed in custom Correlation analysis software, 2DVelocityCorrelation. Which can be found on GitHub (https://github.com/LiamABailey/2DVelocityCorrelation). Work was based off of (Dombrowski et al., 2004; Ganguly et al., 2012). For each frame of PIV, a correlation function was determined and then averaged to generate the correlation for the oocyte. For each oocyte we determined the maximal radius at which the vectors were half correlated and plotted in R using ggplot2. Statistics were run in R using rstatixs package, a one-way ANOVA with Tukey-Kramer post-hoc test to determine significance between genotypes. See graphs for information about p-values generated.

Quantification of Staining (Immunofluorescence and smiFISH)

To determine localization of *osk* mRNA, Spir-mScarlet-HA, and MyosinV, in the oocyte, images were analyzed using the line scan tool in Fiji. 5 or 10µm Z-stack data were collected as previously described above. A maximum intensity projection was made in FIJI. For mRNA localization analysis, the mRNA/Cy3 signal was overlayed with the actin staining to get bounds of the oocyte. Anterior to posterior oocyte (anterior follicle cell) lines were drawn, as well as around the oocyte cortex -excluding the anterior oocyte-nurse cell border. A line width of 20px was used and plotted intensity for the channel of interest. Data were saved from this, intensity and distances measured were normalized using python scripts. Data were then further analyzed in python and plotted in R using ggplot2. Averages for each genotype were smoothed using python, SciPy, Savitzky-Golay filter. From this the maximum peak metrics were determined: full width at half max and peak distance from the posterior oocyte.

Single-Molecule Inexpensive Fluorescence in situ Hybridization (smiFISH)

Was based off of (Calvo et al., 2021; Lu et al., 2023; Tsanov et al., 2016) and generously provided by Lu/Gelfand. Twenty-base-long DNA probes with complementarity to the mRNA *bcd* 3'UTR*, grk* whole mRNA sequence, and *osk* 3'UTR, with 3' FLAP-X complementary probe (5'-CCTCCTAAGTTTCGAGCTGGACTCAGTG-3′) were generated using LGC Biosearch Technologies' Stellaris RNA FISH Probe Designer (masking level five, minimal spacing two bases). 25 probes for each mRNA were ordered from Integrated DNA Technologies (IDT) (probe sequences are listed in Supplement, Table S1). Cy3-FlapX probe was also synthesized by IDT. Ovaries were hybridized in 2µL annealed probe diluted in prewarmed smiFISH Hybridization buffer overnight (>16h) at 37°C in the dark. Egg chambers were counterstained with 0.2µM AlexaFluor647-phallodin (Thermo Fisher Scientific, A22287) for 10 minutes and mounted on slides in Prolong Gold antifade with DAPI (Thermo Fisher Scientific, P36931).

References

Alexandre, C. (2008). Cuticle Preparations of Drosophila embryos and larvae. In *Drosophila: methods and protocols*, pp. 197–205.

Almonacid, M. and Verlhac, M.-H. (2021). A new mode of mechano-transduction shakes the oocyte nucleus, thereby fine tunes gene expression modulating the developmental potential. *C. R. Biol.* 343, 223–234.

Alzahofi, N., Welz, T., Robinson, C. L., Page, E. L., Briggs, D. A., Stainthorp, A. K., Reekes, J., Elbe, D. A., Straub, F., Kallemeijn, W. W., et al. (2020). Rab27a co-ordinates actin-dependent transport by controlling organelle-associated motors and track assembly proteins. *Nat. Commun.* 11, 3495.

Azoury, J., Lee, K. W., Georget, V., Rassinier, P., Leader, B. and Verlhac, M.-H. (2008). Spindle Positioning in Mouse Oocytes Relies on a Dynamic Meshwork of Actin Filaments. *Curr. Biol.* 18, 1514–1519.

Babu, K., Cai, Y., Bahri, S., Yang, X. and Chia, W. (2003). Roles of Bifocal, Homer, and F-actin in anchoring Oskar to the posterior cortex of *Drosophila* oocytes. *Genes Dev.* 18, 138–143.

Bence, M., Jankovics, F., Lukácsovich, T. and Erdélyi, M. (2017). Combining the auxin-inducible degradation system with CRISPR /Cas9-based genome editing for the conditional depletion of endogenous *Drosophila melanogaster* proteins. *FEBS J.* 284, 1056–1069.

Benson, D. A., Cavanaugh, M., Clark, K., Karsch-Mizrachi, I., Lipman, D. J., Ostell, J. and Sayers, E. W. (2012). GenBank. *Nucleic Acids Res.* 41, D36–D42.

Bor, B., Bois, J. S. and Quinlan, M. E. (2015). Regulation of the formin cappuccino is critical for polarity of *D rosophila* oocytes: Capu is Autoinhibited In Vivo. *Cytoskeleton* 72, 1–15.

Bradley, A. O., Vizcarra, C. L., Bailey, H. M. and Quinlan, M. E. (2019). Spire stimulates nucleation by Cappuccino and binds both ends of actin filaments. *Mol. Biol. Cell* 31, 273–286.

Calvo, L., Ronshaugen, M. and Pettini, T. (2021). smiFISH and embryo segmentation for single-cell multi-gene RNA quantification in arthropods. *Commun. Biol.* 4, 352.

Cha, B.-J., Serbus, L. R., Koppetsch, B. S. and Theurkauf, W. E. (2002). Kinesin I-dependent cortical exclusion restricts pole plasm to the oocyte posterior. *Nat. Cell Biol.* 4, 592–598.

Chang, C.-W., Nashchekin, D., Wheatley, L., Irion, U., Dahlgaard, K., Montague, T. G., Hall, J. and St. Johnston, D. (2011). Anterior–Posterior Axis Specification in *Drosophila* Oocytes: Identification of Novel *bicoid* and *oskar* mRNA Localization Factors. *Genetics* 188, 883–896.

Dahlgaard, K., Raposo, A. A. S. F., Niccoli, T. and St Johnston, D. (2007). Capu and Spire Assemble a Cytoplasmic Actin Mesh that Maintains Microtubule Organization in the Drosophila Oocyte. *Dev. Cell* 13, 539–553.

Doerflinger, H., Benton, R., Torres, I. L., Zwart, M. F. and St Johnston, D. (2006). Drosophila Anterior-Posterior Polarity Requires Actin-Dependent PAR-1 Recruitment to the Oocyte Posterior. *Curr. Biol.* 16, 1090–1095.

Doerflinger, H., Zimyanin, V. and St Johnston, D. (2022). The Drosophila anterior-posterior axis is polarized by asymmetric myosin activation. *Curr. Biol.* 32, 374-385.e4.

Dombrowski, C., Cisneros, L., Chatkaew, S., Goldstein, R. E. and Kessler, J. O. (2004). Self-Concentration and Large-Scale Coherence in Bacterial Dynamics. *Phys. Rev. Lett.* 93, 098103.

Emmons, S., Phan, H., Calley, J., Wenliang, C., James, B. and Manseau, L. (1995). cappuccino, a Drosophila maternal effect gene required for polarity of the egg and embryo, is related to the vertebrate limb deformity locus. *Genes Dev.* 9, 2482–2494.

Ephrussi, A., Dickinson, L. K. and Lehmann, R. (1991). oskar Organizes the Germ Plasm and Directs Localization of the Posterior Determinant nanos. *Cell* 66, 37–50.

Ganguly, S., Williams, L. S., Palacios, I. M. and Goldstein, R. E. (2012). Cytoplasmic streaming in Drosophila oocytes varies with kinesin activity and correlates with the microtubule cytoskeleton architecture. *Proc. Natl. Acad. Sci.* 109, 15109–15114.

Glotzer, J. B., Saffrich, R., Glotzer, M. and Ephrussi, A. (1997). Cytoplasmic flows localize injected oskar RNA in Drosophila oocytes. *Curr. Biol.* 7, 326–337.

Gutzeit, H. and Koppa, R. (1982). Time-lapse film analysis of cytoplasmic streaming during late oogenesis of Drosophila. *J. Embryol. exp. Morph* 67, 101–111.

Holubcová, Z., Howard, G. and Schuh, M. (2013). Vesicles modulate an actin network for asymmetric spindle positioning. *Nat. Cell Biol.* 15, 937–947.

Hudson, A. M. and Cooley, L. (2014). Methods for studying oogenesis. *Methods* 68, 207–217.

Jaramillo, A. M., Weil, T. T., Goodhouse, J., Gavis, E. R. and Schupbach, T. (2008). The dynamics of fluorescently labeled endogenous *gurken* mRNA in *Drosophila*. *J. Cell Sci.* 121, 887–894.

Kanca, O., Zirin, J., Garcia-Marques, J., Knight, S. M., Yang-Zhou, D., Amador, G., Chung, H., Zuo, Z., Ma, L., He, Y., et al. (2019). An efficient CRISPR-based strategy to insert small and large fragments of DNA using short homology arms. *eLife* 8, e51539.

Kerkhoff, E., Simpson, J. C., Leberfinger, C. B., Otto, I. M., Doerks, T., Bork, P., Rapp, U. R., Raabe, T. and Pepperkok, R. (2001). The Spir actin organizers are involved in vesicle transport processes. *Curr Biol* 11, 1963–8.

Kim-Ha, J., Smith, J. L. and Macdonald, P. M. (1991). oskar mRNA is localized to the posterior pole of the Drosophila oocyte. *Cell* 66, 23–35.

Krauss, J., López de Quinto, S., Nüsslein-Volhard, C. and Ephrussi, A. (2009). Myosin-V Regulates oskar mRNA Localization in the Drosophila Oocyte. *Curr. Biol.* 19, 1058–1063.

Leader, D. P., Krause, S. A., Pandit, A., Davies, S. A. and Dow, J. A. T. (2018). FlyAtlas 2: a new version of the Drosophila melanogaster expression atlas with RNA-Seq, miRNA-Seq and sex-specific data. *Nucleic Acids Res.* 46, D809–D815.

Lee, P.-T., Zirin, J., Kanca, O., Lin, W.-W., Schulze, K. L., Li-Kroeger, D., Tao, R., Devereaux, C., Hu, Y., Chung, V., et al. (2018). A gene-specific T2A-GAL4 library for Drosophila. *eLife* 7, e35574.

Lu, W., Lakonishok, M., Liu, R., Billington, N., Rich, A., Glotzer, M., Sellers, J. R. and Gelfand, V. I. (2020). Competition between kinesin-1 and myosin-V defines Drosophila posterior determination. *eLife* 9, e54216.

Lu, W., Lakonishok, M. and Gelfand, V. I. (2023). The dynamic duo of microtubule polymerase Mini spindles/XMAP215 and cytoplasmic dynein is essential for maintaining *Drosophila* oocyte fate. *Proc. Natl. Acad. Sci.* 120, e2303376120.

Mallart, C., Netter, S., Chalvet, F., Claret, S., Guichet, A., Montagne, J., Pret, A.-M. and Malartre, M. (2024). JAK-STAT-dependent contact between follicle cells and the oocyte controls Drosophila anterior-posterior polarity and germline development. *Nat. Commun.* 15, 1627.

Manseau, L. J. and Schupbach, T. (1989). cappuccino and spire: two unique maternal-effect loci required for both the anteroposterior and dorsoventral patterns of the Drosophila embryo. *Genes Dev.* 3, 1437–1452.

Nern, A., Pfeiffer, B. D. and Rubin, G. M. (2015). Optimized tools for multicolor stochastic labeling reveal diverse stereotyped cell arrangements in the fly visual system. *Proc. Natl. Acad. Sci.* 112, E2967–E2976.

Öztürk-Çolak, A., Marygold, S. J., Antonazzo, G., Attrill, H., Goutte-Gattat, D., Jenkins, V. K., Matthews, B. B., Millburn, G., dos Santos, G., Tabone, C. J., et al. (2024). FlyBase: updates to the Drosophila genes and genomes database. *Genetics* 227, iyad211.

Parton, R. M., Hamilton, R. S., Ball, G., Yang, L., Cullen, C. F., Lu, W., Ohkura, H. and Davis, I. (2011). A PAR-1–dependent orientation gradient of dynamic microtubules directs posterior cargo transport in the Drosophila oocyte. *J. Cell Biol.* 194, 121–135.

Pfender, S., Kuznetsov, V., Pleiser, S., Kerkhoff, E. and Schuh, M. (2011). Spire-Type Actin Nucleators Cooperate with Formin-2 to Drive Asymmetric Oocyte Division. *Curr. Biol.* 21, 955–960.

Port, F., Chen, H.-M., Lee, T. and Bullock, S. L. (2014). Optimized CRISPR/Cas tools for efficient germline and somatic genome engineering in Drosophila. *Proc. Natl. Acad. Sci. U. S. A.* 111, E2967–E2976.

Quinlan, M. E. (2013). Direct interaction between two actin nucleators is required in Drosophila oogenesis. *Development* 140, 4417–4425.

Quinlan, M. E., Heuser, J. E., Kerkhoff, E. and Dyche Mullins, R. (2005). Drosophila Spire is an actin nucleation factor. *Nature* 433, 382–388.

Ren, X., Housden, B. E., Hu, Y., Roesel, C., Lin, S., Liu, L.-P., Yang, Z., Mao, D., Sun, L., Wu, Q., et al. (2013). Optimized gene editing technology for Drosophila melanogaster using germ line-specific Cas9.

Robinson, D. N. and Cooley, L. (1997). *Drosophila* Kelch Is an Oligomeric Ring Canal Actin Organizer. *J. Cell Biol.* 138, 799–810.

Rongo, C., Gavis, E. R. and Lehmann, R. (1995). Localization of oskar RNA regulates oskar translation and requires Oskar protein. *Development* 121, 2737–2746.

Rosales-Nieves, A. E., Johndrow, J. E., Keller, L. C., Magie, C. R., Pinto-Santini, D. M. and Parkhurst, S. M. (2006). Coordination of microtubule and microfilament dynamics by Drosophila Rho1, Spire and Cappuccino. *Nat. Cell Biol.* 8, 367–376.

Santos, A. C. and Lehmann, R. (2004). Germ Cell Specification and Migration in Drosophila and beyond. *Curr. Biol.* 14, R578–R589.

Scheffler, K., Uraji, J., Jentoft, I., Cavazza, T., Mönnich, E., Mogessie, B. and Schuh, M. (2021). Two mechanisms drive pronuclear migration in mouse zygotes. *Nat. Commun.* 12, 841.

Schuh, M. and Ellenberg, J. (2008). A New Model for Asymmetric Spindle Positioning in Mouse Oocytes. *Curr. Biol.* 18, 1986–1992.

Serbus, L. R. (2005). Dynein and the actin cytoskeleton control kinesin-driven cytoplasmic streaming in Drosophila oocytes. *Development* 132, 3743–3752.

St. Johnston, D., Beuchle, D. and Nusslein-Volhard, C. (1991). staufen, a Gene Required to Localize Maternal RNAs in the Drosophila Egg. *Cell* 66, 51–63.

Stürner, T., Ferreira Castro, A., Philipps, M., Cuntz, H. and Tavosanis, G. (2022). The branching code: A model of actin-driven dendrite arborization. *Cell Rep.* 39, 110746.

Tanaka, T., Kato, Y., Matsuda, K., Hanyu-Nakamura, K. and Nakamura, A. (2011). Drosophila Mon2 couples Oskar-induced endocytosis with actin remodeling for cortical anchorage of the germ plasm. *Development* 138, 2523–2532.

Thielicke, W. and Sonntag, R. (2021). Particle Image Velocimetry for MATLAB: Accuracy and enhanced algorithms in PIVlab. *J. Open Res. Softw.* 9, 12.

Thielicke, W. and Stamhuis, E. J. (2014). PIVlab – Towards User-friendly, Affordable and Accurate Digital Particle Image Velocimetry in MATLAB. *J. Open Res. Softw.* 2,.

Tittel, J., Welz, T., Czogalla, A., Dietrich, S., Samol-Wolf, A., Schulte, M., Schwille, P., Weidemann, T. and Kerkhoff, E. (2015). Membrane Targeting of the Spir·Formin Actin Nucleator Complex Requires a Sequential Handshake of Polar Interactions. *J. Biol. Chem.* 290, 6428–6444.

Trovisco, V., Belaya, K., Nashchekin, D., Irion, U., Sirinakis, G., Butler, R., Lee, J. J., Gavis, E. R. and St Johnston, D. (2016). bicoid mRNA localises to the Drosophila oocyte anterior by random Dynein-mediated transport and anchoring. *eLife* 5, e17537.

Tsanov, N., Samacoits, A., Chouaib, R., Traboulsi, A.-M., Gostan, T., Weber, C., Zimmer, C., Zibara, K., Walter, T., Peter, M., et al. (2016). smiFISH and FISH-quant – a flexible single RNA detection approach with super-resolution capability. *Nucleic Acids Res.* 44, e165–e165.

Vanzo, N. F. and Ephrussi, A. (2002). Oskar anchoring restricts pole plasm formation to the posterior of the *Drosophila* oocyte. *Development* 129, 3705–3714.

Venken, K. J. T., Schulze, K. L., Haelterman, N. A., Pan, H., He, Y., Evans-Holm, M., Carlson, J. W., Levis, R. W., Spradling, A. C., Hoskins, R. A., et al. (2011). MiMIC: a highly versatile transposon insertion resource for engineering Drosophila melanogaster genes. *Nat. Methods* 8, 737–743.

Vizcarra, C. L., Kreutz, B., Rodal, A. A., Toms, A. V., Lu, J., Zheng, W., Quinlan, M. E. and Eck, M. J. (2011). Structure and function of the interacting domains of Spire and Fmn-family formins. *Proc. Natl. Acad. Sci.* 108, 11884–11889.

Weil, T. T., Forrest, K. M. and Gavis, E. R. (2006). Localization of bicoid mRNA in Late Oocytes Is Maintained by Continual Active Transport. *Dev. Cell* 11, 251–262.

Zimyanin, V. L., Belaya, K., Pecreaux, J., Gilchrist, M. J., Clark, A., Davis, I. and St Johnston, D. (2008). In Vivo Imaging of oskar mRNA Transport Reveals the Mechanism of Posterior Localization. *Cell* 134, 843–853.

Chapter 4: Investigation of the direct interaction between Spir and MyosinV in *Drosophila* oocytes

This work was largely carried out by previous Quinlan Lab members, Joseph Ong, Michelle Panzica and Emma Carley. This chapter describes the work I contributed finishing the story. A manuscript is currently in preparation and sections are used with permission from the authors.

Introduction

MyosinV (MyoV) is a processive actin-based motor that is heavily involved in cargo transport (Trybus, 2008). There is no single specific cargo for MyoV, examples include; melanosomes in dendritic cells and melanocytes, pigment granules in photoreceptors, and secretory granules in neurons (Hammer and Sellers, 2012). Three classes of MyoV exist in vertebrates (MyoVa, Vb and Vc) and the specificity of their overall function is influenced by their cargo adapters (Trybus, 2008). Melanophilin is an adapter that forms a tripartite complex between itself, MyoVa, and Rab27a (Li et al., 2005; Wu et al., 2006). In the *Drosophila* rhabdomere, MyoV complexes with Rab11 and *Drosophila* Rab interacting protein 11 (dRip11) (Li et al., 2007). Of interest to our continuing investigation of *Drosophila* oogenesis is the fact that in the analogous actin mesh of the mouse oocyte, Spir and FMN2 colocalize with MyoV on punctae. As mouse oogenesis progresses through metaphase MyoV motor activity creates symmetric diffusion that maintains the nucleus centrally (Schuh and Ellenberg, 2008). Following nuclear envelope breakdown Rab11 positive vesicles allow for migration of the spindle along the mesh and subsequent asymmetric division via polar body extrusion (Holubcová et al., 2013; Scheffler et al., 2021), thereby exemplifying the numerous roles the actin mesh serves during oogenesis.

Drosophila have only one MyoV (*didum*) to carry out numerous cellular functions. *didum* is an essential gene and has a high perdurance, obscuring phenotypic outcomes of its removal (Krauss et al., 2009; Li et al., 2007). The high perdurance renders RNAi insufficient. Instead, germline clones (GLC) and expressing a dominant negative MyoV peptides are the best

methods for studying its removal (Krauss et al., 2009). In the oocyte, MyoV is important for posterior enrichment and localization of *oskar* - presumably through anchoring (Krauss et al., 2009; Lu et al., 2020b). As MyoV colocalizes with Spir and FMN2 on punctae throughout the actin mesh in mouse oocytes (Schuh and Ellenberg, 2008), and mammalian Spir and MyoV directly interact (Pylypenko et al., 2016b) we asked if Spir could be serving as a direct adaptor protein for MyoV in the *Drosophila* oocyte.

Results

Analysis of Streaming Data: Single Copy Sufficiency

To determine the role of the Spir/MyoV interaction in oogenesis we examined the consequence of decreasing levels of Spir and/or MyoV on cytoplasmic flows and polarity establishment. The analysis of cytoplasmic flows is detailed here. Coordination is defined by the half maximal radius of organized streaming patterns (Dombrowski et al., 2004; Ganguly et al., 2012). This is inferred from velocity vectors generated from PIV analysis of streaming movies (Thielicke and Sonntag, 2021; Thielicke and Stamhuis, 2014). Cytoplasmic streaming is described as slow (~20nm/s) and uncoordinated ($C(r)_{0.5}$ = 2.7 ±1.8) during mid-oogenesis, developmental stages 7-10a (wildtype, Figure 4-1). At the onset of late oogenesis at stage 10B, streaming increases in velocity to be described as fast (~300nm/s) and highly coordinated ($C(r)_{0.5}$ = 23.4 ± 10.3), (*data not shown*).

Mutations in a small set of genes, including *spir* and *capu*, cause fast streaming prematurely during mid-oogenesis, with an average velocity of 100 ± 24 nm/s (Figure 4-1B) and increased coordination (here $C(r)_{0.5}$ = 15 ± 5 ; Figure 4-1C;(Ganguly et al., 2012; Quinlan, 2013; Theurkauf, 1994)). We examined two alleles of *didum*: *didum*^{KG04384}, a P-element insertion near the beginning of the coding region, resulting in a presumptive null, and *didum*^{154}, a premature stop at residue 681 which results in expression of most of the motor domain (Krauss et al., 2009). In some cases, phenotypes are more penetrant in germline clones of *didum*^{154} than

didum^{KG04384}, presumably because the expressed motor domain acts as a dominant negative exacerbating the absence of wild type MyoV (Krauss et al., 2009). We also examined two alleles of *spir: spirMI05646,* an insertion, and *spir*^{1}, a premature stop within the first folded domain, aa292, resulting in a presumptive null. We detected no differences between the two alleles and, therefore, pooled the data, (*spir*). No significant differences were detected in the stage 9 streaming velocities of *spir*/+, *didum*^{KG04384}/+, *didum*^{154}/+, or the two *spir*^{1}*/didum** transheterozygous pairs relative to wild type or each other (Figure 4-1B). However, the coordination of movement increased in the +/*didum*^{154} background and for both *spir*^{1}*/didum** transheterozygotes, when compared to wild type (Figure 4-1C), demonstrating a subtle impact of decreasing the amount of MyoV in the oocyte.

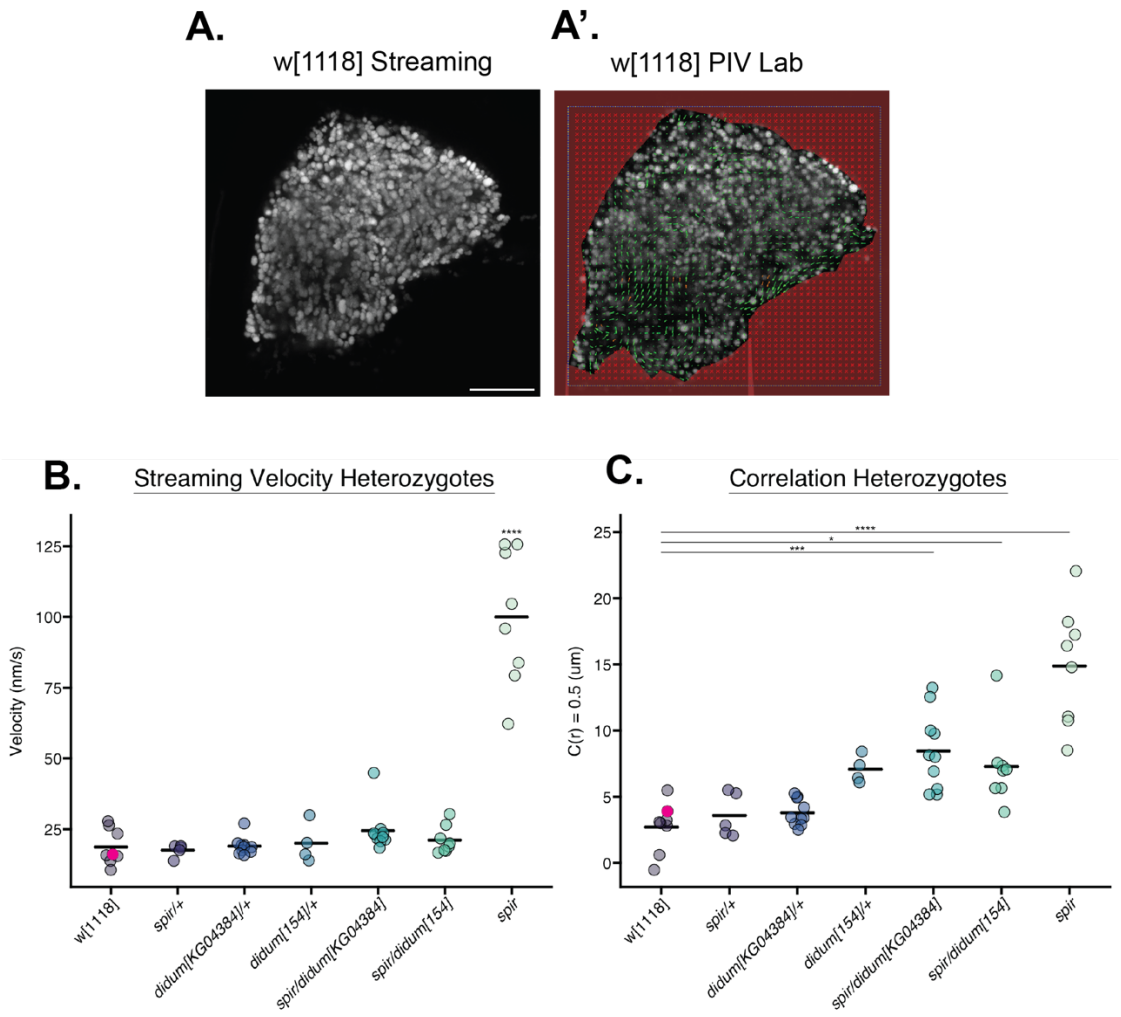

Figure 4-1: Analysis of streaming and mesh in heterozygous backgrounds.

*A) Time lapse projection of yolk granule autofluorescence in a wildtype stage 9 oocyte (magenta dots below are analysis data from these images). A') Frame from PIV analysis shows vectors that reflect velocity and are used to measure correlation of motion. B) Streaming velocity is unchanged in heterozygotes and transheterozygotes. C) Correlation is increased in +/didum[KG], and spir/didum backgrounds, relative to wild type. Statistical analyses are one-way ANOVA, post hoc TKMC. p-values are as indicated: p< 0.1 = *, p<0.05 = **, p<0.01=***, p<0.001 = ****.*

Analysis of Streaming Data: A Streaming Intermediate

Based on the differences in mesh dynamics and fluid flow coordination we observed in *didum* heterozygotic oocytes, we examined streaming in *didum*-GLCs. The mesh forms during mid-oogenesis and has a significant increase in mesh intensity from wild type, which is consistent with reports that *didum* defects do not cause premature streaming (Krauss et al.,

2009)(Figure 4-2A). Likewise, overexpression of MyoVa tail in mouse oocytes does not lead to loss of mesh (Holubcová et al., 2013). However, velocity and $C(r)_{0.5}$ in *didum*-GLCs were significantly increased, relative to wildtype (Figure 4-2B,C). Upon closer examination, we found that the streaming behavior of *didum*-GLCs fell into two classes: about half were indistinguishable from wild type ($C(r)_{0.5}$ = 2.6 ± 0.7, class I) while the other half had a significantly higher $C(r)_{0.5}$ (9.8 ± 3.5 (class II)), (Figure 4-2C). When split according to correlation class, the streaming velocity of *didum*(class II) was 3-fold higher than wild type, with an average velocity of 55 ± 9 nm/s (Figure 4-2B). In contrast, the average velocity for Class II was approximately twice as high (33 ± 8 nm/s) but not significantly different from wild type. It is important to note that MyoV has a high perdurance in the Drosophila oocyte, such that a maternal contribution results in a range of phenotypes (Krauss et al., 2009). In this case, because the motion fell into two classes, as opposed to a continuum and because *didum*(class I) is statistically indistinguishable from wild type, we speculate that a second crossover event occasionally occurred between the *didum* and Ovo^D loci, creating heterozygotes instead of nulls. With this in mind, we focused on *didum*(class II) for further analysis. Confirming that the differences were due to loss of MyoV, both streaming and coordination were restored to wildtype levels upon expression of MyoV-mScarlet in *didum*-GLCs (Figure 4-2B,C).

While the velocity of didum-GLCs is faster than wild type it is also significantly slower than typical premature fast streaming, such as what is observed in a *spir*-null (Figure 4-2B). Slower streaming is presumably due to the presence of the actin mesh, which hinders motion, if not as effectively. Thus, we have identified a new streaming state and a new phenotype caused by the loss of MyoV.

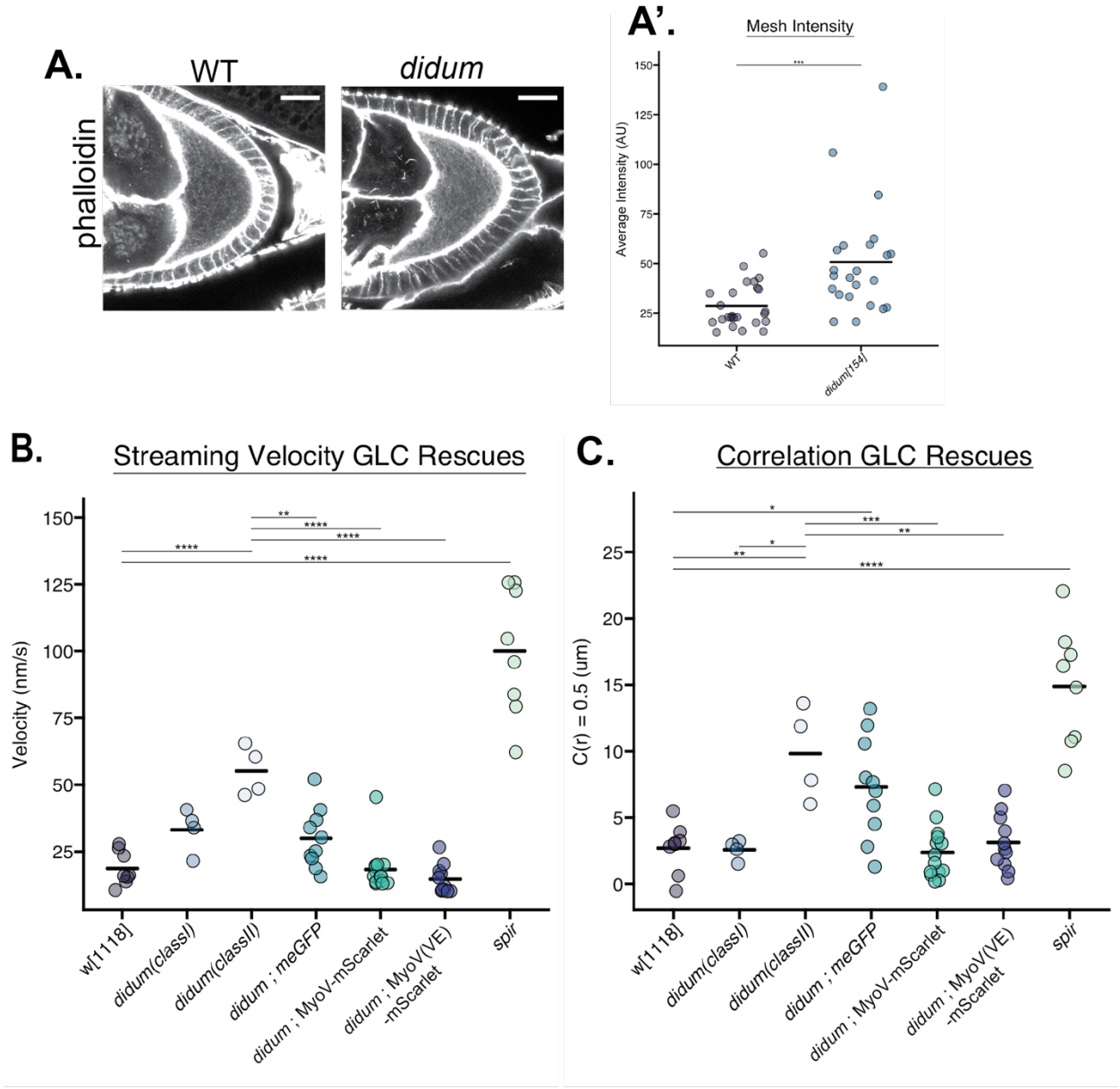

Figure 4-2: A streaming intermediate.

*A) Actin mesh intensity in didum-GLCs forms during mid oogenesis and intensity is significantly increased. B) Streaming velocity is increased in didum-GLC(class II) relative to wild type and rescued by expression of MyoV-mScarlet or MyoV(VE)-mScarlet. C) Correlation of motion is increased in didum-GLC(class II) relative to wild type and rescued by expression of MyoV-mScarlet or MyoV(VE)-mScarlet. Significance determined via one way ANOVA, post hoc TKMC. p-values are as indicated: p< 0.1 = *, p<0.05 = **, p<0.01=***, p<0.001 = ****.*

Loss of Spire-MyoV binding does not disrupt oogenesis

In order to test the significance of the direct interaction between Spire and MyoV to oogenesis, we generated fly lines expressing proteins that cannot interact, based on our in vitro

experiments (*data not shown*): UASp-SpirB(LAIA)-GFP and UASp-MyoV(VE)-mScarlet, using UASp-MyoV-mScarlet for control experiments with mScarlet as a tag. First we compared the genetic rescues of SpirB-GFP and SpirB(LAIA)-GFP (*data not shown*). They both rescued fertility, the actin mesh, and slow streaming of *spir* null oocytes.

We then expressed either MyoV-mScarlet wildtype or Myo(VE)-mScarlet in *didum*-GLCs. Both constructs localized to the cortex of the oocyte and were enriched at the posterior, as observed in MyoV-GFP backgrounds (Figure 4-3). Rescue of fertility was poor but indistinguishable between MyoV-mScarlet and MyoV(VE)-mScarlet, which may reflect a difference between the driver and native expression patterns (*nanos*-Gal4, ~30%) as streaming at mid-oogenesis is rescued to wildtype levels (Figure 4-2B,C). Altogether, these results suggest that mutations sufficient to disrupt SpirB-MyoV binding *in vitro* have little impact on oogenesis.

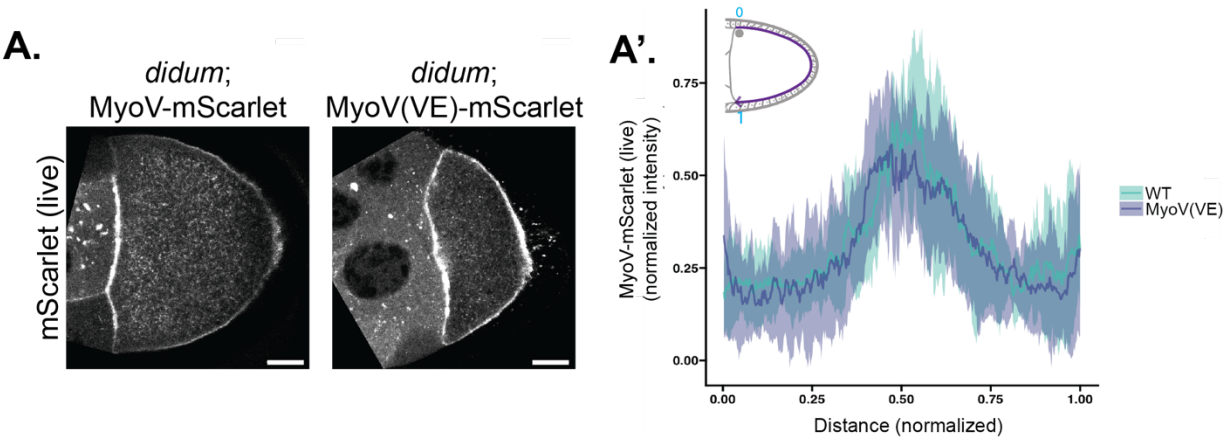

Figure 4-3: Loss of Spire-MyoV binding does not disrupt oogenesis.

A) Localization of MyoV(VE)-mScarlet is indistinguishable from wild type in a didum-GLC background. A') Quantification of cortical mScarlet shows posterior enrichment for all MyoV alleles.

Discussion

Direct interaction between Spir and MyoV is not required for oogenesis.

Through this work we have determined that blocking the Spir, MyoV interaction *in vivo* does not disrupt oogenesis. Spir alone does not stimulate MyoV activity *in vitro* nullifying the

likelihood that Spir is behaving like previously described adaptor proteins such as melanophilin. With removal of MyoV, via *didum* GLCs, we determined that streaming and the correlative pattern of the cytoplasm increases during mid-oogenesis, which is further consistent with our finding that the actin mesh dynamics were altered.

We also observed an enrichment of MyoV at the posterior oocyte. This is consistent with its described role in posterior anchoring (Lu et al., 2020b). Study of oskar/Staufen posterior anchoring in transheterozygote backgrounds reveals no change in posterior anchoring. Suggesting that this background is not sufficient to study the role of Spir/MyoV interaction in polarity establishment.

A tripartite complex?

Rab GTPases regulate membrane trafficking in cells and have been found to be associated with MyoV in the mouse oocyte (Holubcová et al., 2013; Scheffler et al., 2021) and *Drosophila* rhabdomere (Li et al., 2007). It is likely that our work here is lacking another component to permit Spir/MyoV interaction. By abolishing the interacting residues in Spir or MyoV there still could be other interacting residues mediated by a third interacting partner, such as a Rab. Recent biochemical studies have shown that Spire2 and Rab11a synergize to activate mammalian MyoVb (Yao et al., 2024). Both components are required for this effect and it is likely that the interaction between *Drosophila* Spir and MyoV also require Rab11.

Materials and Methods

Drosophila Stocks and Lab Generated Stocks

w[1118] (Bloomington, BDSC 3605), w[*]; P{w[+mC]=His2Av-EGFP.C}2/SM6a (Bloomington, BDSC 24163), w[1118];;*nanos*-Gal4-vp16 (Bloomington, BDSC 4937), y[1]; P{y[+mDint2] w[BR.E.BR]=SUPor-P}didum[KG04384]/CyO (Bloomington, BDSC 14094), y[1] w[*]; Mi{y[+mDint2]=MIC}spir[MI05646] (Bloomington, BDSC 43877), spir[1] cn[1] bw[1]/CyO,

l(2)DTS513[1] (Bloomington, BDSC 5113), P{ry[+t7.2]=hsFLP}12, y[1] w[*]; sna[Sco]/CyO (Bloomington, BDSC 1929), P{w[+mW.hs]=FRT(w[hs])}G13 P{w[+mC]=ovoD1-18}2R/T(1;2)OR64/CyO (Bloomington, BDSC 4434), didum[154] FRT 42B/CyO (Gift from the Ephrussi Lab; Heidelberg, Germany), UASp-SpirB(LAIA)-GFP, UASp-MyoV(VE)-mScarlet, and UASp-MyoV-mScarlet were generated for this study by Michelle Panzica.

Live Imaging of Localization and Analysis

Live egg chambers were dissected under halocarbon 700 oil (Sigma-Aldrich, H8898). Images of MyoV-mScarlet were acquired on a LSM780 platform at 1024 pixels squared with an EC Plan-Neofluar 40x/1.3 Oil DIC M27. For mScarlet excitation, 561 nm laser was used. Z-stacks were collected with a range of 5-10 µm with 1 µm steps. A maximum intensity projection was made in FIJI and analyzed further. A line width of 20px was used and plotted intensity for the channel of interest. Data were saved from this, intensity and distances measured were normalized using python scripts. Data were then further analyzed in python and plotted in R using ggplot2.

Imaging of Streaming and Analysis

Imaging of streaming in *Drosophila* oocytes and analysis of velocity and pattern were performed as described in Chapter 2.

Mesh Staining and Intensity Measurements

Were carried out by JO. Protocol for mesh staining can be found in Chapter 2. For wildtype, ovaries expressing Histone-GFP were used and combined with test ovaries. This allowed fixation and staining conditions to be identical. Data included acquisition of GFP (488) and Alexa-Fluor labeled phalloidin (647). Intensity measurements were made in FIJI and plotted in R using ggplot2. Student's t-test was determined significance in R, rstatix library.

References

Dombrowski, C., Cisneros, L., Chatkaew, S., Goldstein, R. E. and Kessler, J. O. (2004). Self-Concentration and Large-Scale Coherence in Bacterial Dynamics. *Phys. Rev. Lett.* 93, 098103.

Ganguly, S., Williams, L. S., Palacios, I. M. and Goldstein, R. E. (2012). Cytoplasmic streaming in Drosophila oocytes varies with kinesin activity and correlates with the microtubule cytoskeleton architecture. *Proc. Natl. Acad. Sci.* 109, 15109–15114.

Hammer, J. A. and Sellers, J. R. (2012). Walking to work: roles for class V myosins as cargo transporters. *Nat. Rev. Mol. Cell Biol.* 13, 13–26.

Holubcová, Z., Howard, G. and Schuh, M. (2013). Vesicles modulate an actin network for asymmetric spindle positioning. *Nat. Cell Biol.* 15, 937–947.

Krauss, J., López de Quinto, S., Nüsslein-Volhard, C. and Ephrussi, A. (2009). Myosin-V Regulates oskar mRNA Localization in the Drosophila Oocyte. *Curr. Biol.* 19, 1058–1063.

Li, X., Ikebe, R. and Ikebe, M. (2005). Activation of Myosin Va Function by Melanophilin, a Specific Docking Partner of Myosin Va *. *J. Biol. Chem.* 280, 17815–17822.

Li, B. X., Satoh, A. K. and Ready, D. F. (2007). Myosin V, Rab11, and dRip11 direct apical secretion and cellular morphogenesis in developing *Drosophila* photoreceptors. *J. Cell Biol.* 177, 659–669.

Lu, W., Lakonishok, M., Liu, R., Billington, N., Rich, A., Glotzer, M., Sellers, J. R. and Gelfand, V. I. (2020). Competition between kinesin-1 and myosin-V defines Drosophila posterior determination. *eLife* 9, e54216.

Pylypenko, O., Welz, T., Tittel, J., Kollmar, M., Chardon, F., Malherbe, G., Weiss, S., Michel, C. I. L., Samol-Wolf, A., Grasskamp, A. T., et al. (2016). Coordinated recruitment of Spir actin nucleators and myosin V motors to Rab11 vesicle membranes. *eLife* 5, e17523.

Quinlan, M. E. (2013). Direct interaction between two actin nucleators is required in Drosophila oogenesis. *Development* 140, 4417–4425.

Scheffler, K., Uraji, J., Jentoft, I., Cavazza, T., Mönnich, E., Mogessie, B. and Schuh, M. (2021). Two mechanisms drive pronuclear migration in mouse zygotes. *Nat. Commun.* 12, 841.

Schuh, M. and Ellenberg, J. (2008). A New Model for Asymmetric Spindle Positioning in Mouse Oocytes. *Curr. Biol.* 18, 1986–1992.

Theurkauf, W. (1994). Premature microtubule-dependent cytoplasmic streaming in cappuccino and spire mutant oocytes. *Science* 265, 2093–2096.

Thielicke, W. and Sonntag, R. (2021). Particle Image Velocimetry for MATLAB: Accuracy and enhanced algorithms in PIVlab. *J. Open Res. Softw.* 9, 12.

Thielicke, W. and Stamhuis, E. J. (2014). PIVlab – Towards User-friendly, Affordable and Accurate Digital Particle Image Velocimetry in MATLAB. *J. Open Res. Softw.* 2,.

Trybus, K. M. (2008). Myosin V from head to tail. *Cell. Mol. Life Sci. CMLS* 65, 1378–1389.

Wu, X., Sakamoto, T., Zhang, F., Sellers, J. R. and Hammer, J. A. (2006). In vitro reconstitution of a transport complex containing Rab27a, melanophilin and myosin Va. *FEBS Lett.* 580, 5863–5868.

Yao, L.-L., Hou, W.-D., Liang, Y., Li, X. and Ji, H.-H. (2024). Spire2 and Rab11a synergistically activate myosin-5b motor function. *Biochem. Biophys. Res. Commun.* 703, 149653.

Chapter 5: Screening for Rabs that interact with Spir in *Drosophila* oocytes.

Introduction

The C-terminus of Spir contains a conserved region known as the Spir Box, upstream of the mFYVE, a non-canonical zinc finger membrane binding domain (Alzahofi et al., 2020; Tittel et al., 2015). The Spir Box amino acid sequence is similar to the Rab GTPase-binding domain of Rabphilin-3A, making it a putative Rab binding domain (Alzahofi et al., 2020). The C-terminal domains of mammalian Spir have been found to interact with Rab27a (Alzahofi et al., 2020) and Rab11 (Pylypenko et al., 2016b) and mediate distinct processes in different cell types. Rab27a and MyoV in the melanocyte recruit Spir to melanosome membranes. The actin assembly activity of Spir builds actin filaments, on which MyoV migrates, dispersing melanosomes (Alzahofi et al., 2020). Conversely, in the mouse oocyte, Spir- and Rab11- positive vesicles contract and generate a centering force on the mitotic spindle in meiosis (Almonacid and Verlhac, 2021; Holubcová et al., 2013). As we have a strong interest in understanding the regulation and organization of the *Drosophila* actin mesh, we initiated a screen to identify Rabs that interact with *Drosophila* Spire in the oocyte. Characterizing the Rab(s) that bind Spir would improve our understanding of *Drosophila* mesh function by uncovering interactions that favor dispersion or contraction, as observed in mammals.

Rab proteins are a class of small GTPases (Homma et al., 2021). They are well characterized for their role in regulating membrane trafficking and have additional functions including: vesicle trafficking, transmembrane signal transduction, and cytoskeletal rearrangement (Homma et al., 2021; Neumann and Prekeris, 2023). The *Drosophila* genome encodes 33 *Rab* genes that share similarity with vertebrate Rabs (Zhang et al., 2007). Due to the wide breadth of intracellular processes in which Rabs are involved, much effort has gone into generating tools to study Rab functions in the fly. Transgene constructs of 31 *Drosophila* Rabs have been established, expressing fluorescently tagged wildtype, dominant-negative, and constitutively active forms (Zhang et al., 2007). With the discovery of CRISPR/Cas9 (Jinek et al., 2012) greatly facilitating genome editing, 27 fly lines have been developed that each have a

Rab endogenously tagged with an N-terminal YFP-4XMyc tag (Dunst et al., 2015). These lines, and RNAi expressing lines for most Rabs (Perkins et al., 2015), are all commercially available and made the following investigation possible. The Rabs reviewed in this chapter were selected for screening based on their proposed function, oocyte localization (images from FLYtRAB (Dunst et al., 2015), http://rablibrary.mpi-cbg.de/cgi-bin/rab_homepage.pl) and *in vitro* interactions (Figure 5-1A).

Results

Initial Screening of Candidate Rabs

We selected eight Rabs to investigate in our initial screen: Rabs 6, 9, 11, 18, 23, 27, 39 and X1. Using the endogenously tagged lines, we first established wether the localization pattern in the egg chamber were consistent with from published images available on FLYtRAB (Figure 5-1A). As expected, Rabs 27 and 39 were determined to be negative controls for the oocyte. In mammalian melanocytes, a somatic cell type, Rab27a interacts with Spir to regulate transport of melanosomes (Alzahofi et al., 2020). However, in *Drosophila* germline cells, RNA sequencing data indicates low expression of Rab27 (Dunst et al., 2015; Leader et al., 2018). Correspondingly, we observed no positive staining indicating Rab27 expression in any compartment of the egg chamber. Rab39, involved in lysosomal recycling (Lakatos et al., 2021), is expressed in follicle cells but not the oocyte where the actin mesh is built (Figure 5-1A, FLYtRAB (Dunst et al., 2015)).

As a wild-card candidate, we selected RabX1 for its intriguing globule-like localization throughout the nurse cell cytoplasm. RabX1 is involved in the late endosomal compartment and promotes degradation by building tubular connections with lysosomes (Laiouar et al., 2020). This function is known to regulate epithelial morphogenesis in the surrounding follicle cells (Laiouar et al., 2020). While the localization is interesting, we determined RabX1 is unrelated to Spir's function in the actin mesh during oogenesis (Figure 5-1A). In sum, our own staining of

these three eYFP-MYC lines described did not indicate that we should continue our line of inquiry for Rabs 27, 31 or X1.

The following Rabs we screened have a higher possibility of being interactors with Spir in the *Drosophila* oocyte. Pull-down data from a collaborator indicated direct interaction of Rab6 with Spir (*data not shown,* Don van Meyel, McGill University). In the oocyte, Rab6 has also been identified as a posterior regulator of *osk* mRNA localization and organization of microtubules (Coutelis and Ephrussi, 2007; Januschke et al., 2007). The regulation of the posterior is mediated by the recruitment of Dynein to vesicles through interactions with Bicaudal D and Rab6 (Matanis et al., 2002; Short et al., 2002). Rab6 has also been characterized in organizing the germline stem cell cluster (Coutelis and Ephrussi, 2007) and outside of the germline by transporting rhodopsin in neurons (Satoh et al., 2016). Staining for eYFP-MYC-Rab6 with anti-Myc, we observed no specific localization of Rab6 (Figure 5-1A). Therefore, we stained with anti-GFP to label the YFP and observed signal in the egg chamber. We observed different Rab6 localization patterns in the egg chamber including, punctae in the oocyte, throughout the migrating border cell cluster, and aggregates in the nurse cells (Figure 5-1B, b). At the time we elected not to follow up on Rab6. Upon review, we consider this candidate worth further study due to its role in posterior and microtubule organization and direct interaction with Spir *in vitro* (Coutelis and Ephrussi, 2007).

Rab11 is another major player in posterior mRNA localization, being involved in localizing *oskar* to the posterior during mid-oogenesis (Dollar et al., 2002; Jankovics et al., 2001), regulating proper identification during border cell migration, and driving migration of the leading edge (Assaker et al., 2010; Emery and Ramel, 2013; Ramel et al., 2013). We have determined Spir and Capu localize within the migrating border cell cluster (Chapter 1), and therefore hypothesize that Rab11 may interact with Spir at this location. In the mouse oocyte, Rab11 positive vesicles have also been identified to contain Spir (Pylypenko et al., 2016b) and activate MyoV activity (Li et al., 2007; Yao et al., 2024). Aside from the oocyte, Rab11 is

important for embryogenesis via remodeling the actin cytoskeleton and recruitment of the membrane during cleavage furrow formation (Riggs et al., 2003). Staining for Rab11 in the oocyte was generally unimpressive in our hands; attempting to stain for the N-terminal Myc (Figure 5-1A) or YFP (Figure 5-1B, d) exhibited low signal compared to the wildtype, non-expressing control (Figure 5-1B, a). Despite the high precedence in the literature, we decided not to pursue Rab11 any further due to low signal.

Rab18 is highly expressed in the *Drosophila* ovary (Leader et al., 2018) and has a predominant role in regulating lipid droplet formation (Ozeki et al., 2005; Xu et al., 2018). Lipid droplets are generated during mid-oogenesis in the nurse cells and transported to the oocyte (Buszczak et al., 2002). Recently, lipid droplets have been identified as regulators of actin remodeling in nurse cell and follicle cell cortexes via prostaglandin signaling (Giedt et al., 2023). As with the previous Rabs, we stained for Rab18, while there appeared to be localization in follicle cells (Figure 5-1B, e), we did not observe high expression in the oocyte. While there appears to be localization at the follicle cells (Figure 5-1B, e), the lack of signal in the oocyte removed Rab 18 from further screening.

The only described role for Rab9 at this time is in tracheal formation (Dong et al., 2013; Dong et al., 2014). Rab23 also has not been well characterized in *Drosophila,* and is involved in the hexagonal packing of wing cells and formation of body hairs (Pataki et al., 2010). In the immunofluorescence we observed a striking localization pattern at the oocyte cortex for both Rabs (Figure 5-1B, c, f). Rab9 was particularly surprising to us, as it is reported to have low to moderate expression in the female ovary (FlyBase, (Leader et al., 2018)). Our staining of Rab23 in the oocyte demonstrated that it localizes to the nurse cell and oocyte cortex (Figure 5-1A and B, f). Therefore, we found Rab9 and Rab23 to be novel candidates for interaction with Spir during oogenesis.

As Spir, Rab9, and Rab23 localize to the oocyte cortex, we investigated their degree of overlap by co-staining the endogenously tagged Spir-HA and eYFP-Myc Rab (Figure 5-1C). The

first round of co-staining was unsuccessful as the eYFP-Myc-Rab was not efficiently labelled (Rab9 Figure 5-1C a, Rab23 Figure 5-1C b), resulting in a low degree of overlap with Spir (Figure 5-1C, a', b'). We further optimized staining and observed co-incidence of Spir and Rab9 (Figure 5-1D). A high degree of overlap was observed between Rab9 and Spir-HA in the oocyte cortex, suggesting interaction (Figure 5-1D, b"). Since our other experiments suggest that Rab23 may also interact with Spir, we expect that optimization of that staining should also reveal a high degree of overlap. Together, these data imply that Rabs 9 and 23 may be important for organization of the oocyte cortex.

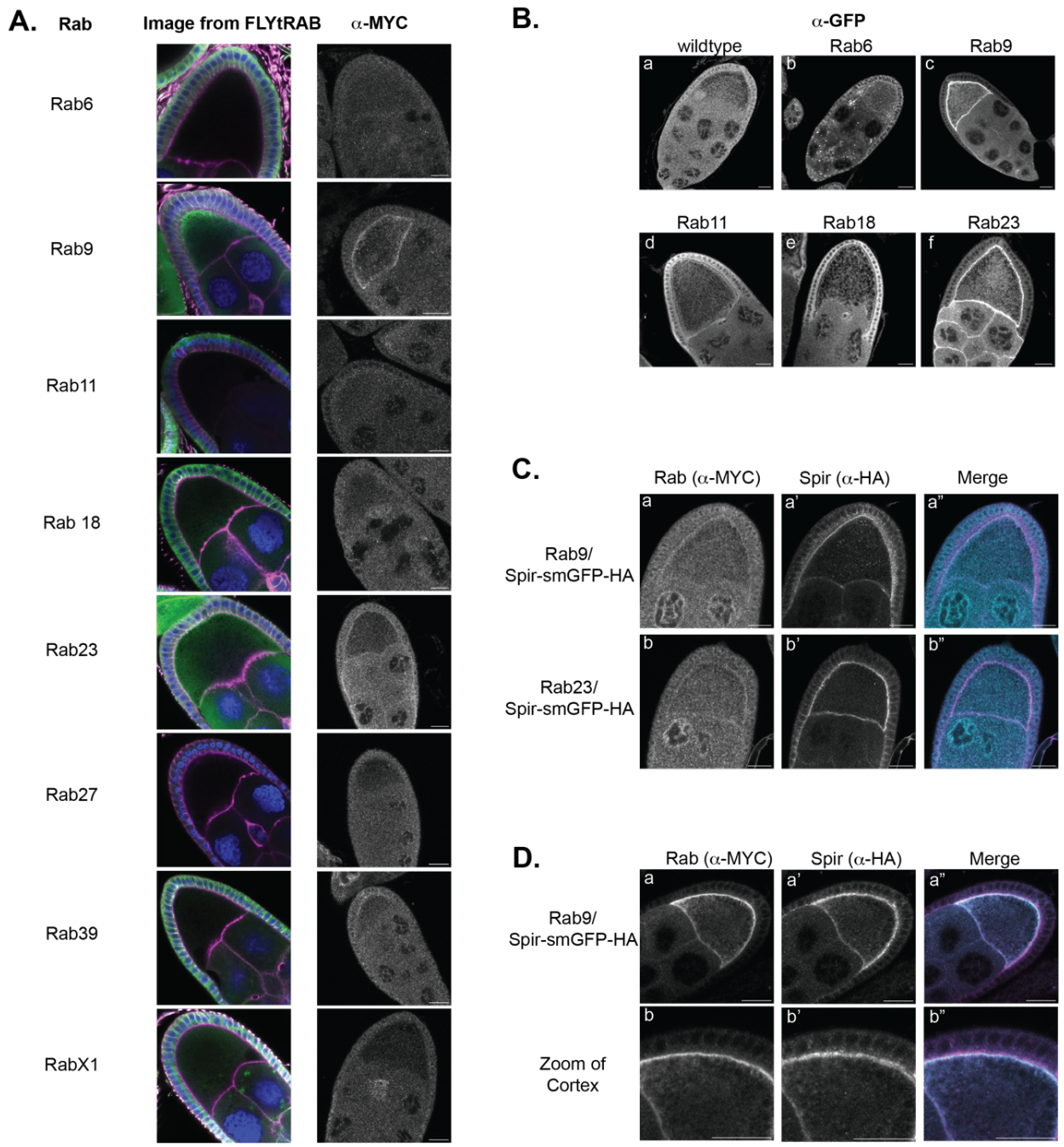

Figure 5-1: Screening of endogenously tagged Rab candidates.

(A.) On the left, full panel of Rabs selected based on images from the FLYtRAB database (http://rablibrary.mpi-cbg.de/cgi-bin/rab_overview.pl) phalloidin/actin in purple, DAPI/nuclei in blue, MYC/RAB in green(Dunst et al., 2015). On the right, our own initial staining of these YFP-4xMYC Rab lines using 1:250 Rabbit anti-MYC(71D10, CST #2278S). (B.) Smaller panel of Rabs screened using Chicken anti-GFP (1:2,000, Abcam ab13970). Rab9 (c) and Rab23 (f) gave strong cortical localization patterns. (C.) Co-staining of endogenously tagged Rabs9 and 23 (1:250 Rabbit anti-MYC(71D10), CST #2278S) with Spir-HA (1:500 Mouse anti-HA(HA.C5), Abcam ab18181). Rab staining was not efficient (a, b). This resulted in a low degree of observed overlap (a", b"). (D.) Co-staining of Rab9 with Spir-HA using new reagents. Higher efficiency of staining for Rab9 (1:500 Mouse anti-MYC (911B), CST #2276S). Spir-HA staining (1:500 Rabbit anti-HA(c29F4), CST #3724S). A higher degree of overlap is observed at the oocyte cortex (b").

Investigating the functional consequence of Rab9 and Rab23 knockdown on oogenesis

To determine if there was a functional role for Rab9 and Rab23 in oogenesis we used the available RNAi lines to induce knockdown. As we aimed to determine the role of these Rabs in regulating the actin mesh, we used *matα*-Gal4 to drive expression of the RNAi. This system induces knockdown following oocyte specification at stage 2 (Lu et al., 2021), allowing for characterization in later stages of oogenesis.

Upon knock-down of Rab9 from the oocyte and staining for actin using AlexaFluor-phalloidin, we uncovered no defects in mesh formation and removal (Figure 5-2A, b-b'). Consistently, small-scale fertility assays of Rab9 depleted females indicated successful oogenesis (Figure 5-2B, b). Our investigation of Rab23 RNAi oocytes identified disrupted morphologies of the nurse cell and oocyte cortexes during mid-oogenesis (Figure 5-2A, c). Oogenesis was not completely stalled upon Rab23 RNAi, as late-stage oocytes were observed (Figure 5-2A, c') and the small-scale fertility assays produced offspring (Figure 5-2B, c). The disrupted actin organization during mid-oogenesis observed in some Rab23 depleted egg chambers indicate that Rab23 plays a role in maintaining the integrity of cellular cortexes in the egg chamber(Figure 5-2A). This is further supported by the highly localized signal of Rab23 to the nurse cell and oocyte cortexes (Figure 5-1B, f).

As overall fertility was not disrupted, we took a closer look for subtle changes to oogenesis. Disruptions to the actin mesh and its organization can be inferred by measuring differences in the yolk granule motion of streaming at mid-oogenesis (Ganguly et al., 2012). We found streaming to be at wildtype levels for the Rab23 knock-down (Figure 5-2C, c) and we did not analyze it further. However, Rab9 knock-down appeared to be different from wild-type (Figure 5-2C, b), and we therefore analyzed the streaming movies further. We used PIV and downstream analysis of the pattern of motion to measure streaming velocities and correlation (Ganguly et al., 2012; Thielicke and Stamhuis, 2014). Rab9 knock-down oocytes on average streamed at a higher velocity than wildtype, similarly to the didum GLCs (**Chapter 3**) (Figure 5-

2C, d). Surprisingly, we found that these oocytes also have a decreased pattern of motion (Figure 5-2C, e). Although this difference is not significant, we found it intriguing and wanted to determine if these changes in streaming were related to Spir function.

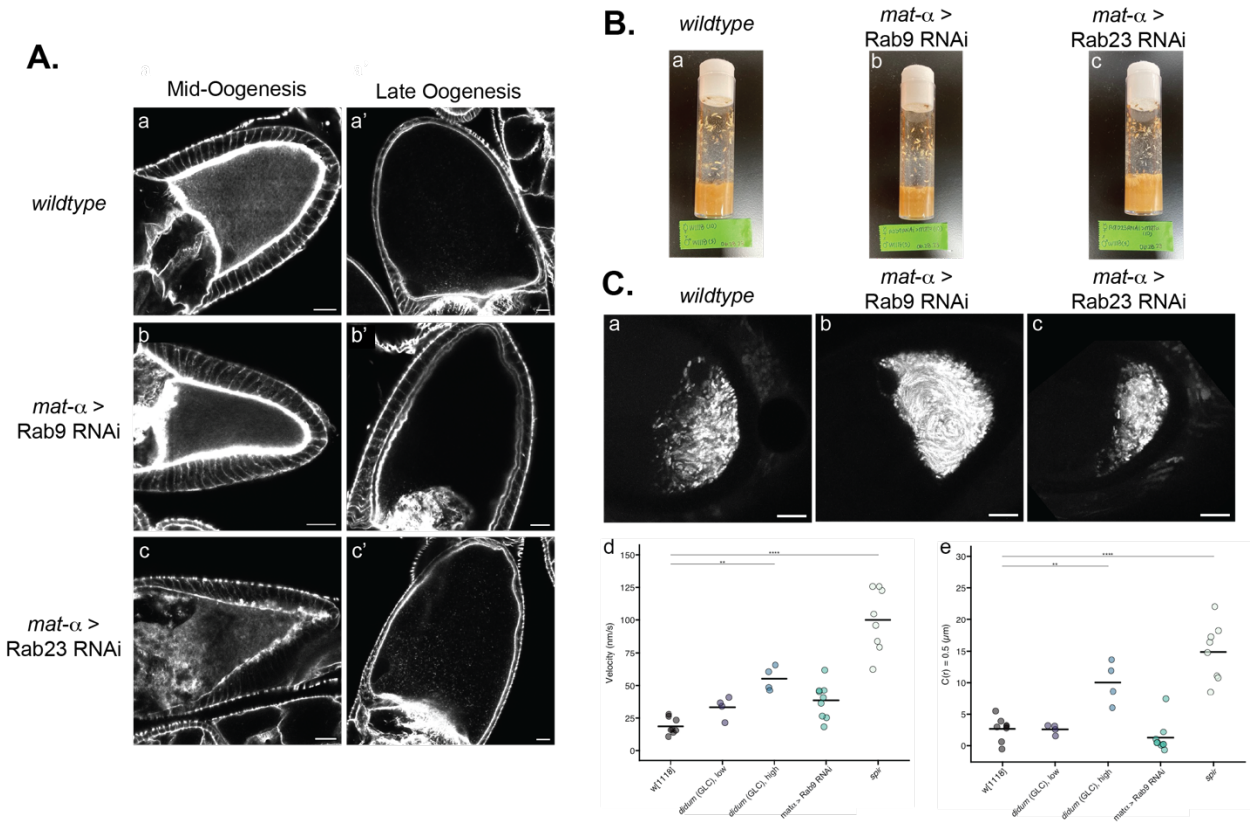

Figure 5-2: RNAi knockdown of Rab9 and Rab23 have varying effect on oogenesis.

(A.) Mesh staining of mid and late-stage egg chambers using AF488-phalloidin. (a-a')Wildtype control, (b-b') Rab9 RNAi, (c) Rab23 in some cases disrupted egg chamber morphology at mid-oogenesis, (c') stage 11 oocytes were still identified. (B.) Small scale fertility assays of (a) wildtype, (b) Rab9 RNAi and (c) Rab23 RNAi. (C.) Overlay of yolk granule motion in mid-stage (a) wildtype, (b) Rab9, and (c) Rab23 RNAi. Streaming analysis of Rab9 RNAi showed a slight increase in streaming velocity (d) and a decrease in the coordination of the pattern (e). This is non-significant (one-way ANOVA with Tukey-Kramer HSD Post Hoc).

With our available tools, we aimed to determine if the removal of Rab9 altered the localization pattern of Spir-HA in the oocyte. Upon staining of Spir-HA in a wildtype (Figure 5-3A, a-a") and Rab9 knock-down background (Figure 5-3A, b-b"), we identified no clear difference in localization pattern at any stage of oogenesis. The lack of observed alteration in localization pattern could be due to additional interacting partners that mediate recruitment or that the

membrane localization is exclusively driven by the mFYVE domain (Pylypenko et al., 2016b; Tittel et al., 2015).

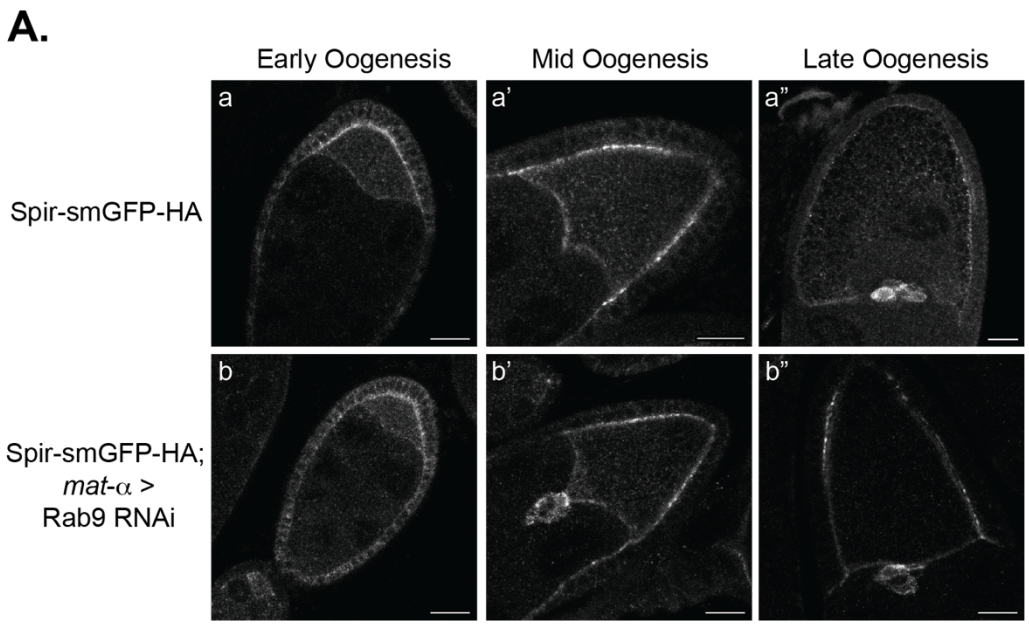

Figure 5-3: Spir localization is unaltered following Rab9 knockdown.

(A.)Staining for Spir-HA (1:1000 Rabbit anti-HA (c29f4), CST #3724S) during all stages of oogenesis in (a-a") wildtype and (b-b") Rab9 knockdown backgrounds.

Discussion

We set out to determine which of the 33 *Drosophila* Rabs interact with Spir in the oocyte. Using the commercially available eYFP-4xMYC-Rab lines, we repeated staining to determine their localization in the oocyte (Dunst et al., 2015). We were especially motivated to repeat staining of the Rabs with reported phenotypes in the oocyte, e.g. Rab6 and Rab11, as Spir functions in the oocyte to build the actin mesh during mid-oogenesis.

To our surprise, we were unable to visualize Rab11 in the oocyte using the eYFP-4xMYC line. We speculate this could be due to inefficient staining and a high degree of background in the immunofluorescence. As there is mounting evidence for a tripartite interaction between Spir,

MyoV, and Rab11, future experiments could reveal further evidence by optimizing the Rab11 staining conditions.

Through our screen we identified Rab9 and Rab23 as strong candidates for Spir interaction. We found their localization in the oocyte cortex, reminiscent of endogenously tagged Spir, indicating a potential site of interaction. We were able to determine that knock-down of Rab23 disrupted the integrity of the oocyte and nurse cell cortexes. While the function of Rab23 at the cortexes remains unclear, it could relate to vesicle formation or interaction with actin (Pataki et al., 2010). We observed altered morphologies in a subset of mid-stage Rab23 RNAi oocytes and we were surprised that fertility was not reduced as a result. To ensure that the Rabs are being removed effectively, western blotting or immunofluorescence following RNAi knock-down would serve as strong controls. We deem this investigation as preliminary. Co-staining of Spir-HA with Rab9 and Rab23 lines needs to be repeated and further analyzed.

We continued with investigation of Rab9, characterizing the effects of Rab9 removal on cytoplasmic streaming and Spir localization. We did not find evidence of a direct linkage between Rab9 and Spir, or on the actin mesh, despite observing co-localization at the oocyte cortex (Figure 5-1D). We speculate that there are multiple interactions that mediate direct linkage to Spir, as in other systems effector proteins form multi-component complexes. For example, in the *Drosophila* rhabdomere, dRip11 mediates the Rab11 and MyoV interaction (Li et al., 2007). Modulating the activity of Rab9 in the oocyte by expressing constitutively active (Bloomington, BDSC 23273) or dominant negative forms (Bloomington, BDSC 23642) (Zhang et al., 2007) could influence this interaction or function at the cortex while allowing for a complex to form. As these tools are UASp constructs, we could quickly investigate the role of activity in the germline.

Outside of their role in the actin mesh, Spir and Capu also mediate endocytosis in the developing oocyte (Tanaka and Nakamura, 2008). Specifically, we have shown that the Spir Box of Spir is crucial for this process, as deleting the Spir Box leads to altered yolk granule size in

the oocyte (A. McQuown *data not shown*). Due to the amino acid sequence similarity of the Spir Box with Rab GTPase binding domain, the yolk granule phenotype could be due to loss of interaction with a Rab. A likely candidate is Rab5, which has been shown to play a role in early endocytosis in the germline and in the regulation of *oskar* at the posterior oocyte (Compagnon et al., 2009; Tanaka and Nakamura, 2008). Investigating the interaction and regulation of Rab5 with Spir serves as a strong direction for future studies. There is also motivation to repeat the original ΔSpir Box experiments with an improved driver of Spir transgene expression, as discussed in **Chapter 1**.

In sum, determining which Rabs interact with Spir will enhance our understanding of the function of the actin mesh and alternative roles of Spir during oogenesis.

Materials and Methods

Drosophila Stocks

w[1118] (Bloomington, BDSC 3605), yw; Spir-smGFP-HA (Quinlan Lab, Chapter 1), w[*]; P{w[+mC]=matalpha4-GAL-VP16}V37 (Bloomington, BDSC 7063), w[1118]; TI{TI}Rab6[EYFP] (Bloomington, BDSC 62544), w[1118]; TI{TI}Rab9[EYFP] (Bloomington, BDSC 62547), w[1118];; TI{TI}Rab9[EYFP](Bloomington, BDSC 62549), y[1] w[1118] TI{TI}Rab18[EYFP] (Bloomington, BDSC 62551), y[1] w[1118];; TI{TI}Rab23[EYFP] (Bloomington, BDSC 62554), y[1] TI{TI}Rab27[EYFP] w[1118] (Bloomington, BDSC 62556), w[1118] TI{TI}Rab39[EYFP] (Bloomington, BDSC 62560), w[1118]; TI{TI}RabX1[EYFP] (Bloomington, BDSC 62562), y[1] sc[*] v[1] sev[21]; P{y[+t7.7]v[+t1.8]=TRiP.HMS02635}attP40 (Bloomington, BDSC 42942), y[1] sc[*] v[1] sev[21]; P{y[+t7.7] v[+t1.8]=TRiP.GL00510}attP2 (Bloomington, BDSC 36091).

Immunofluorescence of oocytes

Immunofluorescence and mesh staining of *Drosophila* oocytes were performed as described in Chapter 2 with the conditions indicated in the associated figures.

Small-scale fertility assays

Small scale fertility assays for ease of screening were utilized for this initial investigation. 10 virgin females expressing the RNAi for the gene of interest by *matα*-Gal4 were crossed to 5 *wildtype* males in vials. A concurrent control cross was established by crossing 10 virgin *wildtype* females with 5 *wildtype males.* The crosses were then left to mature for 10-14 days at 25°C.The number of pupae formed were then counted and compared to the wildtype control for an approximate comparison of fertility.

Live imaging and analysis

Movies of streaming in mid-stage oocytes and analysis of data collected was performed as described in Chapter 2.

References

Almonacid, M. and Verlhac, M.-H. (2021). A new mode of mechano-transduction shakes the oocyte nucleus, thereby fine tunes gene expression modulating the developmental potential. *C. R. Biol.* 343, 223–234.

Alzahofi, N., Welz, T., Robinson, C. L., Page, E. L., Briggs, D. A., Stainthorp, A. K., Reekes, J., Elbe, D. A., Straub, F., Kallemeijn, W. W., et al. (2020). Rab27a co-ordinates actin-dependent transport by controlling organelle-associated motors and track assembly proteins. *Nat. Commun.* 11, 3495.

Assaker, G., Ramel, D., Wculek, S. K., González-Gaitán, M. and Emery, G. (2010). Spatial restriction of receptor tyrosine kinase activity through a polarized endocytic cycle controls border cell migration. *Proc. Natl. Acad. Sci.* 107, 22558–22563.

Buszczak, M., Lu, X., Segraves, W. A., Chang, T. Y. and Cooley, L. (2002). Mutations in the *midway* Gene Disrupt a Drosophila Acyl Coenzyme A: Diacylglycerol Acyltransferase. *Genetics* 160, 1511–1518.

Compagnon, J., Gervais, L., Roman, M. S., Chamot-Bœuf, S. and Guichet, A. (2009). Interplay between Rab5 and PtdIns(4,5) *P* 2 controls early endocytosis in the *Drosophila* germline. *J. Cell Sci.* 122, 25–35.

Coutelis, J.-B. and Ephrussi, A. (2007). Rab6 mediates membrane organization and determinant localization during *Drosophila* oogenesis. *Development* 134, 1419–1430.

Dollar, G., Struckhoff, E., Michaud, J. and Cohen, R. S. (2002). Rab11 polarization of the *Drosophila* oocyte: a novel link between membrane trafficking, microtubule organization, and *oskar* mRNA localization and translation. *Development* 129, 517–526.

Dong, B., Kakihara, K., Otani, T., Wada, H. and Hayashi, S. (2013). Rab9 and retromer regulate retrograde trafficking of luminal protein required for epithelial tube length control. *Nat. Commun.* 4, 1358.

Dong, B., Miao, G. and Hayashi, S. (2014). A fat body-derived apical extracellular matrix enzyme is transported to the tracheal lumen and is required for tube morphogenesis in *Drosophila*. *Development* 141, 4104–4109.

Dunst, S., Kazimiers, T., von Zadow, F., Jambor, H., Sagner, A., Brankatschk, B., Mahmoud, A., Spannl, S., Tomancak, P., Eaton, S., et al. (2015). Endogenously Tagged Rab Proteins: A Resource to Study Membrane Trafficking in Drosophila. *Dev. Cell* 33, 351–365.

Emery, G. and Ramel, D. (2013). Cell coordination of collective migration by Rab11 and Moesin. *Commun. Integr. Biol.* 6, e24587.

Ganguly, S., Williams, L. S., Palacios, I. M. and Goldstein, R. E. (2012). Cytoplasmic streaming in Drosophila oocytes varies with kinesin activity and correlates with the microtubule cytoskeleton architecture. *Proc. Natl. Acad. Sci.* 109, 15109–15114.

Giedt, M. S., Thomalla, J. M., White, R. P., Johnson, M. R., Lai, Z. W., Tootle, T. L. and Welte, M. A. (2023). Adipose triglyceride lipase promotes prostaglandin-dependent actin

remodeling by regulating substrate release from lipid droplets. *Development* 150, dev201516.

Holubcová, Z., Howard, G. and Schuh, M. (2013). Vesicles modulate an actin network for asymmetric spindle positioning. *Nat. Cell Biol.* 15, 937–947.

Homma, Y., Hiragi, S. and Fukuda, M. (2021). Rab family of small GTPases: an updated view on their regulation and functions. *FEBS J.* 288, 36–55.

Jankovics, F., Sinka, R. and Erdélyi, M. (2001). An Interaction Type of Genetic Screen Reveals a Role of the *Rab11* Gene in *oskar* mRNA Localization in the Developing *Drosophila melanogaster* Oocyte. *Genetics* 158, 1177–1188.

Januschke, J., Nicolas, E., Compagnon, J., Formstecher, E., Goud, B. and Guichet, A. (2007). Rab6 and the secretory pathway affect oocyte polarity in *Drosophila*. *Development* 134, 3419–3425.

Jinek, M., Chylinski, K., Fonfara, I., Hauer, M., Doudna, J. A. and Charpentier, E. (2012). A Programmable Dual-RNA–Guided DNA Endonuclease in Adaptive Bacterial Immunity. *Science* 337, 816–821.

Laiouar, S., Berns, N., Brech, A. and Riechmann, V. (2020). RabX1 Organizes a Late Endosomal Compartment that Forms Tubular Connections to Lysosomes Consistent with a “Kiss and Run” Mechanism. *Curr. Biol.* 1177-1188.e5.

Lakatos, Z., Benkő, P., Juhász, G. and Lőrincz, P. (2021). Drosophila Rab39 Attenuates Lysosomal Degradation. *Int. J. Mol. Sci.* 22, 10635.

Leader, D. P., Krause, S. A., Pandit, A., Davies, S. A. and Dow, J. A. T. (2018). FlyAtlas 2: a new version of the Drosophila melanogaster expression atlas with RNA-Seq, miRNA-Seq and sex-specific data. *Nucleic Acids Res.* 46, D809–D815.

Li, B. X., Satoh, A. K. and Ready, D. F. (2007). Myosin V, Rab11, and dRip11 direct apical secretion and cellular morphogenesis in developing *Drosophila* photoreceptors. *J. Cell Biol.* 177, 659–669.

Lu, W., Lakonishok, M. and Gelfand, V. I. (2021). Gatekeeper function for Short stop at the ring canals of the Drosophila ovary. *Curr. Biol.* 31, 3207-3220.e4.

Matanis, T., Akhmanova, A., Wulf, P., Del Nery, E., Weide, T., Stepanova, T., Galjart, N., Grosveld, F., Goud, B., De Zeeuw, C. I., et al. (2002). Bicaudal-D regulates COPI-independent Golgi–ER transport by recruiting the dynein–dynactin motor complex. *Nat. Cell Biol.* 4, 986–992.

Neumann, A. J. and Prekeris, R. (2023). A Rab-bit hole: Rab40 GTPases as new regulators of the actin cytoskeleton and cell migration. *Front. Cell Dev. Biol.* 11, 1268922.

Ozeki, S., Cheng, J., Tauchi-Sato, K., Hatano, N., Taniguchi, H. and Fujimoto, T. (2005). Rab18 localizes to lipid droplets and induces their close apposition to the endoplasmic reticulum-derived membrane. *J. Cell Sci.* 118, 2601–2611.

Pataki, C., Matusek, T., Kurucz, É., Andó, I., Jenny, A. and Mihály, J. (2010). Drosophila Rab23 Is Involved in the Regulation of the Number and Planar Polarization of the Adult Cuticular Hairs. *Genetics* 184, 1051–1065.

Perkins, L. A., Holderbaum, L., Tao, R., Hu, Y., Sopko, R., McCall, K., Yang-Zhou, D., Flockhart, I., Binari, R., Shim, H.-S., et al. (2015). The Transgenic RNAi Project at Harvard Medical School: Resources and Validation. *Genetics* 201, 843–852.

Pylypenko, O., Welz, T., Tittel, J., Kollmar, M., Chardon, F., Malherbe, G., Weiss, S., Michel, C. I. L., Samol-Wolf, A., Grasskamp, A. T., et al. (2016). Coordinated recruitment of Spir actin nucleators and myosin V motors to Rab11 vesicle membranes. *eLife* 5, e17523.

Ramel, D., Wang, X., Laflamme, C., Montell, D. J. and Emery, G. (2013). Rab11 regulates cell–cell communication during collective cell movements. *Nat. Cell Biol.* 15, 317–324.

Riggs, B., Rothwell, W., Mische, S., Hickson, G. R. X., Matheson, J., Hays, T. S., Gould, G. W. and Sullivan, W. (2003). Actin cytoskeleton remodeling during early *Drosophila* furrow formation requires recycling endosomal components Nuclear-fallout and Rab11. *J. Cell Biol.* 163, 143–154.

Satoh, T., Nakamura, Y. and Satoh, A. K. (2016). Rab6 functions in polarized transport in *Drosophila* photoreceptors. *Fly (Austin)* 10, 123–127.

Short, B., Preisinger, C., Schaletzky, J., Kopajtich, R. and Barr, F. A. (2002). The Rab6 GTPase Regulates Recruitment of the Dynactin Complex to Golgi Membranes. *Curr. Biol.* 12, 1792–1795.

Tanaka, T. and Nakamura, A. (2008). The endocytic pathway acts downstream of Oskar in *Drosophila* germ plasm assembly. *Development* 135, 1107–1117.

Thielicke, W. and Stamhuis, E. J. (2014). PIVlab – Towards User-friendly, Affordable and Accurate Digital Particle Image Velocimetry in MATLAB. *J. Open Res. Softw.* 2,.

Tittel, J., Welz, T., Czogalla, A., Dietrich, S., Samol-Wolf, A., Schulte, M., Schwille, P., Weidemann, T. and Kerkhoff, E. (2015). Membrane Targeting of the Spir·Formin Actin Nucleator Complex Requires a Sequential Handshake of Polar Interactions. *J. Biol. Chem.* 290, 6428–6444.

Xu, D., Li, Y., Wu, L., Li, Y., Zhao, D., Yu, J., Huang, T., Ferguson, C., Parton, R. G., Yang, H., et al. (2018). Rab18 promotes lipid droplet (LD) growth by tethering the ER to LDs through SNARE and NRZ interactions. *J. Cell Biol.* 217, 975–995.

Yao, L.-L., Hou, W.-D., Liang, Y., Li, X. and Ji, H.-H. (2024). Spire2 and Rab11a synergistically activate myosin-5b motor function. *Biochem. Biophys. Res. Commun.* 703, 149653.

Zhang, J., Schulze, K. L., Hiesinger, P. R., Suyama, K., Wang, S., Fish, M., Acar, M., Hoskins, R. A., Bellen, H. J. and Scott, M. P. (2007). Thirty-One Flavors of Drosophila Rab Proteins. *Genetics* 176, 1307–1322.

Chapter 6: Candidate based screen to identify regulators of the *Drosophila* actin mesh.

Introduction

Genetic screens for maternal-effect loci led to the identification of *spir* (Spir), *capu* (Capu) and *chickadee* (Profilin) (Manseau and Schupbach, 1989; Manseau et al., 1996). Later it was found that these mutants cause premature fast streaming (Theurkauf, 1994) which is likely due to failure to form the actin mesh (Dahlgaard et al., 2007). Generation of an exhaustive list of meshwork components has proven difficult, due to the requirement of actin-binding proteins in oogenesis prior to mesh formation and impediments when deciphering subtle changes to the actin mesh and streaming (Drechsler et al., 2017; Ganguly et al., 2012). A common approach for characterizing gene function is RNA interference (RNAi). Knockdown via RNAi occurs by expressing double-stranded RNAs in cells, which induces degradation of homologous RNAs that are present (Heigwer et al., 2018). In *Drosophila*, the first RNAi expressing lines generated required co-expression of the ribonuclease Dicer2 for efficient knockdown and cleavage of mRNA (Heigwer et al., 2018). Improved RNAi expression vectors have been generated and inserted, simplifying the genetics required for knockdown. The most common are VALIUM (Vermillion-AttB-Loxp-Intron-UAS-MCS) lines (Ni et al., 2008). For enhanced germline expression, the VALIUM22 and VALIUM21 vectors were utilized in this study. These vectors were specifically engineered to contain the K10 terminator which permits knockdown of genes during oogenesis and do not require co-expression of Dicer2(Ni et al., 2011).

Recently, Lu et al. has had great success investigating the role of proteins during oogenesis by driving RNAi knockdown with *matα*-Gal4 (Lu et al., 2021; Lu et al., 2022; Lu et al., 2023). *matα*-Gal4 knockdown is induced following oocyte specification in early oogenesis (Lu et al., 2021) (Figure 6-1A). This as advantageous as RNAi of essential genes can stall oogenesis prior to oocyte specification, making it impossible to characterize their function in the actin mesh. Therefore, the most efficient system available for knockdown in the oocyte is the combination of VALIUM21/22 RNAi expression vectors driven by *matα*-Gal4.

We have compiled a list of candidate genes that are characterized for regulating the actin cytoskeleton, other cytoskeletal elements, and membrane anchoring of the cytoskeleton (Table 6-1). Encouraged by the Gelfand Lab, we screened an initial subset of candidates of the *Drosophila* actin mesh as described here.

Table 6-1: List of Initial Cytoskeletal Candidates

Common Name	Drosophila Name, abbreviation	Expression level in the ovary (FlyAtlas, FlyBase)	BDSC stock number of available RNAi lines*
actin crosslinkers			
Fascin	*singed, sn*	mid-level expression in germline cells	42615, 57805
Fimbrin	*fimbrin, fim*	high expression in germline cells	32936, 33977
α-actinin	*α-actinin, actn*	low expression in germline cells	3487
	α-actinin 3, actn3	high expression in somatic cells	26737
Filamin	*cheerio, cher*	high expression in nurse cell plasma membrane and oocyte cortex	35755
	jitterbug, jbug	high expression in somatic cells	39070
actin-MT crosslinkers			
Spectraplakin	*short stop, shot*	low to mid-level expression in female germline cells	41858, 64041
Coronin	*pod1, pod1*	mid-level expression in female germline cells	41705
membrane anchoring			
Vinculin	*vinculin, vinc*	low expression in female germline cells	41959
Dystrophin	*dystrophin, dys*	mid expression in female germline cells	41959
Spectrin	*α-Spectrin, a-spec*	low to mid expression in female germline cells	N/A
	β-Spectrin, b-spec	low expression in female germline cells	N/A
actin regulators			
Cofilin	*twinstar, tsr*	high expression in female germline cells	65055
Cyclase associated protein	*CAP, CAP*	mid expression in female germline cells	36616, 36663
	capulet, capt	mid expression in female germline cells	33010
Capping protein	*capping protein α, cpa*	low to mid expression in female germline cells	41685
	capping protein β, cpb	mid expression in female germline cells	50954, 41952
motors			
MyosinV	*didum, didum*	mid expression in female germline cells	55740
Kinesin Heavy Chain	*kinesin heavy chain, khc*	mid expression in female germline cells	35409, 35770
other cytoskeletal organization			
Non-muscle tropomyosin	*tropomyosin1, tm1*	high expression in female germline cells	43542, 77376
VASP	*enabled, ena*	mid to high expression in female germline cells	39034
CLASP	*chromosome bows, chb*	mid to high expression in female germline cells	35442, 34669

**BDSC stock numbers listed are for most efficient expression in germline cells.*

Results

Initial candidate screening yielded interesting phenotypes

The first mesh candidate genes selected for knockdown included Filamin (*cheerio*), both isoforms of Capping Protein (*capping protein α* and *capping protein ß*), and cofilin (*twinstar*). These genes were originally selected for removal using the auxin inducible degradation system (AID). As we did not have success with this method (**Appendix III**), we elected to pivot to RNAi knockdown in the germline. To ensure that *matα*>RNAi worked as described we repeated knockdown of Dynein (*dhc*) and observed the same small-oocyte phenotype described in Lu et al., 2022 (Figure 6-1C, D).

The first candidate selected was Filamin. Filamin, encoded by *cheerio*, is a dimeric F-actin crosslinker that can also bind transmembrane proteins. Initially characterized as a major component of ring canals, recruiting actin filaments (Sokol and Cooley, 1999), *cheerio* mutants also exhibited disrupted contacts between the follicle cells (Sokol and Cooley, 2003). We hypothesized that as a crosslinker of actin, Filamin is important for proper mesh organization. Staining of the actin mesh in *matα* > *filamin* RNAi oocytes, we detected no difference from wildtype (Figure 6-1B, b-b'). Nor did we observe defects in follicle cell contact or ring canal structure. Consistent with our RNAi knockdown not producing defects in oogenesis, fertility was similar to wildtype in small scale assays (Figure 6-1D). The most dramatic conclusion we can draw from these data is that Filamin is not likely to be a major component of the actin mesh. An explanation for the lack of mesh phenotype is that the RNAi was not effective, as we observed no defects matching existing data from nulls. This could be due to inefficiency of the shRNAi expressed, indicating that a higher available percentage of Gal4 is required.

We also screened Capping Protein, as it regulates actin filament assembly by capping the fast growing, barbed end. This activity allows for fine-tuning and regulation of the assembly of filamentous actin (Edwards et al., 2014). Capping Protein forms a heterodimer, with the two components being encoded in *Drosophila* as *capping protein alpha (cpa)* and *capping protein*

beta (cpb). Phenotypes for *cpa* and *cpb* activity have been described for the wing disc epithelium (Janody and Treisman, 2006) and retina (Delalle et al., 2005). During oogenesis, *cpb* has been characterized as a regulator of oocyte specification, nurse cell integrity, and follicle cell migration (including border cell migration) (Ogienko et al., 2013). Our investigation of the actin mesh and fertility upon knockdown of the individual subunits yielded varying results. Knocking down *cpb*, we observed no distinguishable phenotype: the actin mesh (Figure 6-1B, d-d') and fertility (Figure 6-1D) were comparable to wildtype. Conversely, in *matα* > *cpa* RNAi oocytes we observed an increased amount of actin punctae during mid and late oogenesis (Figure 6-1B, c-c'). In addition, a slight decrease in fertility in small scale rescue makes knockdown of *cpa* an interesting target to study further. As *cpa* and *cpb* heterodimerize, we hypothesize that knockdown of both subunits would lead to a more dramatic phenotype and is worth considering when repeating the experiment (Amândio et al., 2014).

The last component from our candidate list that we screened was Cofilin, encoded by *twinstar* (*tsr*). Cofilin is an important regulator of the actin cytoskeleton, severing filamentous actin to trigger remodeling. In *Drosophila,* Cofilin (*tsr*) is a significant regulator of a wide range of processes, including; bristle formation (Wu et al., 2016), neuron integrity (Sudarsanam et al., 2020), and cell motility during oogenesis (Chen et al., 2001). We presume that in the oocyte, Cofilin has strict temporal regulation, as the actin mesh must rapidly be removed at the onset of late oogenesis. Observation of the actin mesh upon Cofilin RNAi revealed sustained actin mesh during late oogenesis and an increased abundance of cortical actin (Figure 6-1B, e-e'). Compression of the actin mesh at the posterior in late-stage oocytes also indicated failed mixing of cytoplasms (Figure 6-1B, e'). We found that fertility was completely lost, as females produced no offspring with the knockdown of Cofilin (Figure 6-1D). These data are consistent with previous description of *tsr* alleles being predominantly lethal with the few survivors being sterile (Chen et al., 2001). As we observe the actin mesh to be sustained through late oogenesis we aimed to determine the effects of modulating Cofilin activity during oogenesis.

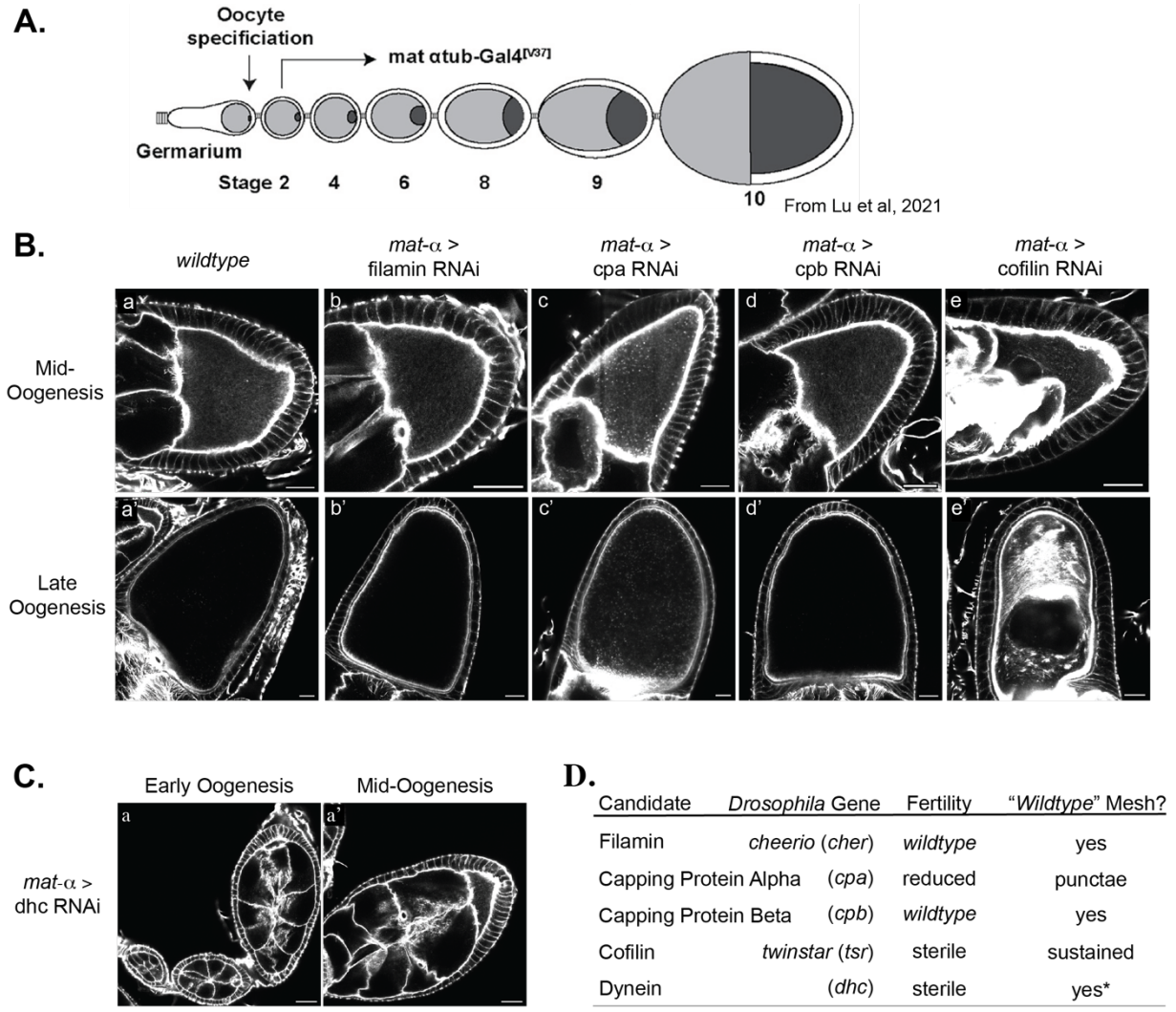

D.

Candidate	*Drosophila* Gene	Fertility	"*Wildtype*" Mesh?
Filamin	*cheerio* (*cher*)	*wildtype*	yes
Capping Protein Alpha	(*cpa*)	reduced	punctae
Capping Protein Beta	(*cpb*)	*wildtype*	yes
Cofilin	*twinstar* (*tsr*)	sterile	sustained
Dynein	(*dhc*)	sterile	yes*

Figure 6-1: Initial screening of actin meshwork components.

*(A.) Schematic of matα-Gal4 expression during Drosophila oogenesis, from (Lu et al., 2021). (B.) Staining of the actin mesh during mid- and late oogenesis with AlexaFluor 488 phalloidin. The genetic backgrounds are as follows: wildtype (a-a'), filamin RNAi (b-b'), capping protein α RNAi (c-c'), capping protein beta RNAi (d-d'), and cofilin RNAi (e-e'). Atypical actin mesh phenotypes were observed in capping protein α (c-c') and cofilin RNAi (e-e'). (C.) Staining of actin structures in dynein heavy chain RNAi. A small oocyte phenotype is observed in early oogenesis (a) and sustained during mid-oogenesis (a'). These egg chambers do not progress to late oogenesis. This phenotype is consistent with published results (Lu et al., 2022). (D.) Summary of findings for initial RNAi knockdown screen. Small scale fertility assays showed consistent findings with actin mesh staining. *RNAi of dynein did not generate late-stage oocytes for observation.*

Further investigation of Cofilin interacting partners

Knockdown of Cofilin, by *matα* > Cofilin RNAi, produced dramatic defects in egg chambers (Figure 6-2A). As removal of Cofilin increased with expression of *matα* in early oogenesis, we observed nurse cells detaching from the surrounding follicle cells and an increase in cortical actin (Figure 6-2A, a-b’’’’). During mid-oogenesis, in egg chambers with a discernable oocyte, we visualize the actin mesh (Figure 6-2A, b-b’’’’). Egg chambers that develop into late oogenesis exhibited a fascinating range of phenotypes, from nurse cell nuclei being dumped into the oocyte (Figure 6-2A, c’) to complete detachment of the oocyte from the follicle cells (Figure 6-2A, c’’’’). Again, in cells with a distinguishable oocyte the actin mesh was sustained through late oogenesis.

In an attempt to restrict knockdown of Cofilin to the oocyte to minimize disruptions to the egg chamber and focus study of the actin mesh, we tested efficiency of Cofilin RNAi with different germline drivers (Figure 6-2B). As commented on by Lu et al., expression of RNAi using *nos*-Gal4 halted oogenesis (Lu et al., 2021). Our own generated *capu*-Gal4 (described in **Chapter 1**) completely halted development of F1 offspring in the larval stage (Figure 6-2C). This suggests that *capu* expression is not limited to germline cells, or more specifically mid-oogenesis. As Spir plays a role in heart development (Xu et al., 2012) and axon growth of neurons (Gates et al., 2011), we presume Capu to also be involved in any number of these processes or others.

From here we tested other commercially available Gal4 drivers. A complete list of GAL4 lines is available on FlyBase and all germline drivers were evaluated as possible candidates for restricting knockdown (https://flybase.org/search/GAL4). From the available Gal4 lines listed on FlyBase, $Gal4^{cb19}$ (cb19) and $Gal4^{cb23}$ (cb23) were selected for study. Annotation of cb19 indicated expression in germline cells, nurse cells and the oocyte, from stages 6-14 and in follicle cells at stages 11-13 (FlyBase). The other Gal4 line selected, cb23, indicated expression in the developing egg chamber from stages 6-14 in the oocyte and stage 11-13 in a few follicle

cells (FlyBase). Although Gal4 expression is not limited to the oocyte, these drivers are described as being expressed later (stage 6) in oogenesis than *matα* (stage 2). The line we received from Bloomington for cb23 (BDSC 6727) did not phenotypically match the stock, yielding no progeny containing the inserted Gal4. Therefore, cb23 experimentation is not described here. We were able to test cb19 and observed that cb19> Cofilin RNAi stalled development similarly to using *capu*-Gal4 (Figure 6-2B, *data not shown*). We hypothesize this is due to cb19-Gal4 expression in other tissues and developmental stages not listed in the annotation.

Cofilin has a number of interacting partners that modulate its severing activity (Figure 6-2D) (Goode et al., 2015). Therefore, in our last attempt to fine-tune Cofilin activity we sought to knock down interacting partners with reported germline expression. Three interacting partners were selected as a small-scale trial; Actin Interacting Protein 1 (AIP1) encoded by *flare* (flr), Mical, and Coronin encoded by *pod1*. AIP1 cooperatively binds actin filaments with Cofilin to enhance efficiency of severing (Ikawa and Sugimura, 2018; Jin et al., 2020). Their direct interaction modulates the amount of actin present around the mitotic spindle during mouse oogenesis (Jin et al., 2020). Interestingly, this is the same time the mouse oocyte is filled with a cytoplasmic actin mesh, built by mammalian homologues of Spir and Capu (Schuh and Ellenberg, 2008). The second candidate, Mical, mediates the oxidation state of filamentous actin, thereby increasing the rate and efficiency of actin severing by Cofilin (as reviewed in (Rajan et al., 2023)). Finally, the last interacting partner we selected was Coronin, which has multiple functions in cytoskeleton regulation. Our initial interest in Coronin (Table 6-1) was as a crosslinker, due to its ability to bind microtubules and actin filaments (Rothenberg et al., 2003). Coronin also enhances recruitment of Cofilin to actin filaments, inducing severing (Mikati et al., 2015). We observed that upon *matα*> RNAi knock down of any of the Cofilin interacting partners described, there was no difference in small-scale fertility (Figure 6-2D). Therefore, we can draw no strong conclusions about their function from this initial investigation. More optimization and

experimentation are required to modulate the effects of Cofilin on oogenesis, focusing on regulation of the actin mesh.

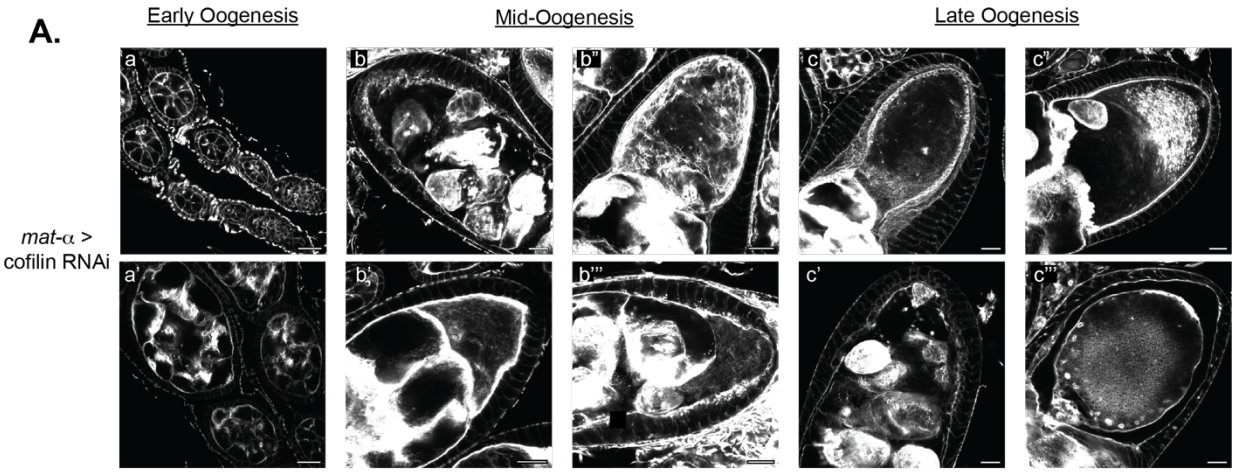

B.

Driver	Bloomington Stock	Result
mat-α	7063	images above
nos	4937	no germ cells
capu	lab generated	no viable adults
cb19	6723	no viable adults

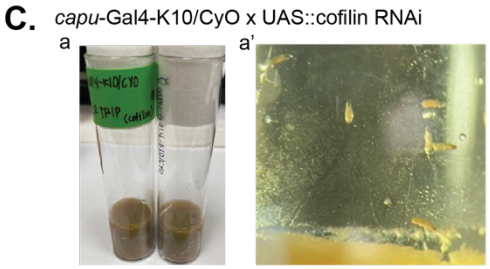

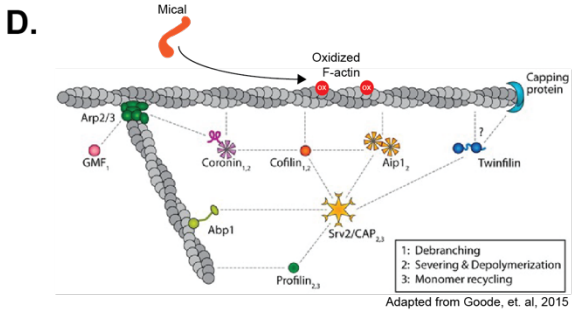

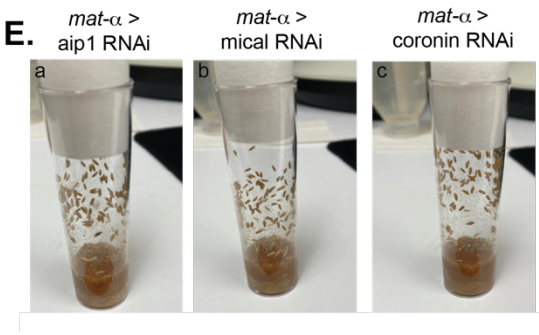

Figure 6-2: Further investigation of Cofilin in actin mesh regulation.

(A.)Phenotypes observed with tsr RNAi, Cofilin knockdown using matα-Gal4 to drive expression. Actin is stained with AlexaFluor488-Phalloidin following the standard mesh staining protocol. (B.) Summary of results using different Gal4 driver lines to drive knockdown of cofilin. (C.) Attempts to cross flies expressing Cofilin RNAi under capu-Gal4 control. No progeny successfully completed pupation. (D.) Overview of cofilin interacting partners screened in this study. Adapted from (Goode et al., 2015) to include Mical. Dashed lines indicate direct interactions. (E.) Small scale fertility assays of RNAi of Cofilin interacting partners using matα-Gal4; (a)Actin Interacting Protein 1(aip1), (b)Mical, (c)Coronin.

Discussion

While new components of the actin mesh remain elusive, this small-scale genetic screen is a promising start to screening candidates. We have identified Capping Protein and Cofilin as likely components, involved in regulating the actin mesh. More experimentation is required to determine the mechanism by which these proteins act on the actin mesh.

A majority of the other RNAi knockdowns presented no observable defects in oogenesis in initial experiments. This could be due to inefficient knockdown of the RNAi. For expression of RNAi lines, the Transgenic RNAi Project (TRiP), suggests using the Maternal Triple Driver (MTD)-Gal4 (Ni et al., 2011). MTD-Gal4 are homozygous insertions of three Gal4 under control *otu* (*ovarian tumor*) with the vp16 terminator, *nos* (*nanos*) with the NGT and vp16 terminators, (BDSC 31777). Together this gives robust expression of Gal4 in the female germline but would stall development prior to actin mesh formation as *nanos* is expressed in the germarium (Wang et al., 1994). Alternatively, increasing expression of the RNAi by driving with two copies of *matα*-Gal4 (BDSC 80361) could improve knockdown efficiency while allowing for oocyte specification.

To control for knockdown, western blotting or IF serves as an important experiment to check for removal in backgrounds where no phenotype is observed. These proposed experiments pose challenges as few antibodies exist for the endogenous genes of interest. Incorporating tagged genes to used epitope labeling is also nontrivial, as the UAS/Gal4 system can have discrepancies in expression patterns and generation of endogenously tagged *Drosophila* is costly and slow. As new endogenously edited *Drosophila* stocks are being generated constantly, availability from Bloomington or other *Drosophila* stock centers would circumvent these limitations in controlling for knockdown.

As exhibited with the Cofilin RNAi, improved spatiotemporal removal of our genes of interest would be beneficial. Further limiting expression of RNAi to stage 6 in oogenesis would minimize effect on other actin structures or stages of *Drosophila* development. Other methods

for temporal regulation, such as optogenetics, could allow for this specificity but again does not permit fast turnaround and evaluation of candidate genes.

It is also important to consider that some phenotypes of the actin mesh may be lost during fixation and staining as large percentages of paraformaldehyde and phalloidin are required for visualization. Therefore, live imaging of mesh dynamics and cytoplasmic streaming would be beneficial to distinguish more subtle changes in mesh organization.

Other projects in the lab include using proteomics and interaction studies to determine components of the actin mesh and more specifically, interactors of Spir and Capu. This study provides support for screening candidates identified through mass spectrometry via RNAi driven by *matα*-Gal4. Further validation on the effects to the actin mesh should include, fertility assays, mesh staining, and streaming analysis. Overall, due to the conservation between actin meshes from other organisms, determining more components to this complex actin network yields high impact and merit.

Materials and Methods

Drosophila Stocks

w[1118] (Bloomington, BDSC 3605), *capu*-Gal4-K10/CyO (Quinlan Lab, unpublished), w[1118];;*nanos*-Gal4-vp16 (Bloomington, BDSC 4937), w[*]; P{w[+mC]=matalpha4-GAL-VP16}V37 (Bloomington, BDSC 7063), y[1] sc[*] v[1] sev[21]; P{y[+t7.7] v[+t1.8]=TRiP.HMS01501}attP2/TM3, Sb[1] (Bloomington, BDSC 35755), y[1] sc[*] v[1] sev[21]; P{y[+t7.7] v[+t1.8]=TRiP.GL00543}attP40 (Bloomington, BDSC 36583), y[1] sc[*] v[1] sev[21]; P{y[+t7.7] v[+t1.8]=TRiP.HMS02249}attP2 (Bloomington, BDSC 41685), y[1] sc[*] v[1] sev[21]; P{y[+t7.7] v[+t1.8]=TRiP.HMS02349}attP2 (Bloomington, BDSC 41952), y[1] sc[*] v[1] sev[21]; P{y[+t7.7] v[+t1.8]=TRiP.HMS00534}attP2 (Bloomington, BDSC 65055).

Mesh staining

For staining and observation of the actin mesh in *Drosophila* oocytes, we followed a standard staining procedure with AlexaFluor488-phalloidin as described in Chapter 1.

Small-scale fertility assays

Small scale fertility assays for ease of screening were utilized for this initial investigation. 10 virgin females expressing the RNAi for the gene of interest by *matα*-Gal4 were crossed to 5 *wildtype* males in vials. A concurrent control cross was established by crossing 10 virgin *wildtype* females with 5 *wildtype males.* The crosses were then left to mature for 10-14 days at 25°C and the number of pupae formed compared to the wildtype control for approximate comparison of fertility.

References

Amândio, A. R., Gaspar, P., Whited, J. L. and Janody, F. (2014). Subunits of the Drosophila Actin-Capping Protein Heterodimer Regulate Each Other at Multiple Levels. *PLoS ONE* 9, e96326.

Chen, J., Godt, D., Gunsalus, K., Kiss, I., Goldberg, M. and Laski, F. A. (2001). Cofilin/ADF is required for cell motility during Drosophila ovary development and oogenesis. *Nat. Cell Biol.* 3, 204–209.

Dahlgaard, K., Raposo, A. A. S. F., Niccoli, T. and St Johnston, D. (2007). Capu and Spire Assemble a Cytoplasmic Actin Mesh that Maintains Microtubule Organization in the Drosophila Oocyte. *Dev. Cell* 13, 539–553.

Delalle, I., Pfleger, C. M., Buff, E., Lueras, P. and Hariharan, I. K. (2005). Mutations in the Drosophila Orthologs of the F-Actin Capping Protein α- and β-Subunits Cause Actin Accumulation and Subsequent Retinal Degeneration. *Genetics* 171, 1757–1765.

Drechsler, M., Giavazzi, F., Cerbino, R. and Palacios, I. M. (2017). Active diffusion and advection in Drosophila oocytes result from the interplay of actin and microtubules. *Nat. Commun.* 8, 1520.

Edwards, M., Zwolak, A., Schafer, D. A., Sept, D., Dominguez, R. and Cooper, J. A. (2014). Capping protein regulators fine-tune actin assembly dynamics. *Nat. Rev. Mol. Cell Biol.* 15, 677–689.

Ganguly, S., Williams, L. S., Palacios, I. M. and Goldstein, R. E. (2012). Cytoplasmic streaming in Drosophila oocytes varies with kinesin activity and correlates with the microtubule cytoskeleton architecture. *Proc. Natl. Acad. Sci.* 109, 15109–15114.

Gates, M. A., Kannan, R. and Giniger, E. (2011). A genome-wide analysis reveals that the Drosophila transcription factor Lola promotes axon growth in part by suppressing expression of the actin nucleation factor Spire. *Neural Develop.* 6, 37.

Goode, B. L., Eskin, J. A. and Wendland, B. (2015). Actin and Endocytosis in Budding Yeast. *Genetics* 199, 315–358.

Heigwer, F., Port, F. and Boutros, M. (2018). RNA Interference (RNAi) Screening in *Drosophila*. *Genetics* 208, 853–874.

Ikawa, K. and Sugimura, K. (2018). AIP1 and cofilin ensure a resistance to tissue tension and promote directional cell rearrangement. *Nat. Commun.* 9, 3295.

Janody, F. and Treisman, J. E. (2006). Actin capping protein α maintains *vestigial* -expressing cells within the *Drosophila* wing disc epithelium. *Development* 133, 3349–3357.

Jin, Z., Yao, X., Wen, L., Hao, G., Kwon, J., Hao, J. and Kim, N. (2020). AIP1 and Cofilin control the actin dynamics to modulate the asymmetric division and cytokinesis in mouse oocytes. *FASEB J.* 34, 11292–11306.

Lu, W., Lakonishok, M. and Gelfand, V. I. (2021). Gatekeeper function for Short stop at the ring canals of the Drosophila ovary. *Curr. Biol.* 31, 3207-3220.e4.

Lu, W., Lakonishok, M., Serpinskaya, A. S. and Gelfand, V. I. (2022). A novel mechanism of bulk cytoplasmic transport by cortical dynein in Drosophila ovary. *eLife* 11, e75538.

Lu, W., Lakonishok, M. and Gelfand, V. I. (2023). The dynamic duo of microtubule polymerase Mini spindles/XMAP215 and cytoplasmic dynein is essential for maintaining *Drosophila* oocyte fate. *Proc. Natl. Acad. Sci.* 120, e2303376120.

Manseau, L. J. and Schupbach, T. (1989). cappuccino and spire: two unique maternal-effect loci required for both the anteroposterior and dorsoventral patterns of the Drosophila embryo. *Genes Dev.* 3, 1437–1452.

Manseau, L., Calley, J. and Phan, H. (1996). Profilin is required for posterior patterning of the Drosophila oocyte. *Development* 122, 2109–2116.

Mikati, M. A., Breitsprecher, D., Jansen, S., Reisler, E. and Goode, B. L. (2015). Coronin Enhances Actin Filament Severing by Recruiting Cofilin to Filament Sides and Altering F-Actin Conformation. *J. Mol. Biol.* 427, 3137–3147.

Ni, J.-Q., Markstein, M., Binari, R., Pfeiffer, B., Liu, L.-P., Villalta, C., Booker, M., Perkins, L. and Perrimon, N. (2008). Vector and parameters for targeted transgenic RNA interference in Drosophila melanogaster. *Nat. Methods* 5, 49–51.

Ni, J.-Q., Zhou, R., Czech, B., Liu, L.-P., Holderbaum, L., Yang-Zhou, D., Shim, H.-S., Tao, R., Handler, D., Karpowicz, P., et al. (2011). A genome-scale shRNA resource for transgenic RNAi in Drosophila. *Nat. Methods* 8, 405–407.

Ogienko, A. A., Karagodin, D. A., Lashina, V. V., Baiborodin, S. I., Omelina, E. S. and Baricheva, E. M. (2013). Capping protein beta is required for actin cytoskeleton organisation and cell migration during *Drosophila* oogenesis. *Cell Biol. Int.* 37, 149–159.

Rajan, S., Terman, J. R. and Reisler, E. (2023). MICAL-mediated oxidation of actin and its effects on cytoskeletal and cellular dynamics. *Front. Cell Dev. Biol.* 11, 1124202.

Rothenberg, M. E., Rogers, S. L., Vale, R. D., Jan, L. Y. and Jan, Y.-N. (2003). Drosophila Pod-1 Crosslinks Both Actin and Microtubules and Controls the Targeting of Axons. *Neuron* 39, 779–791.

Schuh, M. and Ellenberg, J. (2008). A New Model for Asymmetric Spindle Positioning in Mouse Oocytes. *Curr. Biol.* 18, 1986–1992.

Sokol, N. S. and Cooley, L. (1999). Drosophila Filamin encoded by the cheerio locus is a component of ovarian ring canals. *Curr. Biol.* 9, 1221–1230.

Sokol, N. S. and Cooley, L. (2003). Drosophila filamin is required for follicle cell motility during oogenesis. *Dev. Biol.* 260, 260–272.

Sudarsanam, S., Yaniv, S., Meltzer, H. and Schuldiner, O. (2020). Cofilin regulates axon growth and branching of Drosophila γ neurons. *J. Cell Sci.* jcs.232595.

Wang, C., Dickinson, L. K. and Lehmann, R. (1994). Genetics of *nanos* localization in *Drosophila*. *Dev. Dyn.* 199, 103–115.

Wu, J., Wang, H., Guo, X. and Chen, J. (2016). Cofilin-mediated actin dynamics promotes actin bundle formation during *Drosophila* bristle development. *Mol. Biol. Cell* 27, 2554–2564.

Xu, P., Johnson, T. L., Stoller-Conrad, J. R. and Schulz, R. A. (2012). Spire, an Actin Nucleation Factor, Regulates Cell Division during Drosophila Heart Development. *PLoS ONE* 7, e30565.

Chapter 7: Developing Long-Term Live Imaging of the *Drosophila* egg chamber.

Introduction

The mid- to late-stage transition in oogenesis has not been visualized, as egg chambers expire *ex vivo* just prior to the removal of the actin mesh (Gutzeit and Koppa, 1982). The cause of this developmental failure *ex vivo* remains unclear as, egg chambers can be cultured successfully from stage 11 to maturity (Gutzeit and Koppa, 1982). The lack of direct visualization leaves description of *Drosophila* oogenesis incomplete and a gap in our understanding of the actin mesh. To permit the mid- to late-stage transition, we aimed to develop long-term *in vivo* imaging of oogenesis for *Drosophila melanogaster*. The motivation for taking on this endeavor arose from success in performing high-resolution imaging of the midgut in live animals (Martin et al., 2018). Due to the close proximity between the midgut and female ovary in the *Drosophila* abdomen, we determined that modifications to the developed imaging method would be advantageous for visualizing the stage transition in oogenesis. By housing the ovary in its native environment, we hypothesized egg chambers would continue to develop due to sufficient signaling from surrounding tissues.

Producing a full description of the mid- to late-stage transition would complete the description of major events in *Drosophila* oogenesis. Thereby allowing the *Drosophila* community to dream up ways of studying oogenesis and its regulation in greater detail. Specific to our research interests, visualizing the removal of the actin mesh lends to our understanding of the function of this cytoskeletal element. This work is critical, as it allows a greater understanding of higher order actin structures *in vivo* and translates to studies in organisms as the cytoplasmic actin meshwork is conserved in *C. elega*ns (Panzica et al., 2017), mouse (Azoury et al., 2008) and even human oocytes (Trebichalská et al., 2021).

Results

Developing long-term in vivo imaging of oogenesis in Drosophila

The standard methods of studying oogenesis are all *ex vivo* (Gutzeit and Koppa, 1982). This has allowed for characterization of key developmental stages in *Drosophila* oogenesis, including cytoplasmic streaming (Theurkauf, 1994), collective cell migration (Dai and Montell, 2016), and mRNA localization (Becalska and Gavis, 2009). However, we cannot study the removal of the actin mesh, which occurs between stages 10 and 11 in oogenesis as *ex vivo* egg chambers expire before this transition.

Therefore, we set out to adapt Windowmount (Martin et al., 2018). Windowmount is a live-imaging method for visualization of stem cell dynamics within the midgut, which has close proximity to the female ovary (Figure 7-1A). In summary, flies are mounted to an imaging rig (Figure 7-1A', adapted from Martin et al., 2018) and a window in the abdominal cuticle is cut out to expose the ovaries. The exposed ovaries are stabilized in mounting media and agarose to prevent escape of organs and dehydration during long imaging periods (Figure 7-1B, adapted from Martin et a., 2018). The flies are then fitted with a feeding tube and given a sucrose solution inside of a humidity chamber to increase vitality during imaging. Feeder tubes were built using a twisted wire that could pull cotton through a cut capillary tubes (Figure 7-2A, a-a'). We determined the feeder tube was a large source of variation in survival rates (Figure 7-2A, b). If too much cotton or sucrose solution was added to the feeder tube, the fly drowned overnight.

The original Windowmount design described specific dimensions to be milled into metal shims (Trinity Brand Industries, 612H-1) using a laser cutter (Figure 7-1B', adapted from Martin et al., 2018). UCLA does not have a laser cutter capable of milling metal that is available for general use. Therefore, working with the Physical Science Machine Shop and Instrument Fabrication Facility at UCLA (Knudsen Hall, Room 20) we fabricated our own metal shims by manually drilling the approximate shape and size provided from the Windowmount manuscript (Figure 7-1C, c). Ultimately, these shims were not ideal, as the sizes were inconsistent and too

large to properly restrain the abdomen. The dimensions provided from the Windowmount method are for abdomens of pre-fattened flies. The abdomens of the flies we used were smaller as we determined we could not pre-fatten females overnight. Fattening of females led to an increased rate of ovary escape through the window in the cuticle and subsequently increased the rate of imaging failures. Another drawback was that the metal corroded when exposed to the imaging media. Therefore, we turned to alternative materials to fabricate the fly restraint: hand drilling and etching of small holes in different plastic materials available in the lab including the petri dish lids (*data not shown*), weigh boats (Fisherbrand™, 01-549-752, Figure 7-1C, a), and Shrinky Dink (Amazon, Figure 7-1C, b). We found hand drilling to be inconsistent and inefficient. Therefore, we looked for a better solution.

We took measurements of two classes of fly abdomens, “regular” and “smaller”, and devised a new strategy with the Physical Science Machine Shop to build a punch press that could generate consistent mounting shims (Figure 7-1D, a-g). The press works by punching a hole in the center of weigh boats in the shape of a fly abdomen. We had two plates designed to build shims of both sets of dimensions (Figure 7-1D, e-e’). This system allows for rapid and consistent generation of mounting shims. The weigh boats are then glued (DAP 00688, Silicone adhesive) overnight to modified 35mm petri dishes (Corning™, 3294). The petri dishes have a 1cm diameter hole drilled into the center of the top lid, to allow for direct mounting of the fly to the weigh boat shim. A notch is also cut out of the side wall on the top and bottom of the dish for feeder tube access (Figure 7-1F, a-d). With the completed shims, we were able to mount flies on the rigs (Figure 7-1G, a). We determined that mounting the fly laterally, instead of prone, to the objective led to consistent exposure of the ovary upon cuticle removal (Figure 7-1G, b, c). With the rigs we generated from this modified design, we streamlined production and consistency, as the weigh boat serves as both the shim for mounting and reservoir for imaging media.

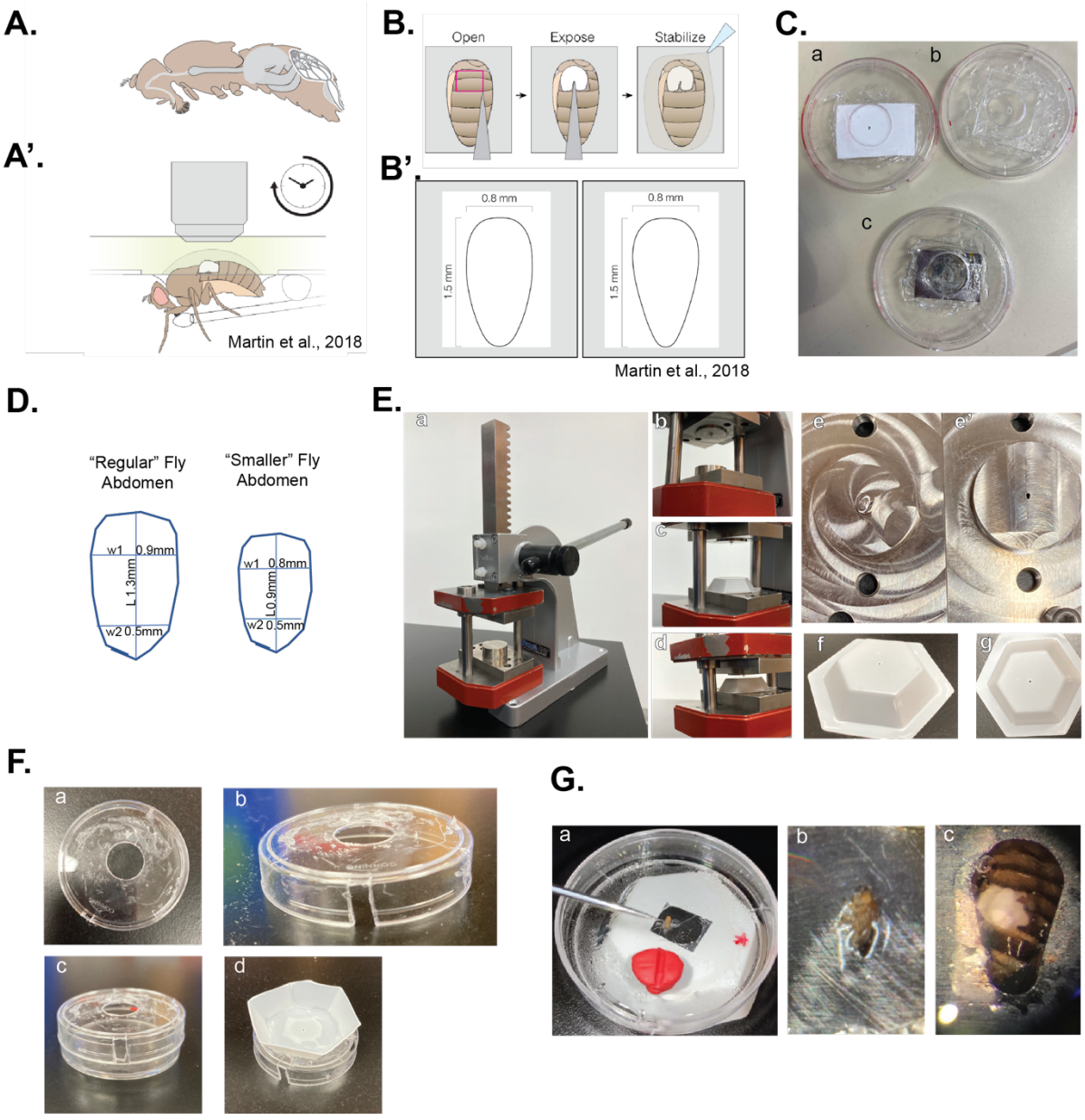

Figure 7-1:Development of imaging rigs for long-term live imaging of Drosophila oocytes.

(A.) Positional similarity of the midgut and ovary in the female abdomen. (A') Depiction of fly mounted to imaging rig, a metal shim is attached to a petri dish while a feeding tube is attached by dental wax and a humidity chamber keeps the fly alive for long periods of imaging (adapted from Martin et al., 2018). (B.) The abdomen of the fly is positioned in the metal shim where the midgut/ovary can be exposed for imaging. (B') The dimensions for milling of the metal shims to mount the abdomen (adapted from Martin et al., 2018). (C.) Our attempts of making shims for mounting out of (a)polystyrene weigh boats, (b)Shrinky Dink and (c)metal. (D.) Measurements of fly abdomens of fed, "Regular" and unfed "smaller" fly abdomens for fabrication of press. (E.) Press used to punch weigh boats for imaging rig fabrication. Two press blocks were fabricated and can easily be swapped out on the press. (F.) Petri dish modified into an imaging chamber. (G.) Fly mounted to the imaging apparatus (a), mounting the fly on its side instead of back (b) allowed for cleaner dissection and visualization of the ovary (c).

The switch from metal to plastic mounting shims made it so the recommended low toxicity silicone adhesive (Kwik-Sil, World Precision Instruments) used to glue the fly did not cure properly. Unfortunately, the flies could drag themselves out of the imaging field, covered in epoxy. Therefore, by recommendation of the Frye Lab, we started using UV curable glue (Amazon) and found success. Curing of the glue and restraint of the fly occurred in 30s (with 10s bursts of exposure). As UV glue dries solid, with no elasticity like epoxy, it was critical to minimize the amount of glue attached to the fly. We found that if improperly restrained, longevity of the mounted fly decreased: this was due to flies being unable to excrete waste, feed, deposit eggs, and move - which in some cases led to self-amputation. Therefore, we built gluing needles (Figure 7-2B) to transfer the smallest amount of UV-curable glue possible.

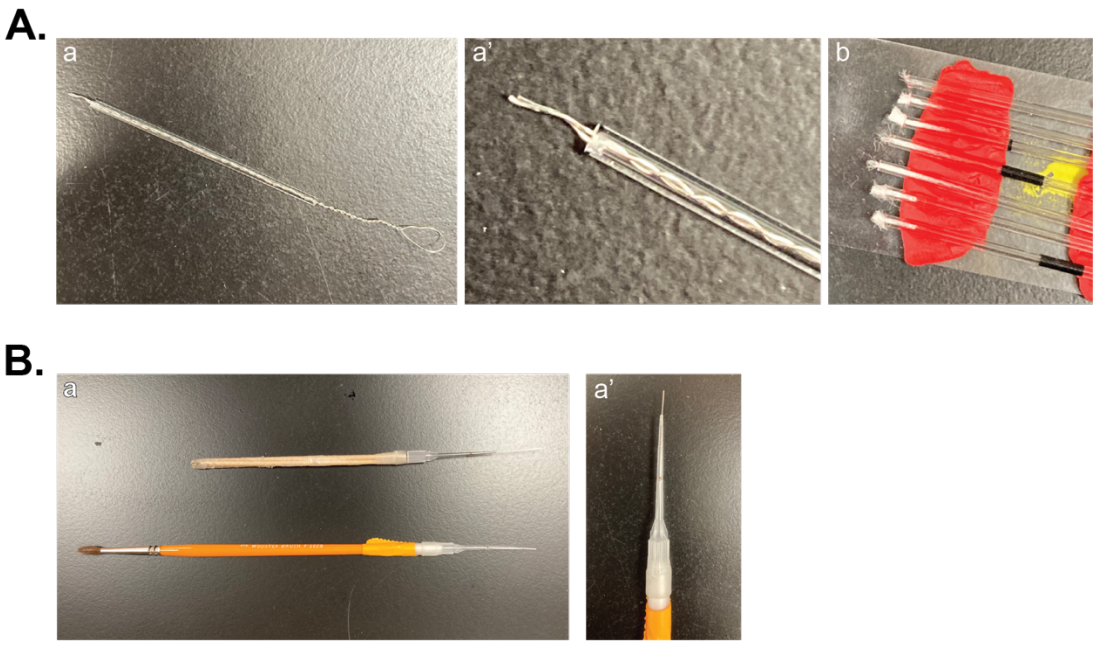

Figure 7-2: Tools fashioned to improve efficiency in imaging set-up.

(A.) A twisted tungsten wire (32 AWG gauge, Amazon) was used to make a hook (a-a') that could grab small amounts of cotton to generate the feeder tubes (b). (B.) Gluing needles built to minimize the amount of UV glue used to restrain the fly (a). Insect pins (VWR, Size 000, 470222-088) are fed into a P20 pipette tip (Rainin, 30389296) and secured on the end of a paint brush or wooden dowel using parafilm (a').

Using modified Long-Term Live Imaging to visualize oogenesis in vivo

We quickly determined that the confocal microscopes available to us did not allow for optimal imaging of the ovary. Ideally, the entire depth of the oocyte will be imaged (ranges from 10μm to >100μm). In general, confocal microscopy works up to 200μm, however, the ooplasm is highly scattering in nature and limits maximal imaging depths to ~20μm *ex vivo*. The layer of agarose to stabilize the exposed ovary also added a variable depth to penetrate. To overcome this limitation in imaging penetration, we used two-photon microscopy (2PM) for vital imaging of the ovary, which itself was novel for studying *Drosophila* oogenesis. Importantly, two-photon illumination is less damaging, allowing for extended periods of continuous imaging.

Thanks to the generosity of the Akin Lab, we were able to use 2PM (Vivo Multiphoton System, Akin Lab, UCLA). Using the mounting strategy described above and in the methods, we were able to sustain immobilized flies for multi-hour windows. We determined success of longevity to be mixed, with approximately half of the mounted and imaged flies surviving for 13-15hrs. Improvements to dissection technique to remove the cuticle, mounting stability of the abdomen, application of UV glue, and proper rate of feeding of the sucrose solution can be made to increase survivability.

To track the oocytes, we used flies endogenously expressing Histone-GFP (BDSC 24163). Using this line, we could clearly visualize nuclei of the nurse cells, oocyte, and surrounding follicle cells (Figure 7-3). To ensure that the ovary was not perturbed and oogenesis was progressing we used SYTOX™ Red (Thermofisher, S34859).

There were several common issues that halted overnight imaging runs (Figure 7-3).

The first issue was tripping of the Photon Multiplier Tubes (PMTs) that halted data acquisition. This shut-off mechanism exists within the microscope software to protect the integrity of the detectors, if the signal collected from the sample is well over the detection threshold and could do damage. Common causes of PMT shut-off included cuticle and hair follicles entering the field of view as they are highly reflective (Figure 7-3A). Another failure to

successfully image the egg chamber overnight occurred due to drift of the ovary in the abdomen. This caused egg chambers to migrate outside of the imaging window and occurred in the XY plane (Figure 7-3B), Z plane (Figure 7-3C), and sometimes a combination of all planes. The motion in these instances were too great to salvage the data using correction plugins available through FIJI (StackReg and Correct 3D Drift). The most common cause of drift was a result of the flies pulling their abdomens and internal organs outside of the imaging plane. We ascertain that minimizing the movement of the fly via further restriction or anesthetics could improve this issue. Lastly, if the cell stayed in the field of view it would often expire, as indicated by changes to cellular morphologies and permeabilization of the SYTOX™ stain (Figure 7-3D).

Not all imaging attempts were failures. Excitingly, we were able to visualize border cell migration (Figure 7-4A). During oogenesis, the migrating border cell cluster delaminates from the anterior follicle cells at stage 9 and migrates to the anterior oocyte cortex by stage 10A (Lamb et al., 2020). Border cells are commonly used as a tool for studying collective cell migration and metastasis (Dai and Montell, 2016; McLaughlin and Bratu, 2015). Although border cell migration can be studied *ex vivo* (Dai and Montell, 2016), we take this as a positive indication that proper oogenesis can occur using our imaging set up and 2PM.

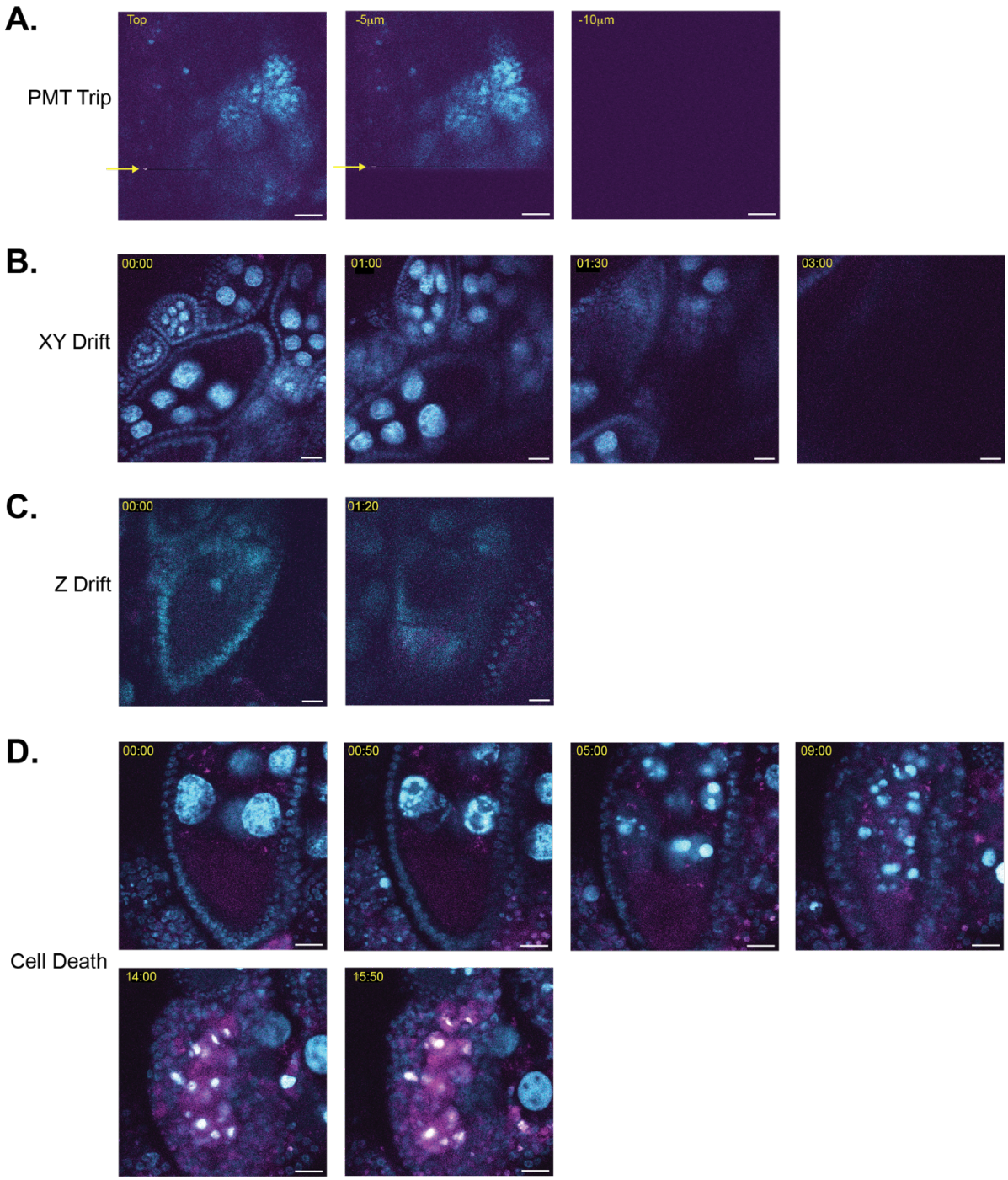

Figure 7-3: Common issues during overnight imaging runs.

All egg chambers are expressing Histone-GFP. (A.) PMT was tripped while acquiring the second image in a z-stack with 5µm depth (yellow arrow). This stopped acquisition and required a reset of the PMT in the software. (B.) Drift of the ovary out of the field of view(FOV) in the XY planes to where very little of the egg chamber is left in the FOV after 3 hours of imaging. (C.) Z-plane drift after an hour of imaging, signal of the oocyte is lost. (D.) Stage 9/10a oocyte imaged over 16 hours, also expressing RFP-Golgi. The first indication of cell death is nuclear breakdown in the nurse cells, begins approximately 1hour into the acquisition. SYTOX™ Red stains the dying cell at 14 hours. Time: HH:MM, Scale Bars: 20µm.

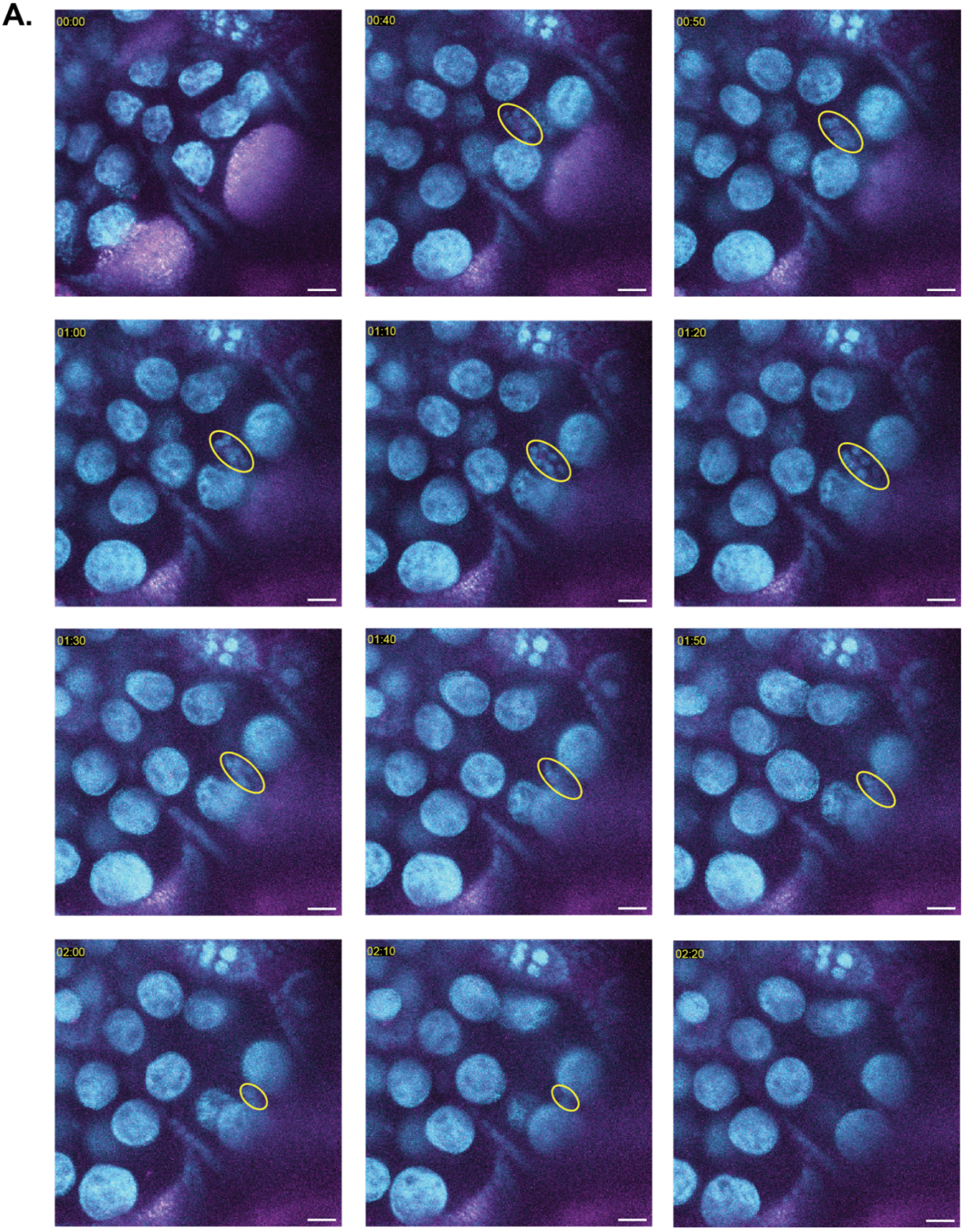

Figure 7-4:Visualization of border cell migration in a mid- to late-stage stage 9 oocyte.

(A.) Stage 9 oocyte imaging over a 140-minute window expressing Histone-GFP (cyan) and GEMs droplets in the oocyte (magenta). Border cells (yellow ellipsoid) become visible at 40 minutes and can be visualized migrating in a 90-minute time period. Time: HH:MM, Scale bars: 20μm.

Discussion

We set out to develop long-term live imaging of the *Drosophila* egg chamber using 2PM to characterize the stage 10 to 11 transition. Our motivation stemmed from gaining a greater understanding of actin mesh removal and establishment of a wild-type description of this stage transition. While our current attempts have not been successful, we have made improvements towards optimizing and streamlining the imaging setup (Figures 7-1 and 7-2). This method is relatively low throughput as a single fly, with one ovary exposed, is imaged overnight. To be able to move past the common issues we ran into during overnight runs (Figure 7-3), further optimization using widefield microscopy would be advantageous over 2PM. In a larger field of view the survival of multiple flies can be tracked overnight. Biasing ovaries to express a higher percentage of mid-stage oocytes would also lead to higher success rates in visualizing the mid- to late-stage transition. Dissection and mounting of flies revealed few stage 9/10a egg chambers in the cuticle window. Using methods such as diapause to generate females with specifically aged germ cells could improve success of finding the appropriate stage upon cuticle removal.

Numerous groups have been working towards improving success of long-term live imaging of *Drosophila* tissues(Balachandra and Amodeo, 2024; Marchetti et al., 2022; Martin et al., 2018). Some success has achieved for *ex vivo* imaging by co-culturing with excised organs (Marchetti et al., 2022). This is interesting to consider using organs in the imaging media for this method, as the extra organs could provide another nutrient source. The Martin lab has also developed “Bellymount” for midgut imaging (Koyama et al., 2020). Briefly, the fly is compressed against a coverslip for direct imaging instead of dissected. “Bellymount” has shown some success with imaging the developing egg chamber (Balachandra and Amodeo, 2024). As the transition from mid- to late-stage-oogenesis remains undescribed in the report, Bellymount could be a feasible next step in the attempts in characterization and leaves room for our research.

Materials and Methods

Drosophila Stocks

w[*]; P{w[+mC]=His2Av-EGFP.C}2/SM6a (Bloomington, BDSC 24163), w[*]; P{w[+mC]=UASp-RFP.Golgi}5 (Bloomington, BDSC 30908), w[*]; P{w[+mC]=matalpha4-GAL-VP16}V37 (Bloomington, BDSC 7063) and yw;;UASP:GEM(w+)M1/TM3 (Gelfand Lab).

Long Term Live Imaging

The method is largely based off of (Martin et al., 2018). The imaging media, sucrose solution, and mounting media have the same components as published. Modifications to the imaging rigs to work with the 2PM set up are described above.

For image acquisition, the Akin lab custom upright Vivo Multiphoton System (3i) was used. The system is equipped with a 20× water immersion objective (Zeiss, W Plan-Apochromat 10x/1.0 DIC) and 2 GaAsP detectors (Hamamatsu). A tunable Ti:Sapphire pulsed laser (Chameleon Ultra II, Coherent) and as well as a fixed wavelength pulsed laser (Axon 1064, Coherent) were used as the light sources. Imaging acquisition parameters were set at 20-35μm Z-stacks with 5μm steps to image the oocyte over 16 hours with 10-minute intervals.

References

Azoury, J., Lee, K. W., Georget, V., Rassinier, P., Leader, B. and Verlhac, M.-H. (2008). Spindle Positioning in Mouse Oocytes Relies on a Dynamic Meshwork of Actin Filaments. *Curr. Biol.* 18, 1514–1519.

Balachandra, S. and Amodeo, A. A. (2024). Bellymount-Pulsed Tracking: A Novel Approach for Real-Time In vivo Imaging of Drosophila Oogenesis. 2024.03.31.587498.

Becalska, A. N. and Gavis, E. R. (2009). Lighting up mRNA localization in Drosophila oogenesis. *Development* 136, 2493–2503.

Dai, W. and Montell, D. J. (2016). Live Imaging of Border Cell Migration in Drosophila. In *Chemotaxis* (ed. Jin, T.) and Hereld, D.), pp. 153–168. New York, NY: Springer New York.

Gutzeit, H. and Koppa, R. (1982). Time-lapse film analysis of cytoplasmic streaming during late oogenesis of Drosophila. *J. Embryol. exp. Morph* 67, 101–111.

Koyama, L. A. J., Aranda-Diaz, A., Su, Y.-H., Balachandra, S., Martin, J., Ludington, W., Huang, K. C. and O'Brien, L. E. (2020). Bellymount enables longitudinal, intravital imaging of abdominal organs and the gut microbiota in adult Drosophila. *PLOS Biol.* 19.

Lamb, M. C., Anliker, K. K. and Tootle, T. L. (2020). Fascin regulates protrusions and delamination to mediate invasive, collective cell migration in vivo. *Dev. Dyn.* 249, 961–982.

Marchetti, M., Zhang, C. and Edgar, B. A. (2022). An improved organ explant culture method reveals stem cell lineage dynamics in the adult Drosophila intestine. *eLife* 11, e76010.

Martin, J. L., Sanders, E. N., Moreno-Roman, P., Jaramillo Koyama, L. A., Balachandra, S., Du, X. and O'Brien, L. E. (2018). Long-term live imaging of the Drosophila adult midgut reveals real-time dynamics of division, differentiation and loss. *eLife* 7,.

McLaughlin, J. M. and Bratu, D. P. (2015). Drosophila melanogaster Oogenesis: An Overview. In *Drosophila Oogenesis* (ed. Bratu, D. P.) and McNeil, G. P.), pp. 1–20. New York, NY: Springer New York.

Panzica, M. T., Marin, H. C., Reymann, A.-C. and McNally, F. J. (2017). F-actin prevents interaction between sperm DNA and the oocyte meiotic spindle in C. elegans. *J. Cell Biol.* 216, 2273–2282.

Quinlan, M. E. (2013). Direct interaction between two actin nucleators is required in Drosophila oogenesis. *Development* 140, 4417–4425.

Theurkauf, W. (1994). Premature microtubule-dependent cytoplasmic streaming in cappuccino and spire mutant oocytes. *Science* 265, 2093–2096.

Trebichalská, Z., Kyjovská, D., Kloudová, S., Otevřel, P., Hampl, A. and Holubcová, Z. (2021). Cytoplasmic maturation in human oocytes: an ultrastructural study †. *Biol. Reprod.* 104, 106–116.

Chapter 8: Conclusion

Introduction

Drosophila oogenesis serves as an important model system for studying development and polarization of cells. A majority of this developmental process has been described in great detail (King, 1970). There are a few gaps that remain in this model system. First, the onset of late oogenesis, and subsequently, fast streaming remains undescribed. This is due to limitations in current imaging methods, as dissected egg chambers arrest at stage 10A. Stage 10A is the developmental stage just prior to the removal of the actin mesh and onset of late oogenesis (reviewed in, Quinlan, 2016). Second, we have a gap in our knowledge of the actin mesh. We do not understand the mechanism of its regulation, its composition, and timing of its removal. Many cytoskeletal regulators play pivotal roles in oogenesis prior to actin mesh formation. Their removal can halt oogenesis at these early stages, making study of their role in the oocyte impossible (Lu et al., 2021). The work in this dissertation was aimed at overcoming these limitations, allowing for a greater understanding of the actin mesh and the role it plays during oogenesis.

Discussion

Improving Transgene Rescue of Spir and Capu

We first set out to better study the role of Spir and Capu during oogenesis, with the aim of understanding the role these actin nucleators play in maintaining the actin mesh. We were able to establish improved transgene rescue of *capu* nulls using a Capu specific driver, *capu*-Gal4 (**Chapter 2**). Which then allowed us to investigate the influence of Capu's localization on oogenesis (**Chapter 3**). We determined that membrane-bound Capu is capable of performing its canonical role, forming the actin mesh, but overall, there is a marked reduction in fertility. Intriguingly, we observed a disruption in posterior pole organization with expression of membrane-bound Capu. Further investigating the organization of the oocyte, such as visualizing microtubule orientation, could assist in understanding the disruption of the posterior anchor. Our

work also hinted at failed embryogenesis with CapuJ rescue. Collaborating with an embryogenesis lab to determine the role Capu is playing in these developmental stages could be fruitful.

As attempts to improve transgene rescue of *spir* null remain unsuccessful (**Chapter 2**), a new *spir*-Gal4 driver is required. Excitingly, the Quinlan Lab recently received such a line from the Gene Disruption Project (Bellen Lab, Baylor College of Medicine). We hope that this version of *spir*-Gal4 proves successful for rescue of *spir* null egg chambers. Testing this driver for rescue using wildtype Spir transgenes is the first step. If the rescue with wildtype transgenes is successful, we could study Spir domains and interactions that yielded mixed phenotypes using *nanos*-Gal4 (Bradley et al., 2019). Similar to Capu, we could also investigate the role Spir's membrane localization plays in actin mesh maintenance and/or removal (Tittel et al., 2015).

To further improve transgene rescue of *spir* and *capu* null egg chambers, trading germline-specific elements (UASp/K10+) for those that express strongly in somatic and germline cells (UASz/p10) should be considered (Masukawa et al., 2021). This work is motivated by somatic cell localization we observed with endogenous Spir/Capu. Understanding the role Spir/Capu play and actin structures they build in these cell types would be a new line of investigation for our lab.

Endogenous tagging of Spir and Capu

We generated numerous endogenously tagged fly lines for Spir and Capu (**Chapter 2**). Overall, these were considered successful and we used immunofluorescence to describe the localization pattern over oogenesis. To our disappointment, the signal from the fluorescent protein tags was below the limit of detection in live samples. As we now have established workflows to endogenously edit Spir and Capu at the C-termini, we can insert any fluorescent tag at the genomic loci. To permit live imaging, we should strongly consider using Halo or SNAPf tags which have improved signals for labeling Drosophila tissues (Sutcliffe et al., 2017).

A major hypothesis we have is that Spir and Capu are important to maintain the actin mesh during mid-oogenesis. We attempted to test this theory by adding the AID motif, part of the Auxin Inducible Degradation system, but we had little success (**Appendix III**). As optogenetics works in the egg chamber (Lu et al., 2022), we should consider using this system for Spir and Capu to restrict their activity in the oocyte. Thereby, allowing for testing of their role in mesh maintenance during mid-oogenesis.

Further improving co-imaging of Spir and Capu is critical for understanding the dynamics of their interactions during oogenesis. One avenue is to improve staining of fixed samples to have consistent, similar relative signal intensities for both channels (Bolte and Cordelières, 2006). Another option is to revisit FRAP, using endogenous tagging or improved transgene rescue established here (**Chapter 2**). As our current colocalization data suggests Capu is working independently from Spir at the posterior oocyte (**Chapter 3**), probing their interactions at this region would be incredibly interesting.

Genetic Screens for Mesh Components

To determine what comprises the actin mesh, outside of Spir, Capu, and profilin (Dahlgaard et al., 2007; Manseau et al., 1996), we employed genetic screens. Motivated by our work studying the Spir/MyosinV interaction (**Chapter 4**), we focused on Rabs (**Chapter 5**) and candidates we established to be other actin meshwork components (**Chapter 6**). These screens are preliminary, a number of the candidates should be revisited – potentially with a stronger RNAi driver 2X *matα*-Gal4 (BDSC 80361). We have determined that Cofilin is involved in actin mesh removal and is critical to many other actin-based structures in the egg chamber. There is no perfect Gal4 line to induce knockdown of Cofilin in only the oocyte, specifically at mid-oogenesis. Optogenetics offers the temporal control we require to further study the role of Cofilin in mesh removal.

At this time, the Quinlan Lab is generating mass spectrometry data for direct interactors of Capu and specific stages in oogenesis. These data will lead to a large list of candidates to test further, with the workflows established in this thesis (**Chapter 6**). For example, using RNAi knockdown will provide a secondary screen to focus the candidates. As discussed, some candidates may have a subtle effect on the actin mesh. Measuring mesh dynamics by direct imaging of actin (mCherry-Lifeact or UtrnCH-GFP) or close analysis of streaming (PIV and 2D Correlation) could lend more information. Overall, due to the conservation between actin meshes from other organisms, determining more components to this complex actin network yields high impact and merit.

Direct Imaging of Actin Mesh Removal

Lastly, an ongoing goal is to directly visualize the removal of the actin mesh and characterize the stage 10 to 11 transition in wildtype egg chambers. We were able to make modifications to an established long-term live imaging protocol (Martin et al., 2018), but did not have enough time to dedicate to getting this method working (**Chapter 7**). If established, the world is our oyster. We could perturb the actin mesh via drug treatment in the imaging media; adding Cytochalasin D or Latrunculin A to induce depolymerization or Phalloidin to stabilize the mesh. We could also use different genetic mutants to alter mesh dynamics and timing of removal. As our most recent results were promising, we should continue to improve this method, but should also consider concurrently trying alternate approaches such as Bellymount (Koyama et al., 2020). Bellymount was recently used to study the developing egg chamber (Balachandra and Amodeo, 2024).

In conclusion, many efforts were made to better understand the *Drosophila* actin mesh. The Quinlan lab has an expanded toolkit to further tackle this endeavor, and we can dream up many lofty goals – as suggested in this conclusion. Accomplishing any number of these

experiments, even one, yields information to broaden our understanding of complex actin networks and the model of *Drosophila* oogenesis. Which is of high value to the scientific community.

References

Balachandra, S. and Amodeo, A. A. (2024). Bellymount-Pulsed Tracking: A Novel Approach for Real-Time In vivo Imaging of Drosophila Oogenesis. 2024.03.31.587498.

Bolte, S. and Cordelières, F. P. (2006). A guided tour into subcellular colocalization analysis in light microscopy. *J. Microsc.* 224, 213–232.

Bradley, A. O., Vizcarra, C. L., Bailey, H. M. and Quinlan, M. E. (2019). Spire stimulates nucleation by Cappuccino and binds both ends of actin filaments. *Mol. Biol. Cell* 31, mbc.E19-09-0550.

Dahlgaard, K., Raposo, A. A. S. F., Niccoli, T. and St Johnston, D. (2007). Capu and Spire Assemble a Cytoplasmic Actin Mesh that Maintains Microtubule Organization in the Drosophila Oocyte. *Dev. Cell* 13, 539–553.

King, R. C. (1970). *Ovarian development in Drosophila melanogaster*. Academic Press.

Koyama, L. A. J., Aranda-Diaz, A., Su, Y.-H., Balachandra, S., Martin, J., Ludington, W., Huang, K. C. and O'Brien, L. E. (2020). Bellymount enables longitudinal, intravital imaging of abdominal organs and the gut microbiota in adult Drosophila. *PLOS Biol.* 19.

Lu, W., Lakonishok, M. and Gelfand, V. I. (2021). Gatekeeper function for Short stop at the ring canals of the Drosophila ovary. *Curr. Biol.* 31, 3207-3220.e4.

Lu, W., Lakonishok, M., Serpinskaya, A. S. and Gelfand, V. I. (2022). A novel mechanism of bulk cytoplasmic transport by cortical dynein in Drosophila ovary. *eLife* 11, e75538.

Manseau, L., Calley, J. and Phan, H. (1996). Profilin is required for posterior patterning of the Drosophila oocyte. *Development* 122, 2109–2116.

Martin, J. L., Sanders, E. N., Moreno-Roman, P., Jaramillo Koyama, L. A., Balachandra, S., Du, X. and O'Brien, L. E. (2018). Long-term live imaging of the Drosophila adult midgut reveals real-time dynamics of division, differentiation and loss. *eLife* 7,.

Masukawa, M., Ishizaki, Y., Miura, H., Hayashi, M., Ota, R. and Kobayashi, S. (2021). Male-biased protein expression in primordial germ cells, identified through a comparative study of UAS vectors in Drosophila. *Sci. Rep.* 11, 21482.

Quinlan, M. E. (2016). Cytoplasmic Streaming in the *Drosophila* Oocyte. *Annu. Rev. Cell Dev. Biol.* 32, 173–195.

Sutcliffe, B., Ng, J., Auer, T. O., Pasche, M., Benton, R., Jefferis, G. S. X. E. and Cachero, S. (2017). Second-Generation *Drosophila* Chemical Tags: Sensitivity, Versatility, and Speed. *Genetics* 205, 1399–1408.

Tittel, J., Welz, T., Czogalla, A., Dietrich, S., Samol-Wolf, A., Schulte, M., Schwille, P., Weidemann, T. and Kerkhoff, E. (2015). Membrane Targeting of the Spir·Formin Actin Nucleator Complex Requires a Sequential Handshake of Polar Interactions. *J. Biol. Chem.* 290, 6428–6444.

Appendix I: Cloning schemes for endogenous editing of Spir and Capu

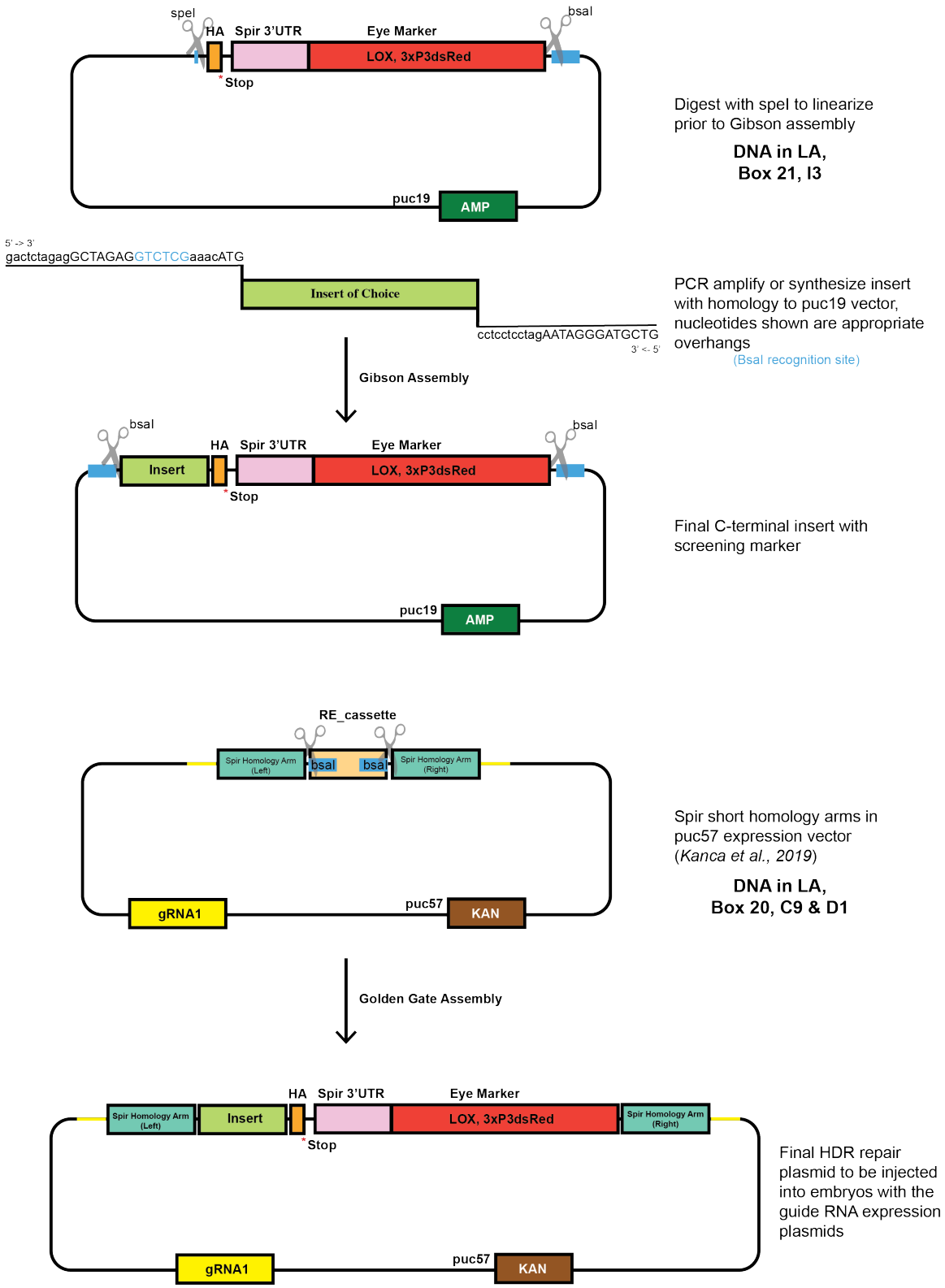

Appendix I - Figure 0-1: Two-step cloning of C-terminal repair plasmid for Spir via CRISPR/cas9 mediated homology directed repair.

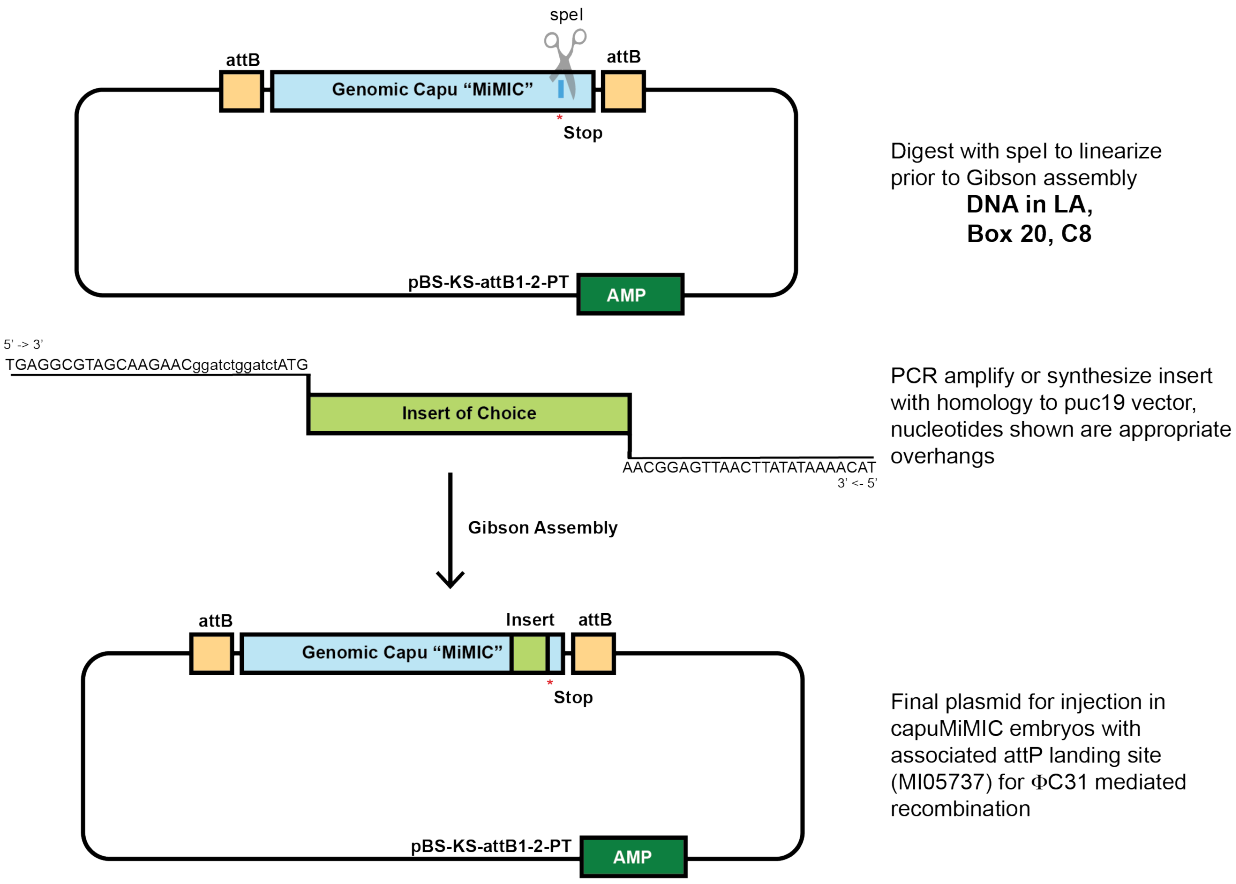

Appendix I - Figure 0-2: One-step cloning of C-terminal repair plasmid for Capu via ΦC31 mediated recombination.

Appendix II: : Primary antibody conditions optimized for immunofluorescence of *Drosophila* egg chambers.

Introduction

The standard lab protocol for immunofluorescence, as described in (Quinlan, 2013; Robinson and Cooley, 1997), was followed. For all primaries tested, optimal staining efficiency was observed with incubation of ovaries overnight at 4°C. When determining optimal staining conditions chambers in a high throughput fashion, 2-3 ovary pairs were treated in 5-7μL of primary antibody solution using Terasaki multiwell plates (Sigma Aldrich, M5812). All secondaries of the appropriate species were used at a 1:200, diluted in a solution of PBS, TritonX-100, and BSA, with an incubation time of 2 hours at room temperature.

Appendix II – Table 1: Primary Antibody Conditions Optimized for IF

Target	Species	Epitope	Concentration	Purchasing Information
HA	Rabbit	HA(c29F4B)	1:1000	CST, 3724S
HA	Mouse	HA(HA.C5)	1:500	Abcam, 18181 (not great)
HA	Mouse	HA(16b12)	1:1000	Enzo, VWR, 76002-614
GFP	Chicken	GFP	1:2000	Abcam, ab13970
OLLAS	Rat	OLLAS	1:2500	Novus Biologicals, NBP1-06713
MYC	Mouse	Myc(9B11)	1:500	CST, 2276S
MYC	Rabbit	Myc(71D10)	1:250	CST, 2278S
Membranes	Mouse	phospho-Tyrosine (pY20)	1:100	Thermofisher, 14-5001-82
Capu	Rabbit	Capu	1:1500	In house, BosterBio (needs further optimized and preabsorbed)
MyosinV (CT)	Rabbit	MyoV(CT)	1:250	Gift from the Ephrussi Lab (preabsorb)
Oskar	Rabbit	Oskar	1:3000	Gift from the Ephrussi Lab
Staufen	Mouse	Staufen	1:50	Gift from the Doe Lab

References

Quinlan, M. E. (2013). Direct interaction between two actin nucleators is required in Drosophila oogenesis. *Development* 140, 4417–4425.

Robinson, D. N. and Cooley, L. (1997). *Drosophila* Kelch Is an Oligomeric Ring Canal Actin Organizer. *J. Cell Biol.* 138, 799–810.

Appendix III: The Auxin Inducible Degradation System

Introduction

Other than the requirement of Spir and Capu, little is known about what other components are necessary for proper mesh organization, stabilization, and removal. To determine other key factors, we sought to establish the Auxin Inducible Degradation (AID) system in our lab. This motivation stems from previously discussed issues with using RNAi for knockdown of candidate genes (**Chapter 6**) and that AID has been shown to work in the female germline (Bence et al., 2017).

Ultimately, we found no success with this method. Other groups have not been able to use AID as well and it has been determined that auxin treatment is disruptive to *Drosophila* (Fleck et al., 2024). Therefore, we have deemed this method is not feasible and not worthwhile to continue optimization. A summary of reagents, conditions, and treatments we tried is reported here.

Materials and Methods

Appendix III - Table 1: Drosophila lines generated

Line	Method	Antibody	Stock (Lab #)
spir-smGFP-HA-AID	CRISPR-cas9 HDR	anti-HA	Q348, Q349
capu-meGFP-AID	MiMIC	anti-GFP	Q386, Q387
didum-MYC-AID	CRISPR-cas9 HDR	anti-Myc	Q335, Q336
yw;+; UASp::OsTir1(F74G)	-	-	Q340, Q341
yw; UASp::OsTir1(F74G)/CyO	-	-	Q342, Q343

Drosophila lines obtained from stock centers

w[*];P{w[+mc]=Ubi-OsTir1.T} (Bloomington, BDSC 91781), w[*];;P{w[+mc]=Ubi-OsTir1.T}/TM3,Ser[1] (Bloomington, BDSC 91782), w[*]; M{w[+mC]=UASp-OsTIR1.myc}ZH-86Fa (Bloomington, BDSC 76124), w[*];;M{w[+mC]=UASp-OsTIR1.myc}ZH-58A (Bloomington, BDSC 76125)

Auxin Analogues

Naphthaleneacetic Acid (K-NAA), (PhytoTech, N610), 5-Ph-IAA (BioAcademia, 30-003), IAA Auxin (3-Indoleacetic acid), (Sigma Aldrich, I2886)

A. Initial experiment

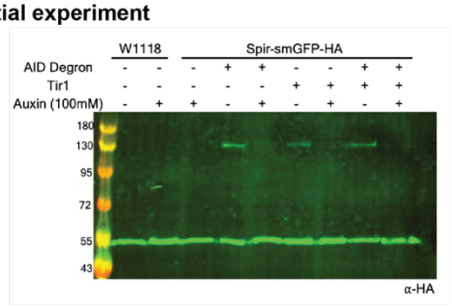

Concentrations of 100mM auxin causes non-specific removal of high molecular weight proteins in a 10 minute treatment window.

B. Auxin analoge comparison

K-NAA

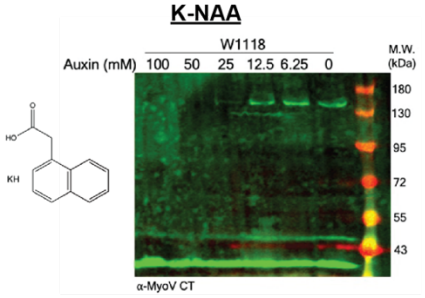

At concentrations >25mM of K-NAA we observe non-specific removal with 10 minute treatment.

IAA

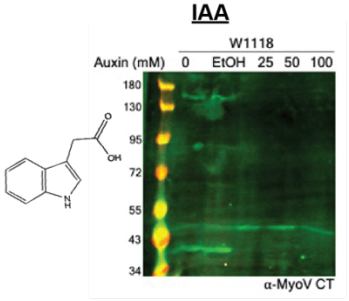

IAA auxin analogue exhibited similar problems and was insoluble.

C. Reducing concentration > 10 fold

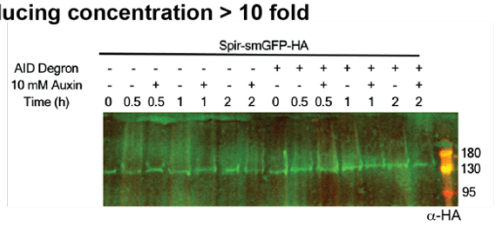

Ovaries can be exposed to 10mM auxin for 2 hours without observing non-specific degradation.

D. Sources of Tir1

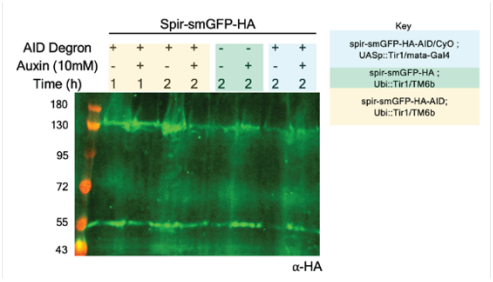

To determine if Tir1 was being expressed properly in the germline we tried comparing driven and ubiquitously expressed sources.

This was inconclusive as no degradation of Spir-AID was observed.

D. Even lower concentrations of auxin

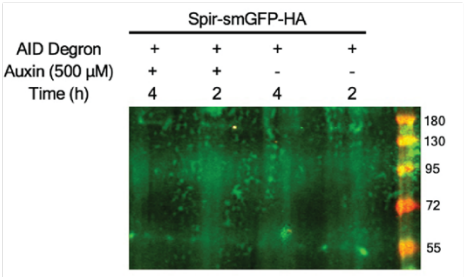

This western blot overall did not work, as the nonspecific band is no longer present. No conclusion can be drawn on the efficiency of removal with 500mM auxin.

Appendix III - Figure 0-1: Results and conclusions from using the AID system in Drosophila egg chambers.

Discussion

K-NAA and IAA were tested and caused nonspecific removal of proteins at concentrations greater than 25mM. Further optimization of auxin treatment could be possible by trying more dilutions and vehicles to get IAA into solution. We did try a range of concentrations from 100mM to 500μM to treat ovaries *ex vivo*. From this we determined that a concentration below 10mM is required to prevent nonspecific removal but not sufficient for removal of AID-tagged proteins. The lack of removal could be due to insufficient treatment time, a range of 10 minutes to 4 hours of incubation of the ovaries in auxin. This is less than ideal, as for this system to be useful to study the actin mesh we need to induce degradation within a 2-hour time period. Our last attempt was using different germline drivers of Tir1. We found that both Ubi::Tir1 and *matα*>Tir1 were unable to induce degradation of the AID-tagged protein. As previously stated, this system is not worth continuing to optimize. Putting effort into optimizing other techniques to induce removal of candidate proteins, such as RNAi or optogenetics, is more worthwhile.

References

Bence, M., Jankovics, F., Lukácsovich, T. and Erdélyi, M. (2017). Combining the auxin-inducible degradation system with CRISPR /Cas9-based genome editing for the conditional depletion of endogenous *Drosophila melanogaster* proteins. *FEBS J.* 284, 1056–1069.

Fleck, S. A., Biswas, P., DeWitt, E. D., Knuteson, R. L., Eisman, R. C., Nemkov, T., D'Alessandro, A., Tennessen, J. M., Rideout, E. and Weaver, L. N. (2024). Auxin exposure disrupts feeding behavior and fatty acid metabolism in adult Drosophila. *eLife* 12, RP91953.